DOE/ER/10612-1

STABLE ISOTOPE STUDIES

Annual Progress Report

for Period March 1, 1980 to February 28, 1981

State University of New York

at

Stony Brook
Stony Brook, New York 11794

October 28, 1980

Prepared by

THE U.S. DEPARTMENT OF ENERGY
OFFICE OF BASIC ENERGY SCIENCES

Under CONTRACT NO. DE-AC02-80ER10612

DISCLAIMER

DOE/ER/10612-1

ANNUAL PROGRESS REPORT
TO
U.S. DEPARTMENT OF ENERGY
OFFICE OF BASIC ENERGY SCIENCES

STABLE ISOTOPE STUDIES

Takanobu Ishida, Principal Investigator
Department of Chemistry
State University of New York
at
Stony Brook
Stony Brook, New York 11794

DE-AC02-80ER10612

October 28, 1980

For Period: March 1, 1980 to February 28, 1981

STABLE ISOTOPE STUDIES

TABLE OF CONTENTS

TABLE OF CONTENTS (cont.)

Annual Progress Report to
U.S. Department of Energy, Office of Basic Energy Sciences
Contract No. DEAC02-80ER10612

STABLE ISOTOPE STUDIES

Abstract

The Bigeleisen-Brooks-Ishida-Ribnikar cryostat has been re-assembled and re-calibrated. The vapor pressures of $^{12}CHF_3$, $^{13}CHF_3$, and $^{12}CDF_3$ have been measured again in the cryostat at temperatures between -147°C and -60°C. The $^{13}CHF_3$-sample used in previous measurements has been found to contain 1.3% of an impurity which escaped our detection earlier and has had to be re-purified. The new data are best represented by

$$T \ln \frac{P'(^{12}CHF_3)}{P\ (^{12}CDF_3)} = \frac{389.2}{T} + 1.511$$

and

$$T \ln \frac{P'(^{12}CHF_3)}{P\ (^{13}CHF_3)} = \frac{72.21}{T} - 0.1313$$

The observed normal isotope effect of the D-for-H substitution with the positive slope in the plot of $T \ln(P'/P)$ vs $1/T$ and the observed inverse isotope effect of the ^{13}C-for-^{12}C substitution with the negative slope in the plot of $T \ln(P'/P)$ vs $1/T$ are simultaneously explanable only in terms of an occurrence of a blue-shift in the C-H stretching frequency upon condensation of fluoroform molecules. The blue-shift is conceivable on the basis of an extensive external-internal interaction through a weak hydrogen bonding.

The vapor pressures of $^{12}CH_3F$, $^{13}CH_3F$, and $^{12}CD_3F$ have been measured in the cryostat at temperatures between -141°C and -60°C. The D-for-H effect in methyl fluoride is a very positively normal isotope effect with a large positive slope and is representable by

$$T \ln \frac{P'(^{12}CH_3F)}{P\ (^{12}CD_3F)} = \frac{2012.6}{T} - 3.161$$

The ^{13}C-for-^{12}C effect in methyl fluoride is a slightly inverse isotope effect with a slightly positive slope and is best expressed by

$$T \ln \frac{P'(^{12}CH_3F)}{P\ (^{13}CH_3F)} = \frac{54.37}{T} - 0.5787$$

The construction of all stainless-steel nitrogen-15 exchange column based on the pressurized NO/N_2O_3 system has been completed. A product

refluxer made of Pyrex after the design of Monse, Spindel, Kauder, and Taylor has been operated under various flow and concentration conditions, which led to a new design for the SO_2-flow control: The reaction zone is more reliably controlled by detecting a rise in temperature by means of a thermistor. Still another reflux system has been designed and constructed, which utilizes the reduction of nitric acid by a ferrous salt solution in dilute sulfuric acid. To facilitate total nitrogen determination at a sub-ppm level, a microanalytical method based on the Devarda's alloy reduction and the Nessler colorimetry has been developed.

Two Fortran programs have been written for studies of differential isotope effect. One of them, DIE, is based on the WIMPER expansion of the isotopic reduced partition function ratio and is designed to test various levels of the approximation for the differential isotope effect. The other program exactly calculates the differential effects of small force constant changes in the liquid $\underset{\sim}{F}$-matrix and produces a compact tabulation of essential data for fitting a liquid $\underset{\sim}{F}$-matrix to observed vapor pressure isotope effects.

This year has been marked by aftermath of the moving from Brooklyn College to Stony Brook. A significant amount of efforts has been expended for re-construction of the equipment. Also, 550 tracks of computer programs and numerical data have been transferred from the IBM-370 system at the City University of New York to the UNIVAC-1100 system at Stony Brook.

II. SUMMARY

II-A. SCOPE OF ACTIVITIES

During the past year one principal investigator, two postdoctoral fellows, four graduate students, and one undergraduate student have participated in various studies of this project. In addition, Dr. William Spindel of National Academy of Sciences collaborated in the studies of nitrogen-15 fractionation systems. We also shared one quarter of a secretary's time with other faculty members of the Chemistry Department on this campus.

Following our move from Brooklyn College, Brooklyn, New York, a substantial effort has been expended in re-construction, re-calibration and re-debugging of the experimental facilities, in particular, those of the precision cryostat, its control systems, nitrogen-15 fractionation systems, mass-spectrometer, and various vacuum systems. At the same time the computer programs and numerical data files which were on 550 tracks of disk storage have been successfully transferred from the IBM-370 system at the University Computer Center of the City University of New York to the UNIVAC-1100 system at the Stony Brook campus of the State University of New York.

Our studies during the year consisted of cryostatic measurements of vapor pressure isotope effects in fluoroform and in methyl fluoride, studies of nitrogen-15 fractionation by exchange between pressurized nitric oxide and liquid dinitrogen trioxide, studies of a new product reflux method for the Nitrox process, and the theoretical investigations that included a study of improved correlation between isotope effect and molecular forces and a study of the differential isotope effect. One manuscript submitted to Journal of Chemical Physics has been accepted. The progresses made in these areas of study during the current year will be summarized in five parts in Section II-C, and their detailed accounts will be presented in Section III, "SCIENTIFIC PROGRESS."

We have not received any support other than this Department of Energy funding in this period.

II-B. PUBLICATIONS

One manuscript has been accepted for publication in Journal of Chemical Physics (tentative issue; February 1, 1981). The manuscript is attached as an Appendix of this report:

"Correlation of the Isotope Chemistry of Hydrogen, Carbon and Oxygen with Molecular Forces by the WIMPER(2) Method,"
J. Bigeleisen, T. Ishida, and M. W. Lee.

II-C. SUMMARY OF SCIENTIFIC INVESTIGATIONS

The following is a five-part summary of various achievements for the current year that are still in progress.

(1) Re-assembly and Re-calibration of Precision Cryostat [cf: Section III-A-1]:

The BBIR-type precision cryostat originally built and used in Brooklyn has been moved, partially dismantled, to the new site here at Stony Brook and has since been re-assemblied. Several improvements that we thought about while operating it in Brooklyn have been instituted. They include rewinding of heater wires, enhancement of heat transfer between the temperature sensors and the radiation shields, elimination of constant heat leak from the sample holder block, installation of a new, 5-position liquid nitrogen level control, and addition of a bellows valve on each sample capillary line to facilitate zeroing of the capacitance gauges in the middle of a run. The quartz spiral gauge for the measurement of absolute pressure of reference isotopic molecules has been calibrated again after the moving against an NBS-certified Ruska dead-weight gauge. We found that the moving did not cause any significant change of calibration over its entire pressure range. The temperature scale of the cryostat has been calibrated again in situ by comparing the vapor pressure of pure ethane of the natural isotopic abundance measured by the quartz spiral gauge as a function of temperature (measured by the platinum resistance thermometer inserted in the sample holder block of the cryostat) to the vapor pressure data of Rossini.

(2) Vapor Pressure Isotope Effects in Fluoroform [cf: Section III-A-2]:

Since we moved we found that the sample specimen of $^{13}CHF_3$ we previously used for the measurements of vapor pressure isotope effect (VPIE) in fluoroform contained 1.3% of chemical impurity, which had escaped our detection due to a particular choice of analytical conditions in gas chromatography. Accordingly, the $^{13}CHF_3$ sample has been re-purified

and re-analyzed, and the VPIE data of fluoroform has been re-taken at temperatures between -147°C and -60°C. The results are reported in Section III-A-2.

The D-for-H substitution in fluoroform yields a normal VPIE, i.e., P'(H)>P(D), at these temperatures, which is best represented by

$$T \ln \frac{P'}{P} = \frac{389.2}{T} + 1.511$$

and the ^{13}C-for-^{12}C VPIE in fluoroform, which is an inverse VPIE, i.e., $P'(^{12}CHF_3)<P(^{13}CHF_3)$, is best expressed as

$$T \ln \frac{P'}{P} = \frac{72.21}{T} - 0.1313$$

Contrary to our last report, the magnitude of the negative slope of the $^{13}C/^{12}C$-VPIE is so small that the second cross-over will not occur in the liquid temperature range. These VPIE-data on the two sets of isotopic pair support the fact that the C-H stretching frequency of fluoroform blue-shifts upon condensation. A correlation between the blue-shifting C-H frequency and an intermolecular hydrogen bonding has been discussed.

(3) Measurements of Vapor Pressure Isotope Effects in Methyl Fluoride [cf: Section III-A-3]:

As a second part of our VPIE studies of fluoromethanes we have conducted the measurements of VPIE in methyl fluoride by using $^{12}CH_3F$ as a reference gas and by taking vapor pressure differences between $^{12}CH_3F$ and $^{12}CD_3F$ and also between $^{12}CH_3F$ and $^{13}CH_3F$. The syntheses, purification, and analyses of the samples of these isotopic molecules had been reported previously.

The D/H-effect in methyl fluoride is a normal isotope effect and can be best represented by

$$T \ln \frac{P'}{P} = \frac{2012.6}{T} - 3.161$$

The $^{13}C/^{12}C$-effect in methyl fluoride is a slightly inverse VPIE with a small positive slope expressed as

$$T \ln \frac{P'}{P} = \frac{54.37}{T} - 0.5787$$

(4) Nitrogen-15 Fractionation Studies [cf: Section III-B]:

After the moving from Brooklyn, the partially disassembled system for nitrogen-15 fractionation studies of the NO/N_2O_3-system has been re-assembled. The isotope exchange column system, except for the product reflux column, was constructed of Type 316 stainless steel. The reflux column system made of Pyrex after the design of Monse, Spindel, Kauder, and Taylor was extensively tested to obtain basic operational data and to gain familiarity with the system. The control for the flow rate of SO_2 has been changed from the photocell system of the original design to a thermistor method, in which the reaction (exothermic) zone in the packed column is detected by a thermistor and the information on the temperature is used to operate a pneumatic valve inserted in a side path of an SO_2 supply line. This method offers much higher versatility and reliability than the photocell method.

A new product reflux system for the reduction of enriched HNO_3 has been conceived and built. This system is based on the reduction of HNO_3 by ferrous salt solution of dilute sulfuric acid, followed by a thermal decomposition of the $FeNO^{2+}$ complex. The ferrous salt can be re-generated by an electrolytic reduction.

To facilitate a quantitative analysis of a sub-ppm concentration of total nitrogen in connection with the nitrogen isotope fractionation studies we have developed a reliable method for the low concentration nitrogen based on the Devarda's metal reduction of nitrate, followed by the Nessler colorimetric determination of ammonia.

(5) Studies of Differential Isotope Effects [cf: Section III-C]:

In the search for a simple approximation method for the effect of a small change in a force constant matrix element on isotope effects, we had last year reported a method based on the WINIMAX expansion of the isotopic reduced partition function ratio. We have now written a Fortran Program, DIE (Differential Isotope Effect), with which we plan to

examine the extent of accuracy with which the various levels of approximation by this short-cut method will predict the differential effect.

In the meanwhile, we have written another Fortran program, P9042D, which computes the differential effect of small force constant changes in liquid $\underset{\sim}{F}$-matrix on the vapor pressure isotope effect. This program employs an exact numerical calculation of the differential effect that involves solutions of the secular equations. The program allows a series of changes in the liquid $\underset{\sim}{F}$-matrix, and produces a compact table of frequencies, ln(fc/fg), and T ln(fc/fg).

II-D. PERSONNEL

The scientific personnel for the current year has consisted of one principal investigator, two postdoctoral fellows, four Ph.D. students, one undergraduate student, and one consulting collaborator. We also shared a secretary with other projects in the Department.

The principal investigator, Professor Takanobu Ishida, spent an average of 25% of his time for the project during the academic year and two full-time months during the summer.

Dr. Takao Oi devoted 100% of his time throughout the project year working on the re-construction of the cryostat and the measurements of vapor pressure isotope effects in fluoroform and methyl fluoride. Dr. Motonari Adachi arrived here in July from Department of Nuclear Chemical Engineering, Institute of Atomic Energy, Kyoto University, Kyoto, Japan. He has since worked full time on the product refluxer for the nitrogen-15 fractionation system.

Two graduate students, Mr. Jan Shulman and Mr. Michael Prencipe, who were midway through their doctoral researches when we moved from Brooklyn, continued their work here at Stony Brook after the moving. Mr. Shulman worked full-time on his study of vapor pressure isotope effect in methyl fluoride for the period through August, during which he was fully supported by this project. Since the beginning of September he, who elected to remain a Ph.D. student at the City University of New York, has been partially supported by the Chemistry Department at Brooklyn College through teaching. During this period he has spent about 75% of his time for the project. Mr. Prencipe, who originally elected to transfer to the State University of New York, has since reversed his decision and has been reactivated as a Ph.D. student of C.U.N.Y. He worked full-time at Stony Brook for his thesis research on the nitrogen-15 fractionation studies.

Two new Stony Brook graduate students, Miss Arundhati Kanungo and Mr. Tseng Ven King, have started to work in this project at the start of the summer. Miss Kanungo is from India, and Mr. King is from People's Republic of China. They are both second year graduate students and want to study vapor pressure isotope effect. Both spent 100% of time during

the summer and 75% of time since September preparing themselves for their thesis researches. The project has fully supported both since June. Miss Kanungo wants to work on the vapor pressure isotope effect in methylene difluoride. Mr. King has not decided on a chemical species the vapor pressure isotope effect of which he wants to investigate. He spent a considerable amount of time in studying and modifying the Schachatschneider programs.

An undergraduate student, Mr. Riazulla Rouhani Manshadi, spent 10 hours per week during the Spring and Fall terms of 1980 and 20 hours per week during the summer months. This Iranian student worked on the improved method of total nitrogen determination. He did this as a special course work during the academic year and received compensation on the hourly basis during the summer.

Dr. William Spindel of the National Academy of Sciences participated in our study of nitrogen-15 fractionation systems and spent a total of 15 days, for which he was compensated by the project.

We closely collaborated with Professor Jacob Bigeleisen's research group. His postdoctoral fellow, Anthony Popowicz, in particular used his expertise in the cryostat assembly and operation, giving his advices and instructions to the students in this project.

We shared Miss Lillian Richardson's time with other members of the Chemistry Department (Drs. Harold Friedman, Philip Johnson, Allen Krantz), who spent 25% of her time for this project throughout the year.

III. SCIENTIFIC PROGRESS

(A) VAPOR PRESSURE ISOTOPE EFFECTS IN FLUOROMETHANES

(A-1) Reassembly and Calibrations of Precision Cryostat

by Takao Oi and Jan Shulman

The system of precision crystotat [1,2], which consists of the modified BBIR-type cryostat, sample-handling vacuum lines, a Mensor spiral quartz gauge, and three differential capacitance gauges, interfaced with an LSI-11 microcomputer (MICROFLOP-11) for experiment control and data acquisition, has been re-assemblied in a fourth floor laboratory at Stony Brook after it was moved, disassembled, from Brooklyn College. Some improvements in design have been instituted during the re-assembly. The quartz spiral gauge has been re-calibrated over its functional range of 0-1500 torr against a Ruska dead-weight gauge. The platinum resistance thermometer in the base of the sample holder block of the cryostat has been calibrated in situ against the known vapor pressure data of ethane.

(A-1-a) Improvements on Cryostat Design: Taking advantage of the moving of the equipment which forced us to partially disassemble the cryostat and the associated plumbing and instrumentation, we have made following improvements in the system. Figures 1 and 2 have been copied from our previous reports for orientation purpose.

During its operation while in Brooklyn we felt that the heater power on the lower radiation shield (LRS) was too low. Therefore, we re-wound the LRS heater with 255 feet of Gauge No. 30 constantan wire, which now provides 671 ohms of resistance at room temperature instead of 297 ohms for the old winding. The heater wire terminals on the radiation shields (the lower (LRS), the upper (URS), and the auxiliary (ARS)) have been re-designed to make them short circuit-proof. Thermal contacts between all platinum resistance thermometers (PRT) and the radiation shields have been increased by building up epoxy cement around the PRTs. Similar

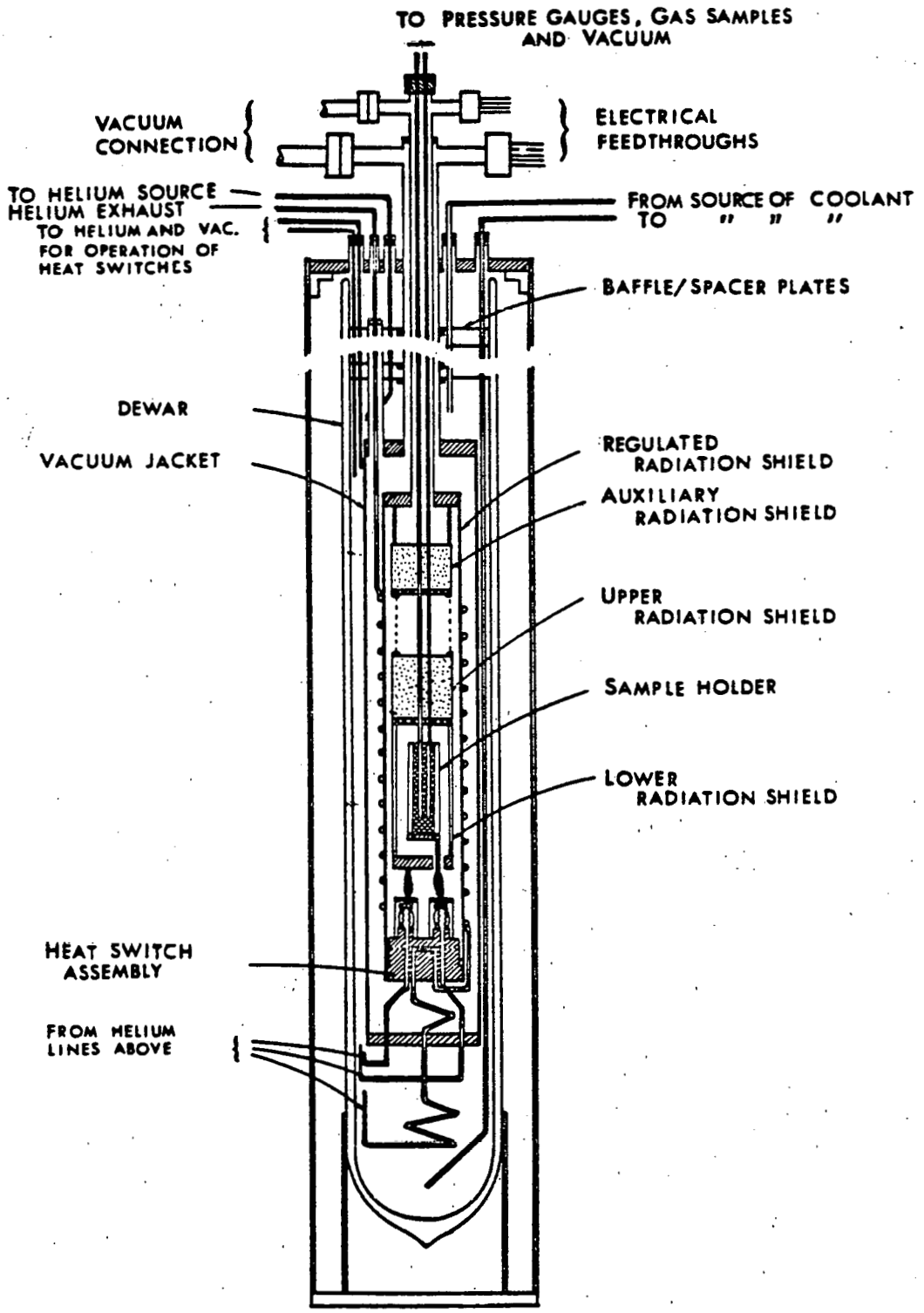

Figure 1. Assembly Drawing of Cryostat

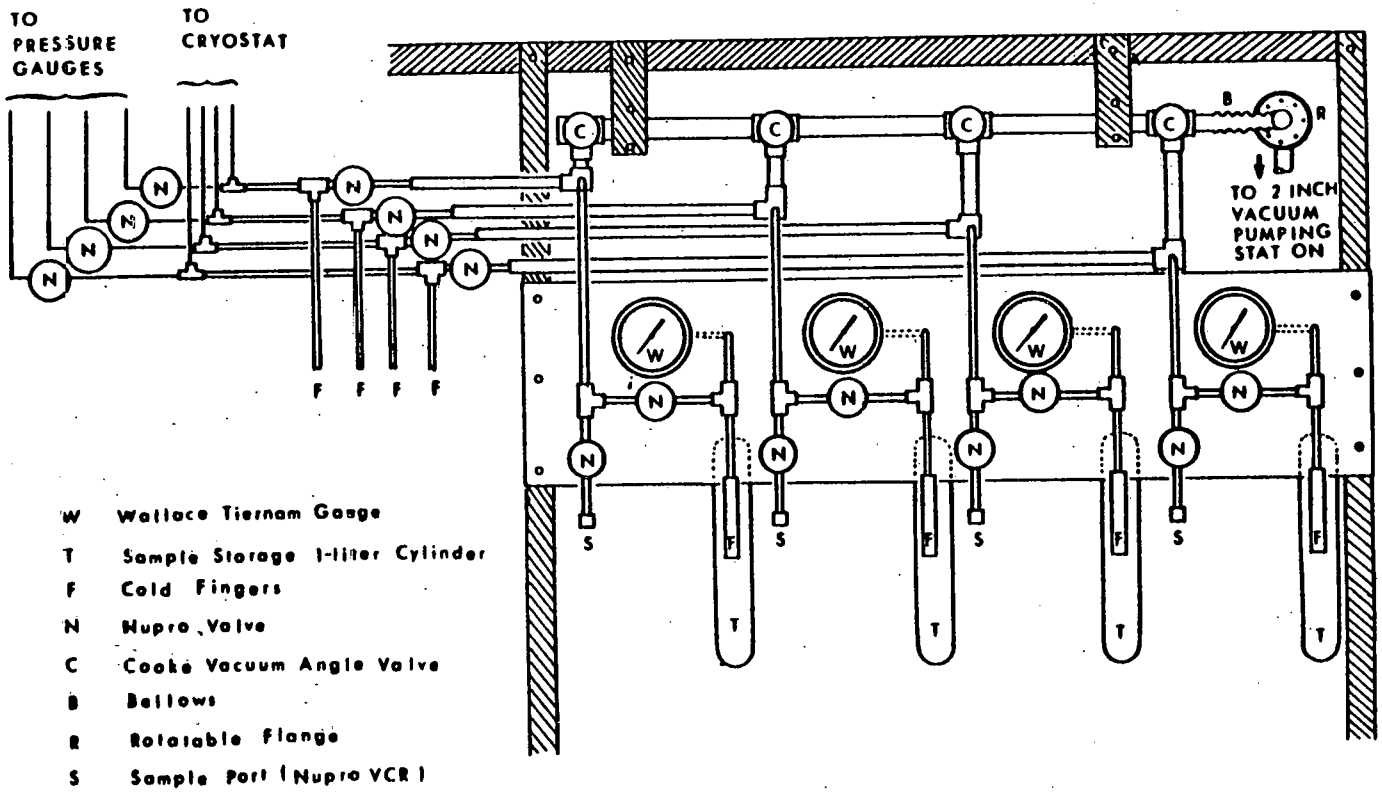

Figure 2. Cryostat Sample-Handling Vacuum Line

improvement has been implemented for the thermocouple junctions. A better thermal contact has been accomplished between the capillary sample lines and the LRS, URS, and ARS by filling with soft metal filler the gap between the capillary lines and the holes through the radiation shields.

The gap between the head of the bellows and the gold-plated contact plate[2] in the thermal switches has been decreased. The pair of copper lines used to provide a constant heat leak between the sample holder (SH) block and the thermal switch base have been completely disconnected to achieve a slower temperature drift of the SH.

In the previous design, levels of liquid nitrogen in the cryostat dewar had been fixed near the elevation of the SH base. To achieve more flexibility in the selection of LN_2 levels we have installed five sensor heads which are selectable by means of a rotary switch. Each sensor head consists of a pair of 1000Ω carbon resistors placed vertically about 1 1/4" apart, one of which acting as a low level sensor and the other as a high level sensor.

To facilitate re-zeroing of the capacitance gauges during vapor pressure measurements, four Nupro bellows valves have been installed along four lines connecting the sample capillary lines of the cryostat and the sample-handling vacuum lines. Referring to Figure 2, the new valves are located (but not shown in the figure) along the vertical lines marked "To Cryostat" on the upper left-hand corner.

(A-1-b) Recalibration: Although the quartz spiral gauge for absolute pressure measurement of reference gases had been calibrated against a Ruska dead-weight gauge while in Brooklyn[1], we felt it advisable to re-calibrate it after the moving. The same Ruska gauge, Model #2460, with the standard weights calibrated by the National Bureau of Standards (Job. #14662) that we used before has been used, a courtesy of Professor Jacob Bigeleisen. One hundred seventy seven points have been taken between 0 torr and 1499 torr at a spiral gauge temperature of 49.36 ± 0.58°C and against the atmospheric pressure as reference. All points line well along a straight line. Result of a least squares fit to the form,

$$P = a Q^3 + b Q^2 + c Q ,$$

where P is the differential pressure in torr and Q the quartz gauge decade counter reading, is as follows:

$$a = -1.8052 \times 10^{-14} \pm 3.628 \times 10^{-16}$$
$$b = 1.4810 \times 10^{-9} \pm 4.536 \times 10^{-11}$$
$$c = 1.5243 \times 10^{-2} \pm 1.300 \times 10^{-6}$$

These calibration points agree very well with 151 points obtained in the previous calibration.[1] This is gratifying since it shows that the moving did not affect the quality of the gauge.

To facilitate a reliable temperature scale for the vapor pressure measurements we have purified ethane of the natural isotopic composition and have used them to calibrate the platinum resistance thermometer (PRT) coaxially inserted in the base of the sample holder block of the cryostat. The sample of ethane purchased from Matheson has been purified by means of a preparative gas-chromatography using a 5 meter column (3/8" O.D.) of molecular sieve (13X, 60-80 mesh) at 40∿60°C. An analysis of combined fractions of the purified ethane showed the following impurities: 10 ppm of CO_2, 20 ppm of H_2O, 25 ppm of ethylene, and a barely detectable (<1 ppm) amount of propane. Vapor pressure of ethane was used to calibrate the PRT output between 128°K and 199°K, and the vapor pressure equation of Rossini,[4]

$$\log_{10} P \text{ (torr)} = - \frac{656.40}{256.00+t(°C)} + 6.80266 , \qquad (1)$$

was applied. The calibration table supplied by the manufacture of the PRT placed in the sample holder of the cryostat yielded a consistently higher temperature by about 0.11°C compared to the Rossini's vapor pressure equation: The least-squares fit of 105 calibration points to the functional form

$$\log_{10} P \text{ (torr)} = \frac{a}{b+t'(°C)} + b \qquad (2a)$$

led to

$$a = -651.71 \pm 0.76$$
$$b = 255.34 \pm 0.10 \qquad (2b)$$
$$c = 6.7892 \pm 0.0026$$

The PRT temperature scale has been modified accordingly.

The re-constructed and calibrated cryostat has then been used to measure the vapor pressure isotope effects in CHF_3 and CH_3F.

(A-2) Vapor Pressure Isotope Effects in Fluoroform

by Takao Oi, Jan Shulman, and Anthony Popowicz

(A-2-a) New Data on Vapor Pressure Isotope Effects in Fluoroform: The vapor pressure isotope effect (VPIE) in fluoroform for the $^{12}CDF_3/^{12}CHF_3$ and $^{13}CHF_3/^{12}CHF_3$ pairs were reported previously[1]. After the cryostat was re-constructed and re-calibrated, its performance was tested by repeating the VPIE measurements for the fluoroform pairs at temperatures between 126.00°K and 212.16°K, which corresponds to the $^{12}CHF_3$ vapor pressures ranging from 1.648 torr to 2203.9 torr. This should be compared to the range of temperatures, 133°K to 193°K corresponding to P = 4.5 torr ∿ 814 torr, that we were able to attain in Brooklyn[1]. The extended temperature range has been made possible due to an improved temperature stability of the sample holder block of the re-constructed cryostat.

These measurements and the last year's VPIE data[1] agreed well for both isotopic pairs, until we noticed a rather sharp apparent increase in the $^{13}CHF_3/^{12}CHF_3$-VPIE at and above 190°K: The plot of T ln $[P(^{12}CHF_3)/P(^{13}CHF_3)]$ against 1/T has a negative slope in the inverse VPIE region, the plot generally approaching the zero-line (zero isotope effect) with an increasing temperature, as illustrated on page 50 of last year's progress report[1]. We then found the sharp break away from the zero-line at about 190°K. The discontinuity was proved reproducible in several test runs.

We decided to analyze the samples of all isotopic fluoroform for chemical impurities, although each isotopic fluoroform had been carefully purified and analyzed to the extent that all impurities were reduced to the order of 10 ppm or better[1] (or, that's what we thought). To our dismay we found in the $^{13}CHF_3$ specimen a new impurity at a level of 1.3%(!), which was originally hidden under the main peak in all the gas-chromatographic analyses. Last year, $^{13}CHF_3$ was purified by a bulb-to-bulb distillation, followed by a passage through a Chromosorb-102 tube at -50°C and then through an Ascarite tube. The sample was analyzed gas-chromatographically using a 6-ft. column of Spherocarb 80/100 at

117° ∿ 227°C. The purified sample contained 7 ppm of CO_2 and 7 ppm of unidentified impurity (retention time relative to CHF_3 = 4.61). After the suspicious VPIE results were obtained, use of an alumina (80/200) column for a GC analysis at 60°C revealed the major impurity (1.3% by area) at a relative retention time of 0.30 (relative to the CHF_3 peak). Other isotopic CHF_3 did not contain this impurity. $^{13}CHF_3$ was re-purified by using a preparative gas-chromatograph with a 5 meter column (3/8" O.D.) of alumina at 0°C. The gases were carried through by a flow of helium at 20 cc/min. The majority of the newly detected impurity was eluted out of the column between 3 1/2 hours and 6 1/2 hours, during which time, only 5% of total charge of fluoroform came out. All the remaining fractions were combined and subsequently used for renewed VPIE measurements.

A new series of cryostatic VPIE measurements of the $^{13}CHF/^{12}CHF_3$-pair have since been carried out using the re-purified sample of $^{13}CHF_3$. The results are summarized in Table 2 and Figure 4. The VPIE data for the $^{12}CDF_3/^{12}CHF_3$-pair are summarized in Table 1 and Figure 3.

The results of Figures 3 and 4 have been least-squares fitted to the form,

$$T \ln \frac{P'}{P} = \frac{A}{T} + B + C\,T \qquad (3)$$

For the $^{13}C/^{12}C$-effect we found

$$\begin{aligned} A &= -56.65 \pm 8.02 \quad (°K^2) \\ B &= -0.3236 \pm 0.0988 \quad (°K) \\ C &= 0.00059 \pm 0.00030 \end{aligned} \qquad (4)$$

For the D/H-effect we found

$$\begin{aligned} A &= 6.72 \pm 28.88 \quad (°K^2) \\ B &= 6.267 \pm 0.357 \quad (°K) \\ C &= -0.01457 \pm 0.00109 \end{aligned}$$

We also fitted the data to the form,

$$T \ln \frac{P'}{P} = \frac{A}{T} + B \qquad (5)$$

which yielded, for the $^{13}C/^{12}C$-effect,

Table 1: Hydrogen Vapor Pressure Isotope Effects in Fluoroform

No.	T (°K)	$10^3/T$ ($°K^{-1}$)	P (Torr)	T $\ln(P'_H/P_D)$	Date
1	126.00	7.936	1.6478	+4.406	09/08
2	126.95	7.877	1.8993	+4.369	09/08
3	127.84	7.822	2.1600	+4.418	09/08
4	128.72	7.769	2.4587	+4.347	09/08
5	129.16	7.742	2.6142	+4.679	10/28
6	129.64	7.714	2.8124	+4.308	09/08
7	129.97	7.694	2.9252	+4.578	10/28
8	130.51	7.662	3.1630	+4.277	09/08
9	131.55	7.602	3.6554	+4.264	09/08
10	132.54	7.545	4.1889	+4.233	09/08
11	133.01	7.518	4.4587	+4.611	10/23
12	133.53	7.489	4.7712	+4.391	08/13
13	133.71	7.479	4.8871	+4.440	10/28
14	133.75	7.477	4.9099	+4.263	09/08
15	134.15	7.454	5.1828	+4.367	08/13
16	134.15	7.454	5.1828	+4.273	09/02
17	134.69	7.424	5.5502	+4.403	10/23
18	135.14	7.400	5.8993	+4.350	08/13
19	135.17	7.398	5.9221	+4.405	10/28
20	135.17	7.398	5.9237	+4.218	09/02
21	135.72	7.368	6.3596	+4.516	10/29
22	136.16	7.344	6.7148	+4.341	08/13
23	136.17	7.344	6.7179	+4.513	10/23
24	136.64	7.319	7.1478	+4.394	10/28
25	136.66	7.317	7.1615	+4.257	09/02
26	137.04	7.297	7.5106	+4.457	10/29

[continued]

[Table 1; continued]

No.	T (°K)	$10^3/T$ ($°K^{-1}$)	P (Torr)	T $\ln(P'_H/P_D)$	Date
27	137.14	7.292	7.5914	+4.317	08/13
28	137.66	7.265	8.1112	+4.470	10/23
29	137.78	7.258	8.2454	+4.267	09/02
30	138.06	7.243	8.5472	+4.406	10/29
31	138.16	7.238	8.6433	+4.307	08/13
32	138.32	7.230	8.8475	+4.247	09/08
33	138.44	7.223	9.0091	+4.202	08/19
34	138.96	7.196	9.5564	+4.243	09/02
35	139.06	7.191	9.6494	+4.361	10/29
36	139.16	7.186	9.8171	+4.183	08/19
37	139.18	7.185	9.7927	+4.426	10/23
38	139.65	7.161	10.422	+4.207	09/08
39	139.75	7.156	10.496	+4.342	10/29
40	140.13	7.137	11.014	+4.233	09/02
41	140.15	7.135	11.052	+4.146	08/19
42	140.43	7.121	11.386	+4.324	10/29
43	140.79	7.103	11.927	+4.314	09/15
44	140.84	7.100	11.979	+4.215	09/08
45	141.15	7.085	12.416	+4.189	08/19
46	141.27	7.079	12.570	+4.311	10/29
47	141.41	7.072	12.778	+4.222	09/02
48	142.05	7.040	13.761	+4.301	10/29
49	142.17	7.034	13.967	+4.238	09/15
50	142.17	7.034	13.985	+4.131	08/19
51	142.53	7.016	14.563	+4.201	09/02
52	142.64	7.010	14.757	+4.198	08/20

[continued]

[Table 1; continued]

No.	T (°K)	$10^3/T$ ($°K^{-1}$)	P (Torr)	T $\ln(P'_H/P_D)$	Date
53	143.02	6.992	15.327	+4.321	10/24
54	143.14	6.986	15.595	+4.192	08/19
55	143.24	6.981	15.723	+4.262	10/29
56	143.64	6.962	16.501	+4.223	09/15
57	143.74	6.957	16.697	+4.213	09/02
58	144.14	6.938	17.438	+4.185	08/19
59	144.64	6.914	18.343	+4.291	10/24
60	144.95	6.899	19.023	+4.238	10/30
61	144.98	6.898	19.102	+4.204	09/02
62	145.14	6.890	19.474	+4.201	09/15
63	145.14	6.890	19.489	+4.165	08/20
64	145.76	6.861	20.773	+4.223	10/30
65	146.13	6.843	21.668	+4.241	09/08
66	146.14	6.843	21.662	+4.248	10/24
67	146.14	6.843	21.712	+4.142	08/20
68	146.55	6.824	22.683	+4.189	09/03
69	146.64	6.819	22.883	+4.203	10/30
70	146.69	6.817	23.019	+4.192	09/15
71	147.15	6.796	24.199	+4.120	08/20
72	147.17	6.795	24.232	+4.118	09/15
73	147.43	6.783	24.923	+4.191	09/08
74	147.55	6.777	25.260	+4.163	09/03
75	147.60	6.775	25.405	+4.148	09/15
76	147.65	6.773	25.484	+4.199	10/24
77	148.15	6.750	26.915	+4.107	08/20
78	148.43	6.737	27.724	+4.145	09/16

[continued]

[Table 1; continued]

No.	T (°K)	$10^3/T$ ($°K^{-1}$)	P (Torr)	T $\ln(P'_H/P_D)$	Date
79	148.56	6.731	28.032	+4.170	10/30
80	148.76	6.722	28.659	+4.143	09/03
81	149.15	6.705	29.816	+4.097	08/20
82	149.16	6.704	29.796	+4.167	10/24
83	149.16	6.704	29.879	+4.170	09/08
84	149.44	6.692	30.689	+4.134	09/16
85	149.94	6.670	32.274	+4.143	10/30
86	149.96	6.668	32.410	+4.125	09/03
87	150.15	6.660	33.048	+4.089	08/20
88	150.44	6.647	33.988	+4.125	09/16
89	150.64	6.638	34.705	+4.147	09/08
90	150.65	6.638	34.661	+4.138	10/24
91	151.13	6.617	36.375	+4.120	10/25
92	151.13	6.617	36.438	+4.103	09/03
93	151.16	6.616	36.546	+4.076	08/20
94	151.44	6.603	37.561	+4.112	09/16
95	151.94	6.581	39.452	+4.087	10/25
96	152.16	6.572	40.374	+4.066	08/20
97	152.18	6.571	40.372	+4.105	10/24
98	152.35	6.564	41.138	+4.081	09/03
99	152.47	6.559	41.613	+4.093	09/16
100	152.66	6.550	42.318	+4.100	10/30
101	152.66	6.550	42.486	+4.078	08/21
102	153.12	6.531	44.415	+4.077	09/11
103	153.14	6.530	44.446	+4.052	08/20
104	153.16	6.529	44.441	+4.068	10/25

[continued]

[Table 1; continued]

No.	T (°K)	$10^3/T$ ($°K^{-1}$)	P (Torr)	T $\ln(P'_H/P_D)$	Date
105	153.55	6.513	46.244	+4.062	09/03
106	153.67	6.508	46.622	+4.086	10/24
107	154.17	6.486	48.907	+4.058	10/25
108	154.36	6.478	49.939	+4.056	08/21
109	154.65	6.466	51.272	+4.077	09/11
110	154.77	6.461	51.919	+4.043	09/03
111	155.15	6.445	53.711	+4.047	10/25
112	155.15	6.445	53.830	+4.042	08/21
113	155.65	6.425	56.470	+4.070	09/08
114	155.94	6.413	57.947	+4.024	09/03
115	155.95	6.412	58.040	+4.062	09/16
116	156.16	6.404	59.009	+4.032	10/25
117	156.16	6.404	59.128	+4.024	08/21
118	157.12	6.365	64.579	+4.042	09/08
119	157.14	6.364	64.607	+4.009	09/03
120	157.16	6.363	64.668	+4.023	10/25
121	157.16	6.363	64.804	+4.009	08/21
122	157.24	6.360	65.183	+4.041	09/11
123	157.43	6.352	66.270	+4.022	10/30
124	157.62	6.344	67.661	+4.036	08/27
125	158.15	6.323	70.803	+3.994	08/21
126	158.17	6.322	70.916	+4.008	10/25
127	158.34	6.316	72.083	+3.987	09/03
128	158.67	6.302	74.251	+4.035	09/12
129	158.95	6.291	76.132	+4.018	09/08
130	159.15	6.283	77.481	+3.978	08/21

[continued]

[Table 1; continued]

No.	T (°K)	$10^3/T$ ($°K^{-1}$)	P (Torr)	T $\ln(P'_H/P_D)$	Date
131	159.23	6.280	77.870	+3.994	10/30
132	159.31	6.277	78.599	+3.997	08/27
133	159.54	6.268	80.177	+3.973	09/03
134	160.16	6.244	84.670	+4.003	09/12
135	160.19	6.243	84.785	+3.998	09/08
136	160.26	6.240	85.247	+3.975	10/30
137	160.74	6.221	89.042	+3.953	09/03
138	160.74	6.221	89.127	+3.977	08/27
139	161.55	6.190	95.287	+3.956	10/30
140	161.68	6.185	96.487	+3.972	09/12
141	161.70	6.184	96.633	+3.940	09/03
142	161.94	6.175	98.582	+3.937	09/03
143	162.07	6.170	99.763	+3.956	08/27
144	162.13	6.168	100.18	+3.944	10/26
145	162.64	6.149	104.63	+3.911	10/21
146	162.94	6.137	107.31	+3.920	09/03
147	163.12	6.131	108.98	+3.946	09/12
148	163.17	6.129	109.12	+3.921	10/26
149	163.26	6.125	110.15	+3.938	08/27
150	163.66	6.110	113.82	+3.898	10/20
151	163.95	6.100	116.49	+3.921	10/30
152	164.15	6.092	118.64	+3.902	09/04
153	164.36	6.084	120.67	+3.917	08/27
154	164.75	6.070	124.41	+3.900	10/26
155	164.75	6.070	124.58	+3.919	09/12
156	165.14	6.056	128.62	+3.920	09/09

[continued]

[Table 1; continued]

No.	T (°K)	$10^3/T$ ($°K^{-1}$)	P (Torr)	T $\ln(P'_H/P_D)$	Date
157	165.16	6.055	128.59	+3.887	10/21
158	165.36	6.048	130.78	+3.885	09/04
159	165.57	6.040	133.12	+3.900	08/27
160	165.86	6.029	136.14	+3.884	10/30
161	166.12	6.020	139.30	+3.907	09/16
162	166.15	6.019	139.39	+3.881	10/22
163	166.27	6.014	140.86	+3.894	09/12
164	166.56	6.004	144.01	+3.868	09/04
165	166.65	6.000	145.31	+3.888	09/09
166	166.75	5.997	146.03	+3.870	10/26
167	166.79	5.996	146.74	+3.881	08/27
168	167.14	5.983	150.76	+3.860	10/21
169	167.50	5.970	155.31	+3.858	09/04
170	167.76	5.961	158.53	+3.851	09/04
171	167.86	5.957	159.48	+3.870	09/12
172	167.97	5.954	161.06	+3.870	08/28
173	168.15	5.947	163.02	+3.849	10/26
174	168.73	5.927	170.70	+3.836	09/04
175	169.09	5.914	175.47	+3.849	09/09
176	169.14	5.912	176.10	+3.832	10/21
177	169.19	5.911	176.96	+3.843	08/28
178	169.45	5.901	180.40	+3.844	09/12
179	169.96	5.884	187.54	+3.816	09/04
180	170.36	5.870	193.42	+3.820	08/28
181	170.44	5.867	194.24	+3.815	10/26
182	171.04	5.847	203.57	+3.819	09/12

[continued]

[Table 1; continued]

No.	T (°K)	$10^3/T$ ($°K^{-1}$)	P (Torr)	T $\ln(P'_H/P_D)$	Date
183	171.14	5.843	205.16	+3.800	09/04
184	171.16	5.842	205.27	+3.808	10/21
185	171.55	5.829	211.46	+3.800	08/28
186	171.65	5.826	212.58	+3.798	10/26
187	172.18	5.808	221.24	+3.797	10/22
188	172.37	5.801	224.62	+3.779	09/04
189	172.76	5.788	231.08	+3.791	09/12
190	172.76	5.788	231.25	+3.782	08/28
191	172.85	5.785	232.60	+3.780	10/26
192	173.56	5.762	244.84	+3.762	09/04
193	173.94	5.749	252.02	+3.764	08/28
194	174.04	5.746	253.60	+3.770	09/09
195	174.16	5.742	255.53	+3.765	10/22
196	174.45	5.732	261.18	+3.763	09/12
197	174.64	5.726	264.29	+3.755	10/26
198	174.74	5.723	266.78	+3.745	09/04
199	175.15	5.709	274.60	+3.746	08/28
200	175.64	5.694	283.80	+3.741	10/26
201	175.66	5.693	284.40	+3.742	09/09
202	175.95	5.684	290.61	+3.728	09/04
203	176.14	5.677	294.46	+3.736	09/12
204	176.17	5.676	294.49	+3.740	10/22
205	176.36	5.670	298.74	+3.728	08/28
206	177.16	5.645	315.69	+3.710	09/04
207	177.53	5.633	323.66	+3.715	10/27
208	177.55	5.632	324.20	+3.713	08/28

[continued]

[Table 1; continued]

No.	T (°K)	$10^3/T$ ($°K^{-1}$)	P (Torr)	T $\ln(P'_H/P_D)$	Date
209	177.84	5.623	330.95	+3.710	09/12
210	178.13	5.614	337.45	+3.709	09/09
211	178.23	5.611	339.15	+3.707	10/22
212	178.44	5.604	344.60	+3.696	09/04
213	178.76	5.594	352.13	+3.695	08/28
214	179.54	5.570	371.16	+3.686	09/13
215	179.56	5.569	370.96	+3.686	10/27
216	179.61	5.568	372.98	+3.682	09/09
217	179.75	5.563	376.52	+3.674	09/04
218	179.95	5.557	381.21	+3.678	08/28
219	180.14	5.551	385.91	+3.681	10/22
220	180.94	5.527	406.58	+3.666	10/27
221	181.05	5.523	410.09	+3.655	09/04
222	181.13	5.521	412.32	+3.666	09/16
223	181.16	5.520	412.87	+3.661	08/28
224	181.25	5.517	415.32	+3.661	09/13
225	181.64	5.505	425.71	+3.668	10/22
226	181.67	5.505	427.08	+3.653	09/09
227	182.30	5.486	444.18	+3.647	10/27
228	182.35	5.484	445.91	+3.637	09/05
229	182.35	5.484	445.98	+3.643	08/28
230	182.95	5.466	463.59	+3.636	09/13
231	183.56	5.448	481.78	+3.627	08/28
232	183.63	5.446	484.25	+3.621	09/05
233	183.64	5.445	484.05	+3.641	10/23
234	184.13	5.431	499.66	+3.620	09/09

[continued]

[Table 1; continued]

No.	T (°K)	$10^3/T$ ($°K^{-1}$)	P (Torr)	T $\ln(P'_H/P_D)$	Date
235	184.58	5.418	512.83	+3.595	10/31
236	184.64	5.416	515.66	+3.611	09/13
237	184.75	5.413	519.55	+3.612	08/28
238	184.97	5.406	526.37	+3.608	09/05
239	185.21	5.399	534.05	+3.615	10/27
240	185.62	5.387	547.73	+3.611	10/23
241	185.94	5.378	558.75	+3.597	08/28
242	186.06	5.375	562.51	+3.601	10/27
243	186.26	5.369	569.64	+3.587	09/05
244	186.35	5.366	572.95	+3.589	09/13
245	187.13	5.344	601.00	+3.579	09/16
246	187.14	5.344	601.28	+3.576	09/09
247	187.14	5.344	601.34	+3.579	08/29
248	187.54	5.332	616.16	+3.570	09/05
249	187.63	5.330	618.52	+3.581	10/23
250	188.13	5.316	638.23	+3.564	09/13
251	188.35	5.309	646.25	+3.560	08/29
252	188.62	5.302	656.53	+3.565	10/27
253	188.86	5.295	666.32	+3.549	09/05
254	189.22	5.285	680.81	+3.555	10/27
255	189.65	5.273	698.61	+3.537	09/10
256	189.66	5.273	698.02	+3.550	10/23
257	189.93	5.265	709.63	+3.536	09/13
258	190.15	5.259	719.08	+3.529	09/05
259	190.54	5.248	735.06	+3.526	10/31
260	191.15	5.232	762.86	+3.516	09/16

[continued]

[Table 1; continued]

No.	T (°K)	$10^3/T$ ($°K^{-1}$)	P (Torr)	T $\ln(P'_H/P_D)$	Date
261	191.24	5.229	766.14	+3.529	10/27
262	191.44	5.224	775.41	+3.509	09/05
263	191.63	5.218	783.28	+3.509	10/23
264	191.67	5.217	785.74	+3.511	09/13
265	192.05	5.207	802.20	+3.514	10/27
266	192.15	5.204	807.74	+3.501	09/10
267	193.02	5.181	847.59	+3.489	10/31
268	193.12	5.178	853.16	+3.489	09/05
269	193.14	5.178	853.41	+3.491	09/16
270	193.63	5.164	875.88	+3.475	10/23
271	194.24	5.148	906.83	+3.492	10/27
272	194.63	5.138	927.92	+3.470	09/10
273	195.12	5.125	952.43	+3.474	10/27
274	195.12	5.125	953.20	+3.464	09/05
275	195.14	5.124	953.96	+3.464	09/16
276	195.65	5.111	980.03	+3.432	10/23
277	196.02	5.101	1000.9	+3.433	10/31
278	197.05	5.075	1056.9	+3.432	10/27
279	197.12	5.073	1063.4	+3.441	09/10
280	197.15	5.072	1063.8	+3.437	09/16
281	197.15	5.072	1064.1	+3.440	09/05
282	197.66	5.059	1091.8	+3.412	10/23
283	198.10	5.048	1118.5	+3.408	10/31
284	198.64	5.034	1150.5	+3.418	10/27
285	199.15	5.021	1183.8	+3.416	09/05
286	199.61	5.010	1210.9	+3.378	10/23

[continued]

[Table 1; continued]

No.	T (°K)	$10^3/T$ ($°K^{-1}$)	P (Torr)	T $\ln(P'_H/P_D)$	Date
287	199.66	5.008	1215.0	+3.386	10/31
288	200.15	4.996	1247.2	+3.407	09/10
289	201.15	4.971	1313.6	+3.392	09/05
290	203.14	4.923	1452.6	+3.385	09/16
291	203.17	4.922	1455.6	+3.357	09/05
292	205.14	4.875	1607.6	+3.324	09/16
293	207.13	4.828	1770.6	+3.271	09/16
294	212.16	4.713	2237.2	+3.179	09/16

Table 2: Carbon Vapor Pressure Isotope Effects in Fluoroform

No.	T (°K)	$10^3/T$ ($°K^{-1}$)	P (Torr)	T $\ln(P'_{12}/P_{13})$	Date
1	133.71	7.479	4.8871	-0.6646	10/28
2	134.69	7.424	5.5502	-0.6732	10/23
3	135.17	7.398	5.9221	-0.6742	10/28
4	135.72	7.368	6.3596	-0.6664	10/29
5	136.17	7.344	6.7179	-0.6576	10/23
6	136.64	7.319	7.1478	-0.6642	10/28
7	137.04	7.297	7.5106	-0.6417	10/29
8	137.66	7.265	8.1112	-0.6544	10/23
9	138.06	7.243	8.5472	-0.6459	10/29
10	139.06	7.191	9.6494	-0.6444	10/29
11	139.18	7.185	9.7927	-0.6461	10/23
12	139.75	7.156	10.496	-0.6510	10/29
13	140.43	7.121	11.386	-0.6500	10/29
14	141.27	7.079	12.570	-0.6449	10/29
15	142.05	7.040	13.761	-0.6313	10/29
16	143.02	6.992	15.327	-0.6174	10/24
17	143.24	6.981	15.723	-0.6324	10/29
18	144.64	6.914	18.343	-0.6404	10/24
19	144.95	6.899	19.023	-0.6227	10/30
20	145.76	6.861	20.773	-0.6312	10/30
21	146.14	6.843	21.662	-0.6366	10/24
22	146.64	6.819	22.883	-0.6302	10/30
23	147.65	6.773	25.484	-0.6246	10/24
24	148.56	6.731	28.032	-0.6102	10/30
25	149.16	6.704	29.796	-0.6246	10/24
26	149.94	6.670	32.274	-0.6134	10/30

[continued]

[Table 2; continued]

No.	T (°K)	$10^3/T$ ($°K^{-1}$)	P (Torr)	T $\ln(P'_{12}/P_{13})$	Date
27	150.65	6.638	34.661	-0.6160	10/24
28	151.13	6.617	36.375	-0.6061	10/25
29	151.94	6.581	39.452	-0.6126	10/25
30	152.18	6.571	40.372	-0.6089	10/24
31	152.66	6.550	42.318	-0.6028	10/30
32	153.16	6.529	44.441	-0.6026	10/25
33	153.67	6.508	46.622	-0.6070	10/24
34	154.17	6.486	48.907	-0.6000	10/25
35	155.15	6.445	53.711	-0.5947	10/25
36	156.16	6.404	59.009	-0.5901	10/25
37	157.16	6.363	64.668	-0.5859	10/25
38	157.43	6.352	66.270	-0.5944	10/30
39	158.17	6.322	70.916	-0.5828	10/25
40	159.23	6.280	77.870	-0.5906	10/30
41	160.26	6.240	85.247	-0.5926	10/30
42	160.61	6.226	87.963	-0.5752	10/21
43	161.55	6.190	95.287	-0.5852	10/30
44	162.13	6.168	100.18	-0.5716	10/26
45	162.64	6.149	104.63	-0.5764	10/21
46	163.17	6.129	109.12	-0.5716	10/26
47	163.95	6.100	116.49	-0.5752	10/30
48	164.75	6.070	124.41	-0.5649	10/26
49	165.16	6.055	128.59	-0.5687	10/21
50	165.86	6.029	136.14	-0.5737	10/30
51	166.75	5.997	146.03	-0.5593	10/26
52	167.14	5.983	150.76	-0.5592	10/21

[continued]

[Table 2; continued]

No.	T (°K)	$10^3/T$ ($°K^{-1}$)	P (Torr)	T $\ln(P'_{12}/P_{13})$	Date
53	168.15	5.947	163.02	-0.5580	10/26
54	169.14	5.912	176.10	-0.5578	10/21
55	170.44	5.867	194.24	-0.5511	10/26
56	171.16	5.842	205.27	-0.5522	10/21
57	171.65	5.826	212.58	-0.5492	10/26
58	172.18	5.808	221.24	-0.5608	10/22
59	172.85	5.785	232.60	-0.5476	10/26
60	174.16	5.742	255.53	-0.5551	10/22
61	174.64	5.726	264.29	-0.5428	10/26
62	175.64	5.694	283.80	-0.5419	10/26
63	176.17	5.676	294.49	-0.5485	10/22
64	177.53	5.633	323.66	-0.5370	10/27
65	178.23	5.611	339.15	-0.5470	10/22
66	179.56	5.569	370.96	-0.5329	10/27
67	180.14	5.551	385.91	-0.5417	10/22
68	180.94	5.527	406.58	-0.5310	10/27
69	181.64	5.505	425.71	-0.5223	10/22
70	182.30	5.486	444.18	-0.5283	10/27
71	183.64	5.445	484.05	-0.5203	10/23
72	184.58	5.418	512.83	-0.5244	10/31
73	185.21	5.399	534.05	-0.5197	10/27
74	185.62	5.387	547.73	-0.5206	10/23
75	186.06	5.375	562.51	-0.5218	10/27
76	187.63	5.330	618.52	-0.5161	10/23
77	188.62	5.302	656.53	-0.5140	10/27
78	189.22	5.285	680.81	-0.5140	10/27

[continued]

[Table 2; continued]

No.	T (°K)	$10^3/T$ ($°K^{-1}$)	P (Torr)	T $\ln(P'_{12}/P_{13})$	Date
79	189.66	5.273	698.02	-0.5155	10/23
80	190.54	5.248	735.06	-0.5104	10/31
81	191.24	5.229	766.14	-0.5050	10/27
82	192.05	5.207	802.20	-0.5064	10/27
83	193.02	5.181	847.59	-0.5057	10/31
84	194.24	5.148	906.83	-0.4955	10/27
85	195.12	5.125	952.43	-0.4961	10/27
86	196.02	5.101	1000.9	-0.5054	10/31
87	197.05	5.075	1056.9	-0.4977	10/27
88	198.10	5.048	1118.5	-0.4914	10/31
89	198.64	5.034	1150.5	-0.4916	10/27
90	199.66	5.008	1215.0	-0.4824	10/31

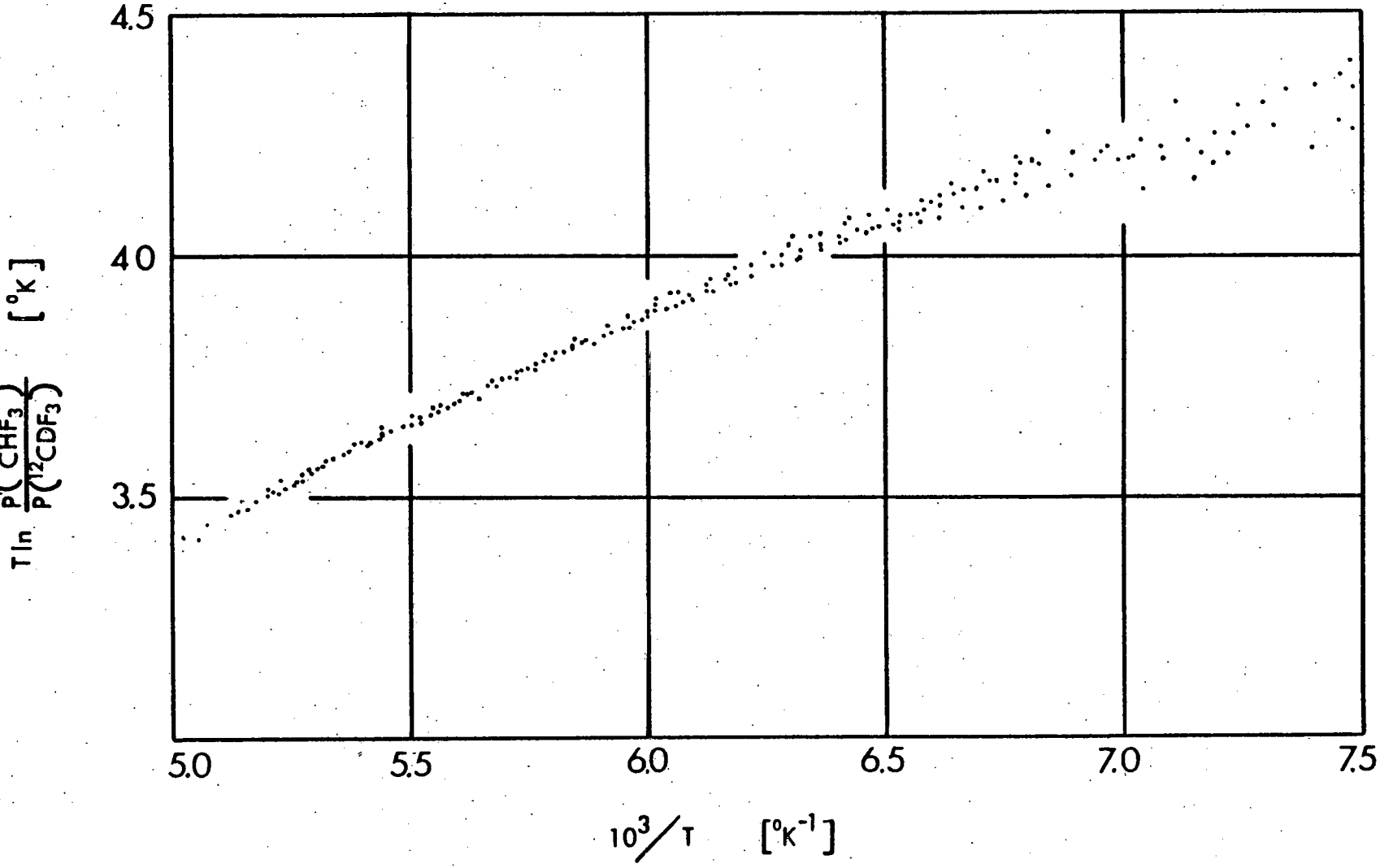

Figure 3. D/H Vapor Pressure Isotope Effect in Fluoroform

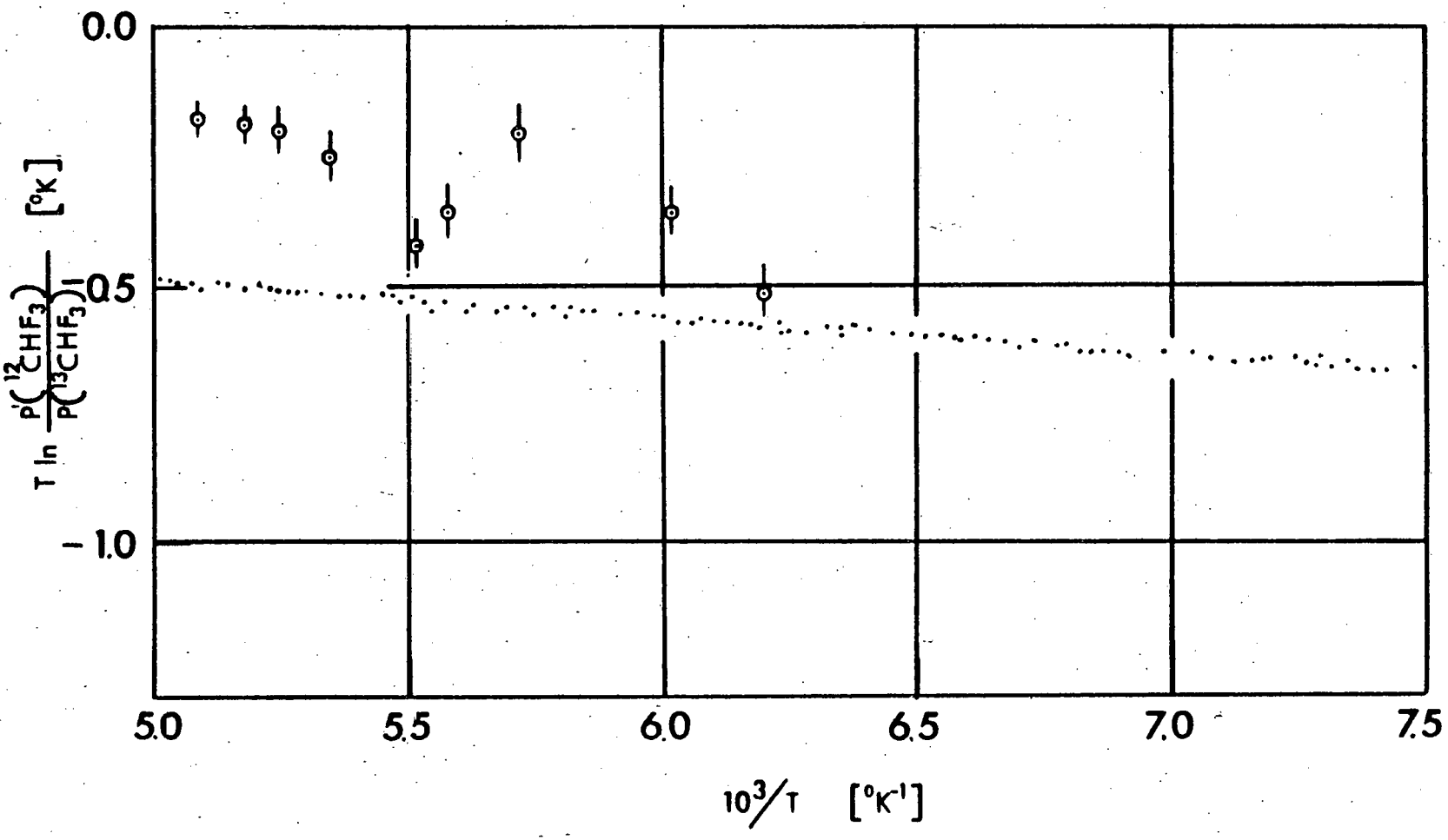

Figure 4. $^{13}C/^{12}C$ Vapor Pressure Isotope Effect in Fluoroform

$$A = -72.21 \pm 0.85$$
$$B = -0.1313 \pm 0.0053 \qquad (6)$$

and, for the D/H-effect,

$$A = 389.2 \pm 4.4 \quad (°K^2)$$
$$B = 1.511 \pm 0.028 \quad (°K) \qquad (7)$$

(A-2-b) Discussion:

It is noted in Figure 4 that the plot is now much less steep than the corresponding plot of last year, a consequence of removal of the newly found chemical impurity in the $^{13}CHF_3$ sample. In Figure 4 we also included the data obtained by Borodinsky, Wieck, Mayfield, and Ishida.[5] They compare well with the present data, especially in view of the fact that their data were obtained by the much less precise method of cryogenic distillation of fluoroform of natural isotopic composition.

However, the force constant matrix, $\underset{\sim}{F}$, of liquid fluoroform they published leads to an inverse VPIE not only for the $^{13}C/^{12}C$-effect but also for the H/D-effect, the fact that Boroduisky et al. did not have a means for checking because they measured only the $^{13}C/^{12}C$-effect. We are in the process of fitting a liquid $\underset{\sim}{F}$-matrix which would reproduce (i) the observed frequencies[6,7] of liquid $^{12}CHF_3$ and (ii) the D/H- and $^{13}C/^{12}C$- VPIE of Figures 3 and 4.

Although we have not finalized the liquid $\underset{\sim}{F}$-matrix, it seems that the VPIE data we have obtained for fluoroform will support the following conclusions: (i) The normal VPIE with the positive slope for the D/H-effect and the inverse VPIE with the negative slope for the $^{13}C/^{12}C$-effect can be simultaneously explained only by a blue-shift of the C-H stretching frequency of fluoroform upon condensation. (ii) We will have to employ large external-internal interaction force constants to reproduce both observed D/H-VPIE and $^{13}C/^{12}C$-VPIE. Such extensive interactions seem to be in agreement with specific, short-range intermolecular interactions such as the hydrogen bonding between the molecules of fluoroform. In the following we will summarize the reasons for these tentative conclusions.

Figure 3 shows for the D-for-H substitution a normal vapor pressure

isotope effect at all temperatures we investigated and a positive slope of the plot of T ln P'/P vs 1/T. On the other hand, Figure 4 shows for the ^{13}C-for-^{12}C substitution an inverse VPIE at all temperatures and a negative slope in the plot. How is this marked difference between two substitutions possible? In both substitutions the molecular symmetry does not change (C_{3v}). The molecular mass increases by the similar amount (by 1 amu) in both cases, so that the translational contributions to the overall T ln(P'/P), contained in the A/T-term of Eq. (6), is similar for both cases. The change in the principal moments of inertia in the D/H-substitution is somewhat greater for the D/H substitution than for the $^{13}C/^{12}C$ substitution, because the latter substitution is made near the center of mass of the molecule. However, the magnitude of the change even in the former is not large, because the fluoroform has three heavy (F) atoms at the peripheral positions. Thus, the rotational contribution to T ln(P'/P) would not be so different between the two isotopic substitutions.

Vibrational contributions to T ln(P'/P) may be expressed as a sum of 3N-6 independent contributions. In the form of Eq. (5) the vibrational contributions appear as the constant B-term, which corresponds to the zero-point energy approximation for the contribution: When the temperature is not sufficiently high ($h\nu_i >> kT$), the vibrational excited states are not accessible and they do not contribute appreciably to the partition functions. These contributions to T ln(P'/P) are depicted in Figure 5. It is noted that the internal vibrations usually red-shift upon condensation and only in rare occasions does a vibrational frequency blue-shift upon condensation. When it does, an analysis of the functional form of the reduced partition function ratio shows that such an internal vibration contributes positively to ln(P'/P). As the Boltzmann excitation sets in with an increasing temperature, the magnitude of vibrational contribution starts to decrease toward zero.

With these trends shown in Figure 5 in mind, the marked difference observed between the D/H-VPIE and the $^{13}C/^{12}C$-VPIE is explanable as follows. The isotope shift of the C-H stretching frequency in fluoroform is very large in the D-for-H substitution, while it is small for the ^{13}C-for-^{12}C substitution. If the C-H stretching frequency red-shifts upon

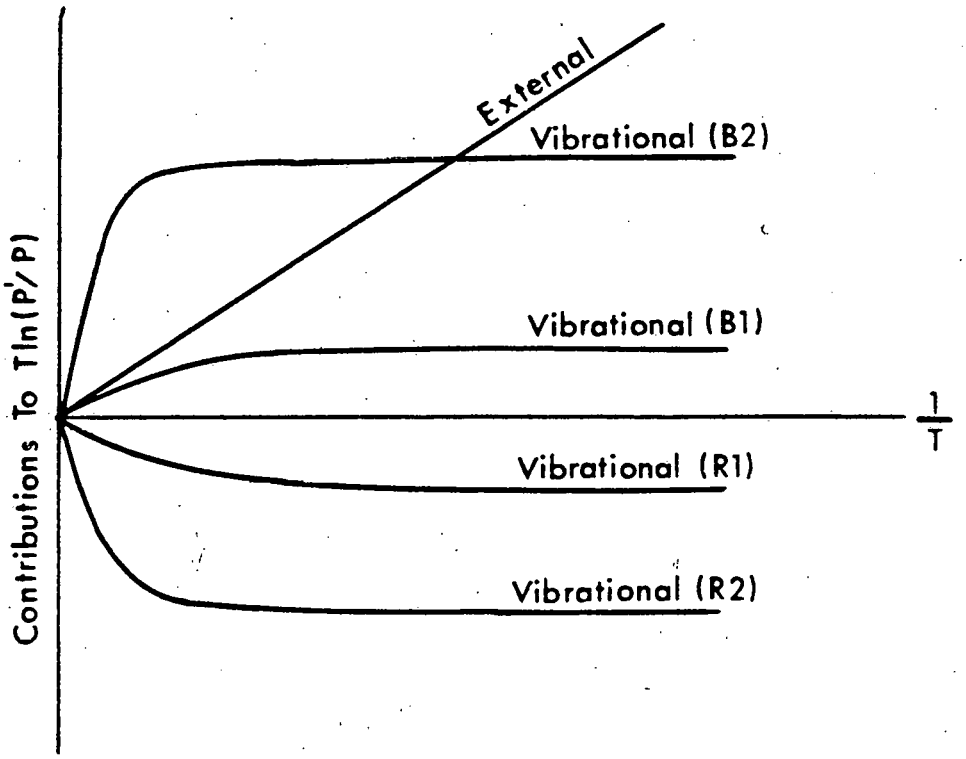

Figure 5: Schematic Plots of Various Contributions to T ln(P'/P).

Vibrational R1: Frequencies that red-shift upon condensation, Low frequency and/or small isotope shift.

Vibrational R2: Frequencies that red-shift upon condensation, High frequency and/or large isotope shift.

Vibrational B1: Frequencies that blue-shift upon condensation, Low frequency and/or small isotope shift.

Vibrational B2: Frequencies that blue-shift upon condensation, High frequencies and/or large isotope shift.

condensation, its contribution to T ln(P'/P) is that of the R2-line of Figure 5 for D/H and that of the R1-line of Figure 5 for $^{13}C/^{12}C$. Since all the other vibrational frequencies red-shift upon condensation, the sum of the "External" line and all the red-shift lines should yield a plot for the D/H-substitution which would lie below (more inverse than) the corresponding plot for the $^{13}C/^{12}C$-substitution. Figures 3 and 4 show otherwise. The normal VPIE with a positive slope for the D/H-effect is possible only if the contribution of the C-H stretching motion looks like the B1 or B2 line of Figure 5. Thus, for the D/H-substitution, the C-H stretching contribution is like that of the B2-line, while for the $^{13}C/^{12}C$-effect, the contribution is that of the B1-line. The sum of the "External" line and B2-line thus yields a straight line with the positive slope in the positive VPIE-region when the temperatures are not sufficiently high for the Boltzmann excitation to set in for the C-H stretching mode. On the other hand, since the isotope shift upon ^{13}C-for-^{12}C substitution is so small (10 cm^{-1} for $^{13}C/^{12}C$, as compared to 780 cm^{-1} for D/H), the magnitude of its contribution to T ln(P'/P) is very small (B1-line), resulting in the negative VPIE largely due to the effects of other red-shifting frequencies.

Thus, we feel our VPIE data support the blue-shifting of the C-H stretching frequency upon condensation. A blue-shift had in fact been reported by Glockler[6] and Rank[7]: In liquid CHF_3 at -95°C it is 3062 cm^{-1}, while the gas value for CHF_3 is 3035[10] or 3031.[11,12]

The next question is: What type of interaction is responsible for the blue-shift? We had explored[3] the possibility of hydrogen-bonding by carrying out a molecular orbital study using Gaussian-70 program with the STO-3G basis set of functions. We then found several dimer configurations of fluoroform which exhibited a small stabilization energy. One of such stable configurations (called DT-A in Reference 3) and the energy plot of the DT-A configuration as a function of H_1-F_{21} distance are reproduced in Figures 6 and 7, respectively.

Thus, the DT-A dimer configuration shows a stabilization energy of -0.72 kcal/mole dimer (or -0.36 kcal/mole monomer) with the equilibrium H···F distance of 2.34 Å, corresponding to the carbon-to-carbon intermolecular separation of 4.83 Å. These are in fair agreement with a

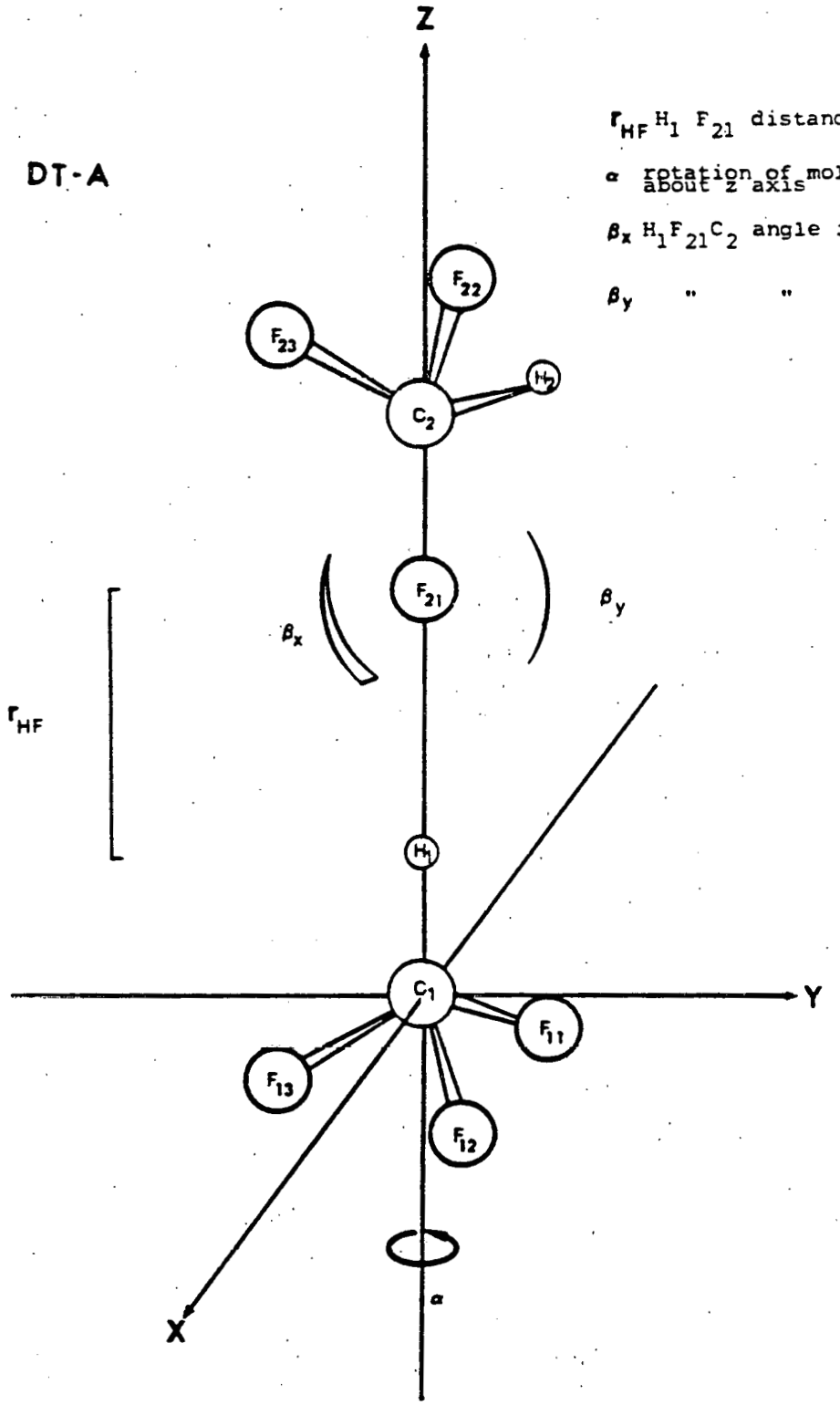

Figure 6. DT-A Configuration of Fluoroform Dimer

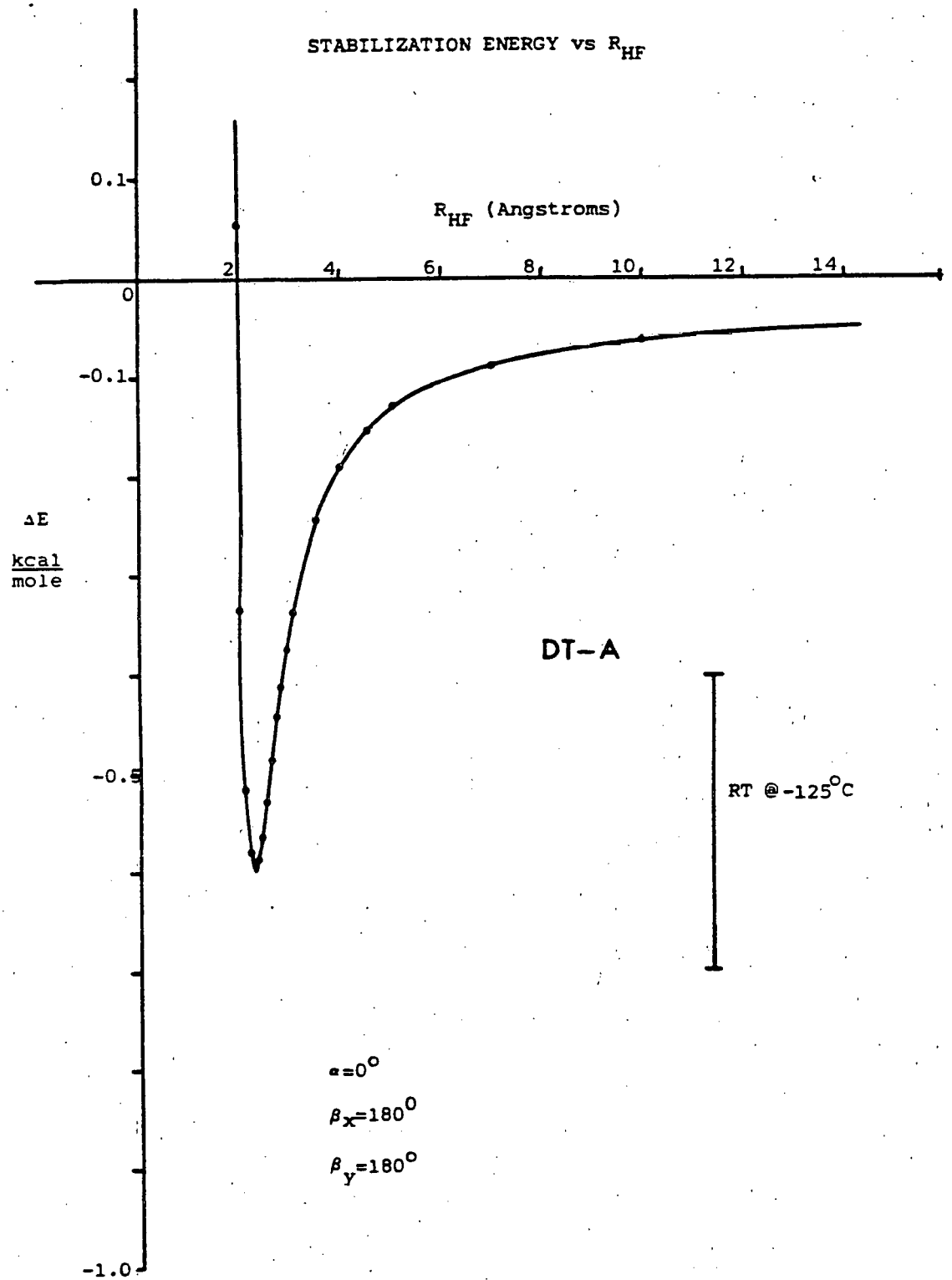

Figure 7. Stabilization Energy vs R_{HF} for DT-A Configuration of Fluoroform Dimer

published[8] Lennard-Jones' 12-6 potential constants ϵ = 0.391 kcal/mole and σ = 4.26 Å, the latter being obtained from the second virial coefficient of gaseous CHF_3. These equilibrium intermolecular separations are also in surprisingly good agreement with the molecular volume data: At -95°C (178°K), the molar volume of liquid fluoroform[9] is 25.33 ml/mole, the corresponding diameter of a molecular sphere being 4.314 Å.

A hydrogen bond with an energy of the order of 0.4 kcal/mole is a very weak one compared to bona-fide hydrogen bonds having the bond energies of the order of 5 ∿ 20 kcal/mole. The fact that the liquid molecular volume data gives the average intermolecular separation (4.31 Å) which is similar to the equilibrium distance (4.83 Å) obtained by our M.O. calculation indicates that on the average the intermolecular forces of the magnitudes similar to that of our "hydrogen bond" are acting between every pair of molecules in the liquid. This is so in spite of the fact that any CHF_3 molecule can contribute only one hydrogen to the hydrogen bonding. Such an extra interaction could be the London dispersion force in its nature. This is possible in view of the fact that we at least did not account for it when we computed the energy surface such as Figure 7 because, in the calculation, we held the internal structure of both molecules rigid.

A question was then raised: Can a hydrogen bonding account for the blue-shift in the C-H stretching frequency upon condensation? As far as we can find, the literature on hydrogen bonding contains not a single instance of blue-shift of X-H stretching frequency upon formation of a X-H····Y bond: The X-H stretching frequency always red-shifts upon a hydrogen bond formation. The explanation is that the formation of a hydrogen bond necessarily modifies the electronic charge distribution around the X-H bond, making it less stiff. But, then, the literatures on hydrogen bonding concern themselves with bona fide hydrogen bonds and sometimes even regard a bond energy of 5 kcal/mole marginal in order to qualify to be a hydrogen bond. If a "hydrogen bond" is as weak (∿0.4 kcal/mole monomer) as in our CHF_3, could it be that the shift in electronic distribution around the X-H bond upon formation of the C-H····F bond is so small that other effects, such as an effect of the new H····F

bond on the C-H stretching frequency, more than just compensate for the weakening of the C-H bond?

Chloroform, an accepted and well studied proton donor, undergoes no shift of its C-H stretching frequency[13] when dissolved in such electron donor solvents as ketones and nitriles. In CCl_4 solutions of strong proton acceptors such as pyridine-d_5 and dimethyl sulfoxide-d_6, the spectral shifts were found[14] to be in the order $CHBr_3 > CHI_3 > CHCl_3$, with fluoroform exhibiting inconclusive results. This is not so surprising, because there are abundant evidence in the literature of the fact that the role of bond polarity in the hydrogen bond strength is not a major one.

In the simplest model of hydrogen bonding one would assume that carbon and fluorine atoms are infinitely heavy and can be simulated by two solid walls. In this model the potential energy and the kinetic

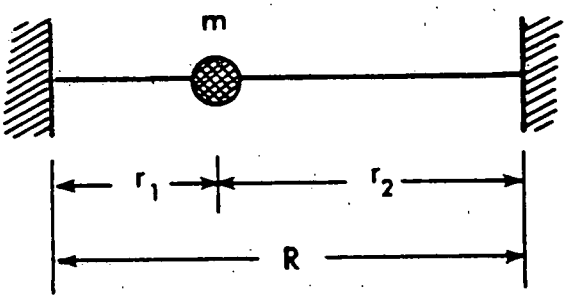

energy are given by

$$2V = f_1 (r_1-r_{10})^2 + f_2 (r_2-r_{20})^2$$

$$= f_1 (\Delta r_1)^2 + f_2 (\Delta R-\Delta r_1)^2$$

$$= (f_1+f_2) (\Delta r_1)^2 - 2f_2 \Delta R\Delta r_1 + f_2(\Delta R)^2 , \qquad (8)$$

and

$$2T = m(\Delta \dot{r}_1)^2 + M(\Delta \dot{R})^2 , \qquad (9)$$

where f_1 and f_2 are the harmonic force constants, r_{10} and r_{20} are the equilibrium distances, $\Delta r_1=r_1-r_{10}$, $\Delta R_2=R_2-R_{20}$, and $\Delta R=R-R_e$, R_e being equal to $r_{10}+r_{20}$, and M is a certain reduced mass of the two-wall system.

The eigenvalues of this two-dimensional problem are:

$$\lambda_{\pm} = \frac{1}{2mM} \left\{ [M(f_1+f_2)+mf_2] \pm \sqrt{[M(f_1+f_2)+mf_2]^2-4mMf_1f_2} \right\} \qquad (10)$$

λ_+ of Eq. (10) corresponds to the C-H stretching frequency, and it can be approximated by

$$\frac{\lambda_+}{\lambda_o} = \frac{[1+(1+\frac{m}{M})\frac{f_2}{f_1}]^2 - \frac{m}{M}\frac{f_2}{f_1}}{1+(1+\frac{m}{M})\frac{f_2}{f_1}} , \qquad (11)$$

where $\lambda_o = f_1/m$, the eigenvalue of a free C-H stretching motion. When f_2 tends to zero, Eq. (11) reduces to

$$\frac{\lambda_+}{\lambda_o} = 1 \quad , \qquad (12)$$

as it should. When M tends to infinity, Eq. (11) reduces to

$$\frac{\lambda_+}{\lambda_o} = \frac{f_1+f_2}{f_1} \quad , \qquad (13)$$

which implies a blue-shift of the C-H stretching frequency, unless the value of f_1 in the numerator becomes smaller than the f_1 value in the denominator. Apparently for bona fide hydrogen bonds, f_1 in the H-bonded configuration which we might call f_1' is so small compared to the f_1-value of a free C-H configuration that the relation,

$$f_1' + f_2 < f_1 \quad , \qquad (14)$$

is satisfied, thus leading to the red-shift. A further analysis of the quantity λ_+/λ_o given by Eq. (11) as a function of two ratios, m/M and f_2/f_1, has proved that λ_+ is always greater than λ_o as long as f_2 is positive. Therefore, the condition, $f_1'<f_1$, is the necessary condition for the red-shift under all circumstances. The minimum value of the decrease in f_1 that one should have for the red-shifting depends on the ratios m/M and f_2/f_1 and can be obtained by solving a simultaneous equation consisting of Eq. (11) and

$$\frac{\lambda_+}{\lambda_o} = \frac{f_1}{f_1'} \quad .$$

If this minimum decrease in f_1 is not met, the frequency will blue-shift.

The more sophisticated models of hydrogen bond lead to the qualitatively same conclusion. We have tried two additional harmonic oscillator models. One consists of two masses, m_H and m_F, oscillating between two walls. This model corresponds to a rigid intermolecular separation. The other model is a linear triatomic model with the center of its mass kept stationary. In the last model we examined the effect of an off-diagonal $\underset{\sim}{F}$-matrix element:

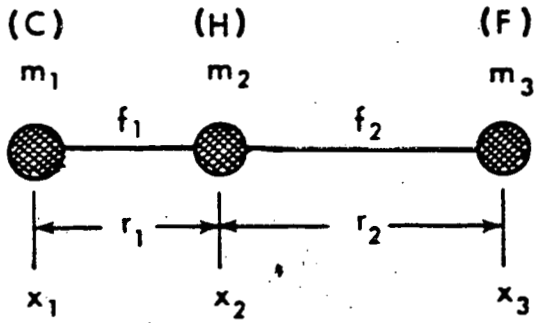

$$2V = f_1(x_2-x_1-r_{10})^2 + f_2(x_3-x_2-r_{20})^2 + 2f_{12}(x_2-x_1-r_{10})(x_3-x_2-r_{20})$$

and $2T = m_1\dot{x}_1^2 + m_2\dot{x}_2^2 + m_3\dot{x}_3^2$

The standard transformation to the internal coordinate system yielded

$$2V = f_1(\Delta r_1)^2 + f_2(\Delta r_2)^2 + 2f_{12}(\Delta r_1)(\Delta r_2) \quad , \tag{15}$$

$$2T = \mu_{1-23}(\Delta\dot{r}_1)^2 + \mu_{3-12}(\Delta\dot{r}_2)^2 + 2\frac{m_1m_3}{M}(\Delta\dot{r}_1)(\Delta\dot{r}_2) \quad , \tag{16}$$

where $\frac{1}{\mu_{1-23}} = \frac{1}{m_1} + \frac{1}{m_2+m_3}$,

and $\frac{1}{\mu_{3-12}} = \frac{1}{m_3} + \frac{1}{m_1+m_2}$.

One of the roots of this secular problem λ_+ can be approximated by

$$\frac{\lambda_+}{\lambda_o} = (1 + \frac{f_2-2f_{12}}{f_1})(1 - \frac{m_2}{m_1})(1 - x) \quad , \tag{17}$$

where

$$\lambda_o = \frac{f_1}{\mu_{12}} = \frac{f_1(m_1+m_2)}{m_1 m_2} \quad ,$$

$$x = \frac{2m_2(m_1+m_3)}{m_1 m_3} \; \frac{(f_1 f_2 - f_{12})^2}{(f_1+f_2-2f_{12})^2} \quad .$$

Eq. (17) reduces to Eq. (13) when $f_{12} = 0$, $m_2 << m_1$ and $m_2 << m_3$. In the limit of heavy m_1 and m_3,

$$\frac{\lambda_+}{\lambda_o} = \frac{f_1+f_2-2f_{12}}{f_1} \quad , \tag{18}$$

which clearly shows the role of off-diagonal force constant between the "internal" motion, which is the C-H stretching motion, and the "external" motion represented by the distance between m_2(H) atom and m_3(F) atom. A positive f_{12} tends to give a red shift, while a negative f_{12} tends to lead to a blue shift. Numerical restriction on the absolute magnitude of f_{12} in a stable configuration is given by $f_{12} < (f_1 f_2)^{1/2}$. Since $f_1 >> f_2$, $|f_{12}|$ may be bigger than f_2 and thus become more important than f_2 in its role in the blue-shift/red-shift argument. The possibility of $|f_{12}| > f_2$ has been demonstrated by Borodinsky et al[4] in their $\underset{\sim}{F}$-matrix for the liquid fluoroform.

We are in the process of obtaining a liquid $\underset{\sim}{F}$-matrix that contain rather large external-internal interaction force constants and which reproduces the observed D/H- and $^{13}C/^{12}C$- isotope effects as well as the observed frequencies of liquid $^{12}CHF_3$.

(A-3) Vapor Pressure Isotope Effects in Methyl Fluoride

by Takao Oi and Jan Shulman

The synthesis and purificiation of $^{13}CH_3F$, $^{12}CD_3F$, and $^{12}CH_3F$ have been reported in previous years.[1,2] This year, the re-constructed and re-calibrated cryostat has been used to obtain data on the vapor pressure isotope effects in these methyl fluoride samples. Results of chemical analyses of these samples are summarized below:

Table 3: Chemical Analyses of Methyl Fluorides

Impurities	$^{12}CH_3F$	$^{12}CD_3F$	$^{13}CH_3F$
carbon dioxide	<10 ppm	< 5 ppm	<10 ppm
water	< 5 ppm	ND	ND
others	ND*	CD_3Cl<10 ppm	$^{13}CH_3Cl$<10 ppm x <15 ppm

* None detectable, i.e., < 1 ppm.

The $^{12}CH_3F$ was used as a reference gas for the capacitance gauges. The measurements have been carried out between temperatures 132.52°K (= ∿ 140.63°C, P = 3.712 torr) and 213.12°K (= ∿ 60.03°C, P = 1887.1 torr). The results have been summarized in Table 4 and Figure 8 for the $^{12}CD_3F/^{12}CH_3F$-effect and in Table 5 and Figure 9 for the $^{13}CH_3F/^{12}CH_3F$.

These results have been least-squares fitted to the functional form of Eq. (3) which yielded, for the $^{13}C/^{12}C$-effect,

$$\begin{aligned} A &= 11.21 \pm 15.58 \quad (°K^2)\,, \\ B &= -0.0481 \pm 0.1906 \quad (°K)\,, \\ \text{and} \quad C &= -0.00160 \pm 0.00057\,, \end{aligned} \tag{19}$$

and, for the D/H-effect,

$$\begin{aligned} A &= 1954.1 \pm 39.0 \quad (°K^2)\,, \\ B &= -2.451 \pm 0.472 \quad (°K)\,, \\ \text{and} \quad C &= -0.00211 \pm 0.00140\,. \end{aligned} \tag{20}$$

Table 4: Hydrogen Vapor Pressure Isotope Effects in Methyl Fluoride

No.	T (°K)	$10^3/T$ ($°K^{-1}$)	P (Torr)	T $\ln(P'_H/P_D)$	Date
1	132.52	7.546	3.7118	+12.162	10/06
2	133.25	7.505	4.0852	+11.971	10/06
3	133.63	7.483	4.3139	+12.088	10/13
4	133.63	7.483	4.3276	+12.045	10/13
5	133.87	7.470	4.4602	+11.937	10/13
6	133.88	7.470	4.4587	+11.988	10/13
7	134.03	7.461	4.5288	+11.866	10/06
8	134.06	7.460	4.5654	+11.919	10/13
9	134.81	7.418	4.9877	+11.641	10/06
10	135.33	7.389	5.3230	+11.685	10/06
11	135.74	7.367	5.6081	+11.596	10/06
12	136.26	7.339	5.9877	+11.566	10/06
13	136.85	7.307	6.4587	+11.598	10/14
14	137.06	7.296	6.6051	+11.505	10/07
15	137.70	7.262	7.1737	+11.484	10/14
16	137.97	7.248	7.3917	+11.410	10/07
17	138.06	7.243	7.4923	+11.434	09/29
18	138.08	7.242	7.5091	+11.325	10/10
19	138.16	7.238	7.5685	+11.318	10/10
20	138.27	7.232	7.6783	+11.292	10/10
21	138.44	7.223	7.8460	+11.360	10/14
22	138.44	7.223	7.8505	+11.403	10/14
23	138.84	7.202	8.2012	+11.344	10/07
24	139.13	7.188	8.5030	+11.287	09/29
25	139.37	7.175	8.7332	+11.283	10/07
26	139.75	7.156	9.1585	+11.225	09/29

[continued]

[Table 4; continued]

No.	T (°K)	$10^3/T$ ($°K^{-1}$)	P (Torr)	T $\ln(P'_H/P_D)$	Date
27	140.13	7.137	9.5884	+11.153	09/29
28	140.36	7.124	9.8339	+11.151	10/07
29	140.74	7.105	10.294	+11.105	09/30
30	141.36	7.074	11.018	+11.056	10/07
31	141.74	7.055	11.537	+11.010	09/30
32	142.36	7.025	12.310	+10.906	10/07
33	142.36	7.025	12.326	+10.958	10/07
34	142.64	7.010	12.706	+10.904	10/07
35	142.74	7.006	12.874	+10.922	09/30
36	143.16	6.985	13.487	+10.849	10/15
37	143.64	6.962	14.193	+10.805	10/07
38	143.72	6.958	14.350	+10.833	09/30
39	144.14	6.938	14.998	+10.698	10/16
40	144.26	6.932	15.185	+10.693	10/16
41	144.76	6.908	16.010	+10.702	10/07
42	144.76	6.908	16.043	+10.737	09/30
43	145.35	6.880	17.045	+10.600	10/16
44	145.86	6.856	18.015	+10.649	09/30
45	145.87	6.855	18.021	+10.594	10/07
46	146.41	6.830	19.068	+10.510	10/16
47	146.53	6.825	19.283	+10.530	10/16
48	146.94	6.805	20.163	+10.561	09/30
49	146.96	6.805	20.169	+10.505	10/07
50	147.55	6.777	21.464	+10.424	10/16
51	148.05	6.754	22.618	+10.404	10/07
52	148.05	6.754	22.633	+10.445	09/30

[continued]

[Table 4; continued]

No.	T (°K)	$10^3/T$ ($°K^{-1}$)	P (Torr)	T $\ln(P'_H/P_D)$	Date
53	148.62	6.728	23.982	+10.427	10/01
54	149.15	6.705	25.304	+10.347	09/30
55	149.72	6.679	26.831	+10.299	10/01
56	150.24	6.656	28.226	+10.243	09/30
57	150.82	6.630	29.926	+10.198	10/01
58	151.37	6.606	31.510	+10.167	09/30
59	151.92	6.582	33.269	+10.106	10/01
60	153.02	6.535	36.974	+10.015	10/01
61	153.57	6.512	38.917	+10.010	10/01
62	154.15	6.487	41.081	+9.912	10/01
63	154.84	6.458	43.863	+9.860	10/02
64	155.44	6.433	46.311	+9.780	10/08
65	156.04	6.409	48.943	+9.768	10/02
66	156.66	6.383	51.751	+9.664	10/08
67	157.24	6.360	54.512	+9.678	10/02
68	157.86	6.335	57.585	+9.557	10/08
69	158.58	6.306	61.298	+9.557	10/02
70	159.84	6.256	68.433	+9.458	10/02
71	161.16	6.205	76.595	+9.354	10/02
72	162.47	6.155	85.401	+9.255	10/02
73	163.12	6.131	90.232	+9.190	09/23
74	163.74	6.107	94.956	+9.156	10/02
75	164.63	6.074	102.09	+9.070	09/23
76	165.16	6.055	106.34	+9.027	09/24
77	165.67	6.036	110.72	+9.017	10/02
78	166.19	6.017	115.40	+8.962	09/23

[continued]

[Table 4; continued]

No.	T (°K)	$10^3/T$ ($°K^{-1}$)	P (Torr)	T $\ln(P'_H/P_D)$	Date
79	167.14	5.983	124.28	+8.886	09/24
80	167.35	5.975	126.34	+8.894	10/02
81	168.66	5.929	139.59	+8.780	09/24
82	169.45	5.901	148.29	+8.729	10/08
83	170.15	5.877	156.34	+8.677	09/24
84	170.96	5.849	165.92	+8.621	10/08
85	171.65	5.826	174.56	+8.578	09/24
86	173.15	5.776	194.55	+8.478	09/24
87	174.52	5.730	214.52	+8.387	09/24
88	174.86	5.719	219.72	+8.367	09/24
89	176.24	5.674	241.78	+8.276	09/25
90	177.93	5.620	271.48	+8.166	09/25
91	179.17	5.581	294.83	+8.098	10/02
92	179.63	5.567	304.05	+8.060	09/25
93	181.18	5.519	336.56	+7.972	10/02
94	181.35	5.514	340.24	+7.956	09/25
95	183.00	5.464	378.15	+7.854	09/25
96	184.14	5.431	405.98	+7.788	09/25
97	184.77	5.412	422.45	+7.748	09/25
98	185.87	5.380	451.84	+7.684	09/25
99	187.54	5.332	500.11	+7.589	09/25
100	188.52	5.305	529.77	+7.532	10/08
101	189.26	5.284	553.15	+7.496	09/25
102	190.22	5.257	585.37	+7.435	10/09
103	190.95	5.237	610.25	+7.402	09/25
104	192.73	5.189	675.46	+7.300	09/25

[continued]

[Table 4; continued]

No.	T (°K)	$10^3/T$ ($°K^{-1}$)	P (Torr)	T $\ln(P'_H/P_D)$	Date
105	194.83	5.133	759.89	+7.179	09/25
106	196.15	5.098	815.85	+7.115	10/02
107	196.71	5.084	841.31	+7.081	09/25
108	197.95	5.052	898.83	+7.021	10/02
109	198.73	5.032	936.57	+6.975	10/09
110	199.04	5.024	951.40	+6.942	09/25
111	199.94	5.001	998.08	+6.914	10/02
112	200.86	4.979	1046.9	+6.864	10/03
113	200.86	4.979	1045.7	+6.857	09/25
114	201.96	4.951	1106.6	+6.811	10/03
115	202.65	4.935	1145.4	+6.780	10/09
116	202.84	4.930	1157.8	+6.759	10/03
117	204.17	4.898	1236.1	+6.677	09/26
118	204.85	4.882	1279.6	+6.661	10/03
119	205.56	4.865	1324.1	+6.642	10/09
120	205.94	4.856	1348.3	+6.582	09/26
121	206.84	4.835	1408.8	+6.555	10/03
122	207.74	4.814	1470.3	+6.492	09/26
123	207.74	4.814	1471.4	+6.514	10/09
124	208.82	4.789	1548.0	+6.451	10/03
125	209.51	4.773	1602.8	+6.381	09/26
126	209.84	4.766	1622.7	+6.397	10/09
127	211.13	4.736	1724.5	+6.328	10/03
128	211.33	4.732	1738.9	+6.314	09/26
129	213.12	4.692	1887.1	+6.217	09/26

Table 5: Carbon Vapor Pressure Isotope Effects in Methyl Fluoride

No.	T (°K)	$10^3/T$ ($°K^{-1}$)	P (Torr)	T $\ln(P'_{12}/P_{13})$	Date
1	132.52	7.546	3.7118	-0.1684	10/06
2	133.25	7.505	4.0852	-0.1851	10/06
3	133.25	7.505	4.0852	-0.2053	10/06
4	133.63	7.483	4.3139	-0.1687	10/13
5	133.63	7.483	4.3276	-0.1910	10/13
6	133.87	7.470	4.4602	-0.2261	10/13
7	133.88	7.470	4.4587	-0.1818	10/13
8	134.03	7.461	4.5288	-0.2168	10/06
9	134.06	7.460	4.5654	-0.1989	10/13
10	134.81	7.418	4.9877	-0.1704	10/06
11	135.33	7.389	5.3230	-0.1649	10/06
12	135.62	7.374	5.5715	-0.2058	10/14
13	135.62	7.374	5.5715	-0.2228	10/14
14	135.74	7.367	5.6081	-0.1575	10/06
15	136.26	7.339	5.9877	-0.1792	10/06
16	137.06	7.296	6.6051	-0.1943	10/07
17	137.33	7.282	6.8383	-0.1742	10/15
18	137.37	7.280	6.8978	-0.1738	10/15
19	137.97	7.248	7.3917	-0.1924	10/07
20	138.08	7.242	7.5091	-0.2089	10/10
21	138.16	7.238	7.5685	-0.2039	10/10
22	138.27	7.232	7.6783	-0.2077	10/10
23	138.44	7.223	7.8505	-0.1169	10/14
24	138.84	7.202	8.2012	-0.2059	10/07
25	139.37	7.175	8.7332	-0.2014	10/07
26	139.84	7.151	9.2622	-0.1783	10/15

[continued]

[Table 5; continued]

No.	T (°K)	$10^3/T$ ($°K^{-1}$)	P (Torr)	T $\ln(P'_{12}/P_{13})$	Date
27	139.98	7.144	9.4085	-0.1694	10/15
28	140.36	7.124	9.8339	-0.2119	10/07
29	140.86	7.099	10.444	-0.1742	10/15
30	141.36	7.074	11.018	-0.2137	10/07
31	141.76	7.054	11.555	-0.1713	10/15
32	141.91	7.047	11.747	-0.1638	10/15
33	142.36	7.025	12.310	-0.1385	10/07
34	142.36	7.025	12.326	-0.2326	10/07
35	142.45	7.020	12.465	-0.1948	10/10
36	142.60	7.013	12.644	-0.1753	10/10
37	142.64	7.010	12.706	-0.1464	10/07
38	143.16	6.985	13.487	-0.1780	10/15
39	143.64	6.962	14.193	-0.1739	10/07
40	144.14	6.938	14.998	-0.1913	10/16
41	144.26	6.932	15.185	-0.1799	10/16
42	144.76	6.908	16.010	-0.1880	10/07
43	145.35	6.880	17.045	-0.2009	10/16
44	145.87	6.855	18.021	-0.1988	10/07
45	146.41	6.830	19.068	-0.2104	10/16
46	146.53	6.825	19.283	-0.1969	10/16
47	146.96	6.805	20.169	-0.2077	10/07
48	147.55	6.777	21.464	-0.2112	10/16
49	148.05	6.754	22.618	-0.2119	10/07
50	148.62	6.728	23.982	-0.1980	10/01
51	149.34	6.696	25.830	-0.2057	10/16
52	149.72	6.679	26.831	-0.2108	10/01

[continued]

[Table 5; continued]

No.	T (°K)	$10^3/T$ ($°K^{-1}$)	P (Torr)	T $\ln(P'_{12}/P_{13})$	Date
53	150.82	6.630	29.926	-0.2169	10/01
54	151.92	6.582	33.269	-0.2182	10/01
55	153.02	6.535	36.974	-0.2215	10/01
56	153.57	6.512	38.917	-0.2160	10/01
57	154.15	6.487	41.081	-0.2245	10/01
58	154.84	6.458	43.863	-0.2289	10/02
59	155.44	6.433	46.311	-0.2299	10/08
60	156.04	6.409	48.943	-0.2270	10/02
61	156.66	6.383	51.751	-0.2401	10/08
62	157.24	6.360	54.512	-0.2263	10/02
63	157.86	6.335	57.585	-0.2454	10/08
64	158.58	6.306	61.298	-0.2346	10/02
65	159.84	6.256	68.433	-0.2367	10/02
66	161.16	6.205	76.595	-0.2394	10/02
67	162.47	6.155	85.401	-0.2423	10/02
68	163.12	6.131	90.232	-0.2463	09/23
69	163.74	6.107	94.956	-0.2461	10/02
70	164.63	6.074	102.09	-0.2452	09/23
71	165.16	6.055	106.34	-0.2526	09/24
72	165.67	6.036	110.72	-0.2486	10/02
73	166.19	6.017	115.40	-0.2460	09/23
74	167.14	5.983	124.28	-0.2558	09/24
75	167.35	5.975	126.34	-0.2527	10/02
76	168.66	5.929	139.59	-0.2588	09/24
77	169.45	5.901	148.29	-0.2587	10/08
78	170.15	5.877	156.34	-0.2613	09/24

[continued]

[Table 5; continued]

No.	T (°K)	$10^3/T$ ($°K^{-1}$)	P (Torr)	T $\ln(P'_{12}/P_{13})$	Date
79	170.96	5.849	165.92	-0.2641	10/08
80	171.65	5.826	174.56	-0.2640	09/24
81	173.15	5.776	194.55	-0.2662	09/24
82	174.52	5.730	214.52	-0.2701	09/24
83	174.86	5.719	219.72	-0.2685	09/24
84	176.24	5.674	241.78	-0.2709	09/25
85	177.93	5.620	271.48	-0.2727	09/25
86	179.17	5.581	294.83	-0.2718	10/02
87	179.63	5.567	304.05	-0.2755	09/25
88	181.18	5.519	336.56	-0.2769	10/02
89	181.35	5.514	340.24	-0.2784	09/25
90	183.00	5.464	378.15	-0.2806	09/25
91	184.14	5.431	405.98	-0.2829	09/25
92	184.77	5.412	422.45	-0.2832	09/25
93	185.87	5.380	451.84	-0.2845	09/25
94	187.54	5.332	500.11	-0.2878	09/25
95	188.52	5.305	529.77	-0.2881	10/08
96	189.26	5.284	553.15	-0.2906	09/25
97	190.22	5.257	585.37	-0.2922	10/09
98	190.95	5.237	610.25	-0.2934	09/25
99	192.73	5.189	675.46	-0.2971	09/25
100	194.83	5.133	759.89	-0.3016	09/25
101	196.15	5.098	815.85	-0.2977	10/02
102	196.71	5.084	841.31	-0.3078	09/25
103	197.95	5.052	898.83	-0.3013	10/02
104	198.73	5.032	936.57	-0.3021	10/09

[continued]

[Table 5; continued]

No.	T (°K)	$10^3/T$ ($°K^{-1}$)	P (Torr)	T $\ln(P'_{12}/P_{13})$	Date
105	199.94	5.001	998.08	-0.3045	10/02
106	200.86	4.979	1046.9	-0.3080	10/03
107	201.96	4.951	1106.6	-0.3088	10/03
108	202.65	4.935	1145.6	-0.3020	10/09
109	202.84	4.930	1157.8	-0.3133	10/03
110	204.85	4.882	1279.6	-0.3125	10/03
111	205.56	4.865	1324.1	-0.3004	10/09
112	206.84	4.835	1408.8	-0.3230	10/03
113	207.74	4.814	1470.3	-0.3547	09/26
114	208.82	4.789	1548.0	-0.3310	10/03
115	209.84	4.766	1622.7	-0.3315	10/09
116	211.13	4.736	1724.5	-0.3390	10/03

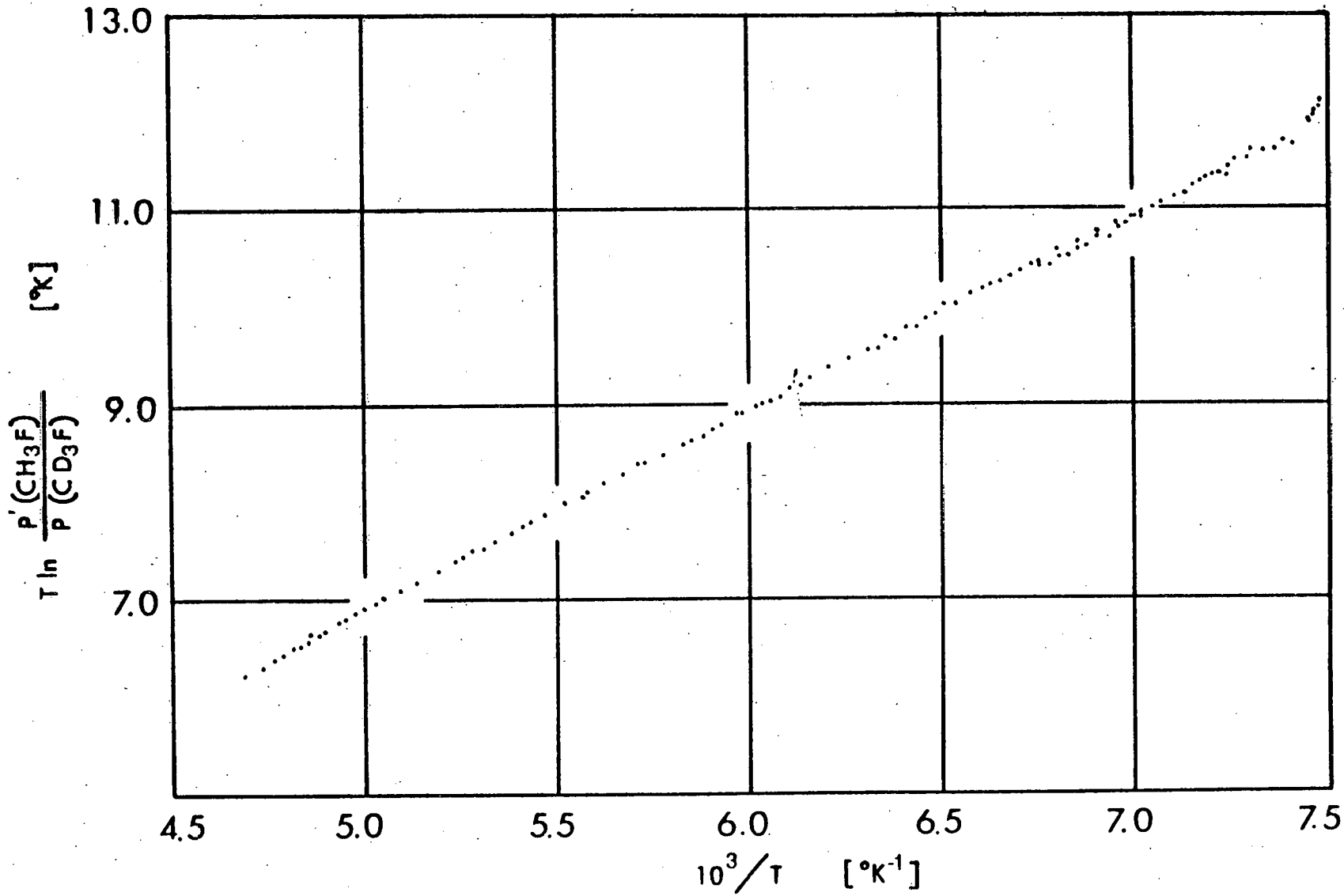

Figure 8. D/H Vapor Pressure Isotope Effect in Methyl Fluoride

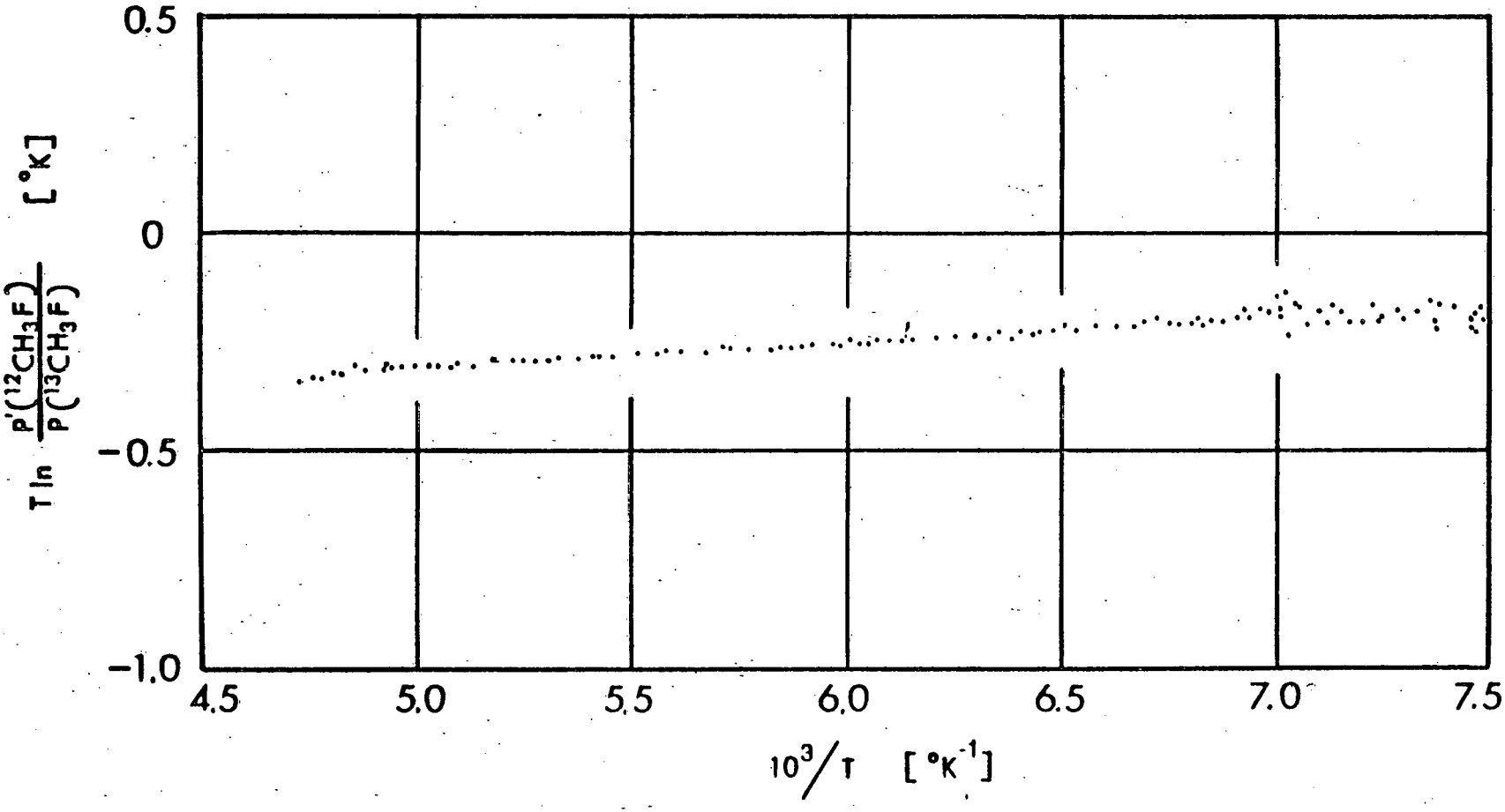

Figure 9. $^{13}C/^{12}C$ Vapor Pressure Isotope Effect in Methyl Fluoride

We also fitted the data to the linear form of Eq. (5) which yielded, for the $^{13}C/^{12}C$-effect,

$$\begin{aligned} A &= 54.37 \pm 1.86 \quad (°K^2) \ , \\ \text{and} \quad B &= -0.5787 \pm 0.0118 \quad (°K) \ , \end{aligned} \tag{21}$$

and, for the D/H-effect,

$$\begin{aligned} A &= 2012.6 \pm 4.5 \quad (°K^2) \ , \\ \text{and} \quad B &= -3.161 \pm 0.028 \quad (°K) \ . \end{aligned} \tag{22}$$

Studies of these results for a plausible explanation have just been started.

(B) NITROGEN ISOTOPE FRACTIONATION

(B-1) Studies of NO/N_2O_3 System

by Michael Prencipe

As reported previously,[2,15] an increase in the nitric oxide partial pressure in gas phase should increase the effective stage separation factor of ^{15}N-fractionation which utilizes the isotope exchange between the gaseous nitric oxide and liquid dinitrogen trioxide. The constructions of all-stainless steel exchange system and a product refluxer made of Pyrex have been completed. The system had to be disassembled to facilitate the moving from Brooklyn College, Brooklyn, New York to the present site at Stony Brook. The dismantled system has been re-assembled and tested for leaks. To facilitate the discussion that follows, Figure 10 has been reproduced from last year's progress report.

For the last several months we have been learning how to operate the product reflux column, including the procedures for its start up and shut down. While experimenting with the product refluxer we found a room for improvement in its design concerning its control of the reaction zone.

This Pyrex refluxer column was built in accordance with the design by Monse, Spindel, Kauder and Taylor,[16] which utilizes a controlled flow of SO_2 for the reduction of HNO_3 from the exchange column. The SO_2 flow control is achieved by a photocell mounted on a short side arm attached on the packed reflux column at an elevation near the reaction zone in which the reduction takes place. The photocell receives a light transmitted through a green filter. When the elevation of the reaction zone becomes too low, brown NO_2 gas generated causes the photocell current to decrease below a threshold, and a solenoid valve is opened to supply an extra SO_2 through a branch path in the SO_2 supply line.

However, the sensitivity of detection of the reaction band by the photocell method changes as the concentration of HNO_3 from the exchange column and the flow rate of dilute sulfuric acid fed at the upper end of the reflux column change. (The flow rate of the H_2SO_4 feed, along with

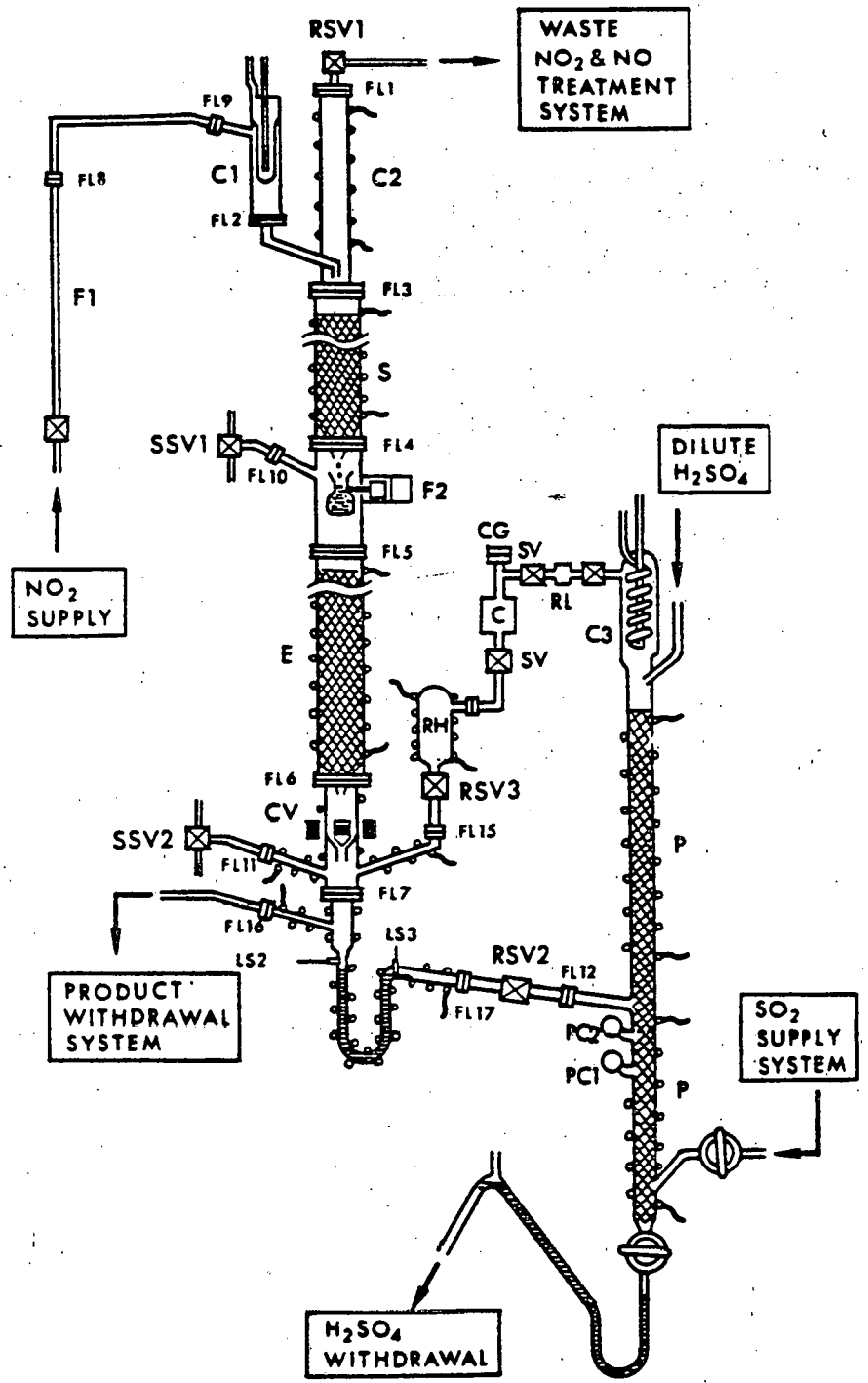

Figure 10. NO/N_2O_3 System for ^{15}N-Fractionation

the rate of cooling of the condenser (C3 in Figure 10), is used to maintain an equilibrium chemical composition of the "nitric oxide" returned to the exchange column.) Besides, the detection of NO_2 gas is delayed while the SO_2 gas trapped in the photocell side-arm is consumed as the band continues to move down the column. The SO_2 gas fills up the photocell side-arm when the reaction band moves upward past the side-arm during the period when the extra supply of SO_2 is fed through the solenoid valve line. Sometimes the reaction zone moves unevenly and the brown zone would channel down one side of the column, leaving the other side of the column colorless. As a result of these reasons, we frequently observed the reaction zone moving downward past the photocell level by as much as 3 inches before sufficient NO_2 is accumulated to trigger the photocell.

Furthermore, we have become aware of the difficulties involved in operating a process consisting of two pressure zones. We proposed last year that, to operate the NO/N_2O_3 system under an elevated pressure ($10 \sim 20$ atm), we would employ a relief valve on the path of enriched HNO_3 from the exchange column, which is at the elevated pressure, to the product refluxer, which is at the atmospheric pressure, and a use diaphragm compressor to compress the nitric oxide generated by the refluxer before the gas is returned to the exchange column. However, we have since learned the difficulties in the maintenance of such a compressor necessary for its reliable operation and difficulties in controlling and balancing the flow rates of HNO_3 coming out and NO going back. If this is proved to be the case, we should consider a feasibility of operating the refluxer at the same elevated pressure as the exchange column.

Aside from the pressure level of refluxer, the photocell method has room for improvement, as explained earlier. Accordingly, we have designed, constructed, and operated a new SO_2-flow control system based on detection of reaction zone by means of temperature sensing with a thermistor. We will present its design and operation in Section (B-1-a) and the considerations for a pressurized refluxer design in Section (B-1-b). In Section (B-1-c) a step-by-step procedures of operations of the Pyrex reflux system is given for the sake of record.

(B-1-a) Thermistor Control of Reaction Zone: We have installed an 1/8" diameter well on the side wall between two photocell ports of the existing Pyrex refluxer. Figure 11 shows the thermistor well as well as the SO_2-handling system. The electronic circuit for the SO_2-flow control is shown in Figure 12.

In this circuit the common emitter inverter is used as a switch, the information transmitted being simply the presence or absence of a positive signal which result in the transmitter being in the state of saturation or cutoff, respectively.

The positive and negative voltages (V_o) are generated by the operational amplifier in the following manner. V_+ is chosen by changing R_p so that $V_+ > V_-$ is achieved with the lower end of the reaction zone slightly above the level of the thermistor well. Then, the resistance of the thermistor (R_T) is not so small, $V_+ > V_-$, and therefore $V_o = +14V$, the transistor being in saturation. The relay thus causes a solenoid valve for a supply of compressed air to open, which keeps the pneumatically operated valve in the auxiliary SO_2 line (V_3 in Figure 11) closed. The value of V_+ at which the valve V_3 is shut off is given by

$$V_+(h) = V_i \frac{1}{1+R_p||R_f} \simeq \frac{V_i}{1+R_p} ,$$

R_p being much less than R_f. In this equation the resistance values are in kilo-ohms. The h in $V_+(h)$ indicates the "high" trigger point, when the reaction band reaches its highest level.

As the reaction zone falls, i.e., as more SO_2 becomes needed, the temperature of the thermistor increases, R_T decreases, and V_- increases. When V_- becomes greater than V_+, V_o becomes -14V, and no current flows through the relay, thereby allowing more SO_2 to flow to the product refluxer. The value of V_+ when the auxiliary SO_2 line opens is given by

$$V_+(\ell) = \frac{V_i}{1+R_p} - \frac{V_o}{1+R_f} ,$$

where the resistance values are in kilo-ohms. $V_+(\ell)$ can be chosen to be different from $V_+(h)$ by appropriately changing R_f. By properly chosing the values of $V_+(h)$ and $V_-(\ell)$ one can adjust the detector sensitivity. We found that the amplitude of fluctuation of the level of reaction zone

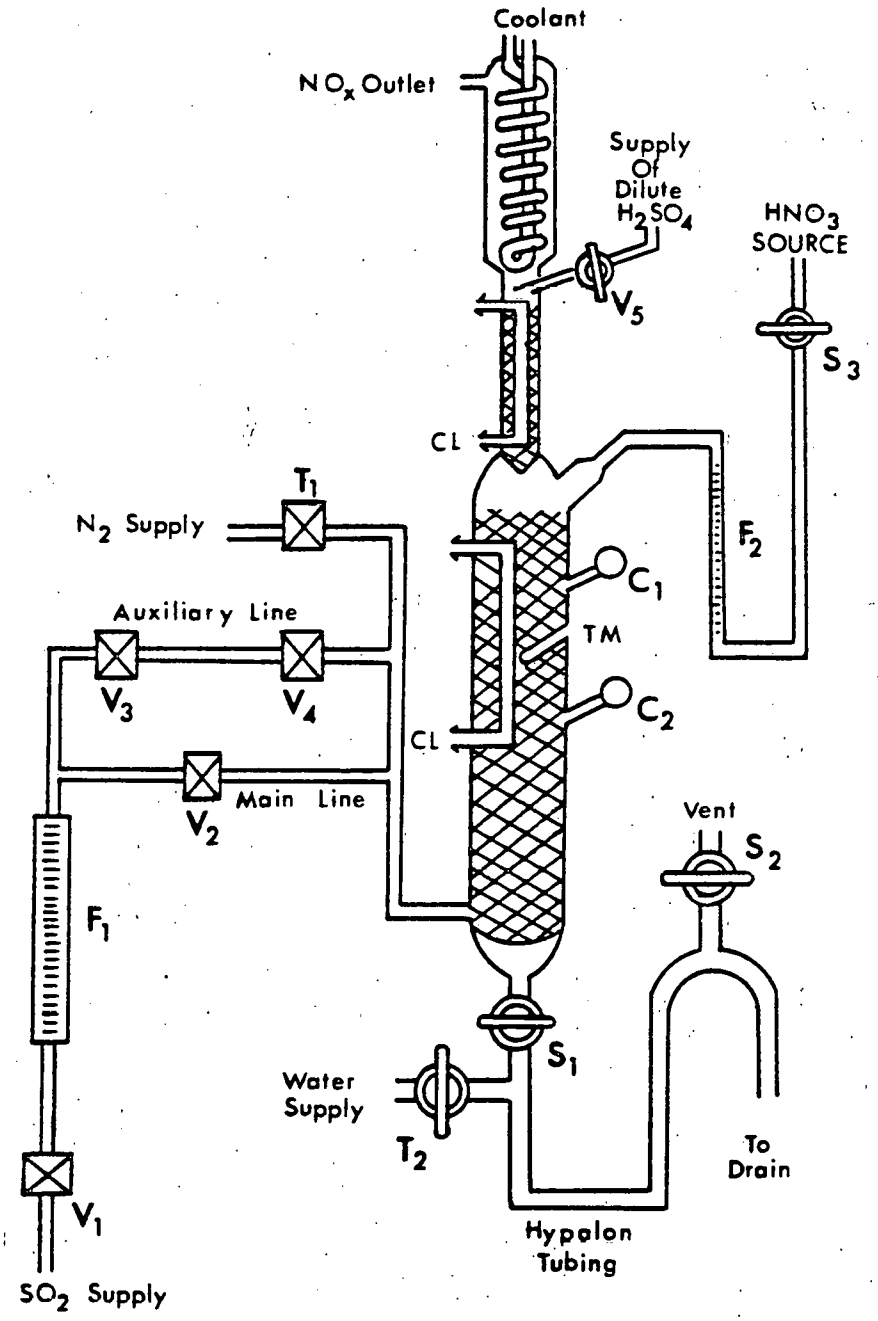

Figure 11. HNO_3-Refluxer System

[Legends for Figure 11 will be found on page 65.]

Figure Legends for Figure 11

C_1 and C_2 : Photocell detectors

CL : Coolant

F_1 and F_2 : Flowmeters

S_1, S_2, S_3 : Teflon-plug stopcocks

T_1 and T_2 : Teflon bellows valves

TM : Thermistor well

V_1 : Stainless steel shut-off valve

V_2 : Stainless steel regulating/shut-off valve

V_3 : Stainless steel, bellows-sealed, pneumatic valve, actuated by air pressure controlled by a solenoid valve.

V_4 : Stainless steel needle valve.

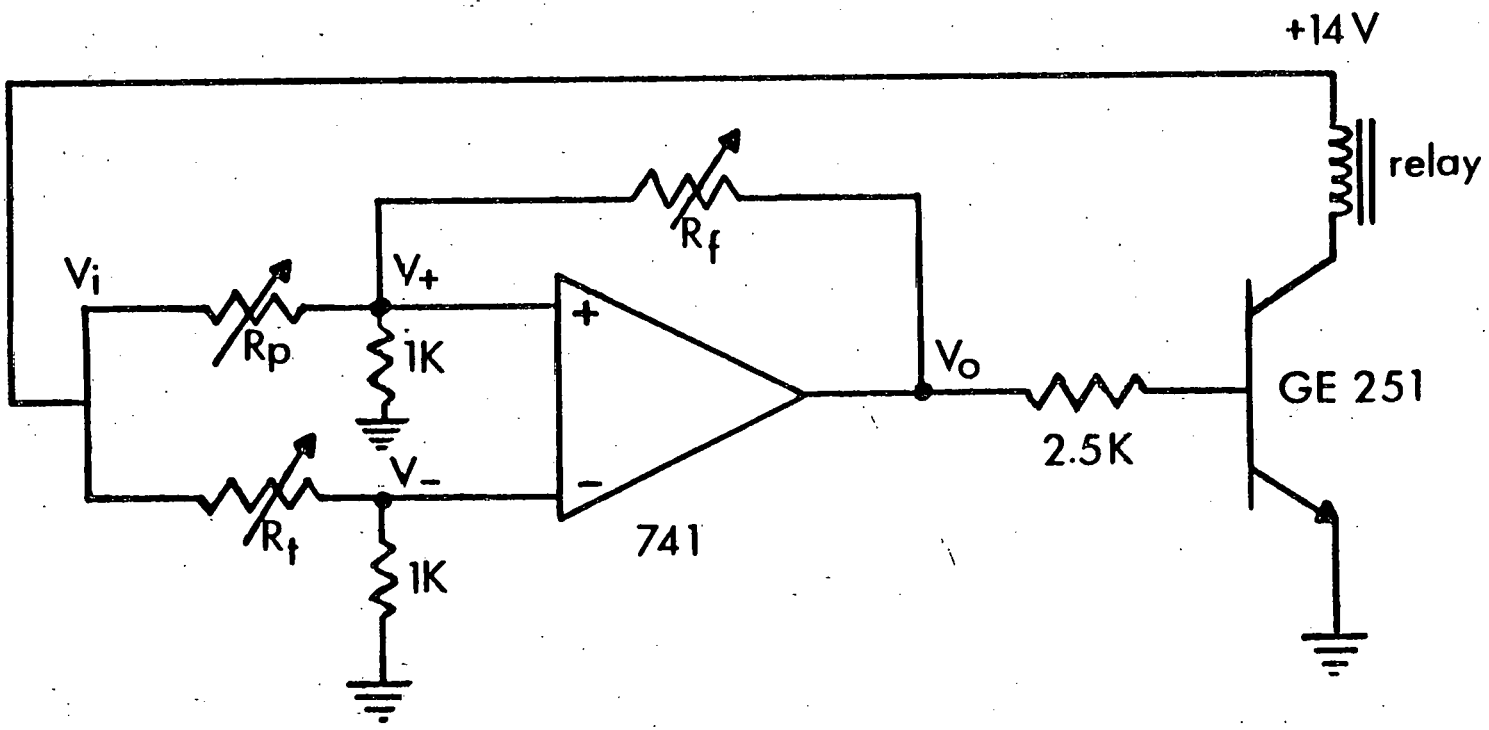

Figure 12. Sulfur Dioxide Flow Control Circuit using Thermistor as Reaction Zone Sensor

[Legends for Figure 12 will be found on page 67.]

Figure Legends for Figure 12

R_p : 1K ohm potentiometer

R_T : 10K thermistor

R_f : 50K ohm potentiometer

741 : Operational amplifier LM741

GE251 : NPN silicon, general purpose switching (20W), transistor

can be adjusted from a few millimeters to a few centimeters, but an amplitude of about 1 cm is adequate.

We have operated the reflux column using this control for extended periods of time ranging up to 24 hours and have found it much more reliable than the photocell method. We also found it more versatile than the photocell system, because it gives us two different trigger points rather than just one. This is very useful since the electronic noise or any slight changes in any of the operating conditions would not interfere with the automatic control. Besides, the thermistor system is suitable for adaptation to the elevated pressure operation of refluxer, while the photocell method is not. We plan to use the thermistor method throughout the remainder of this ^{15}N-fractionation study.

(B-1-b) Feasibility of Refluxer Operation under Elevated Pressure: If the product refluxer is to be operated at the same elevated pressure as the exchange column, a major modification of its design will be necessary. Following consideration is based on a reflux pressure of 10 atmosphere.

All the feed streams to such a reflux column must be pressurized. There are three feed streams, i.e., the HNO_3 from the exchange column, the dilute sulfuric acid line to the top of the column, and the SO_2 gas line to the bottom of the column. The HNO_3 line has no problem, because HNO_3 is already at the operating pressure of exchange column. The dilute sulfuric acid will have to be pressurized but it offers little problem, because we don't have to worry about the loss and the holdup of H_2SO_4 during the compression, which was the case when we considered a compressor for the enriched nitric oxide. However, the SO_2 supply will have to be heated, because its vapor pressure at room temperature is only 34 psig. The vapor pressure of SO_2 reaches 10 atm at 55.5°C. Therefore, a 2.5 gallon, Type 304 stainless steel, high pressure (1800 psig) cylinder has been purchased. Prior to a fractionation run, SO_2 will be transferred to this special cylinder from the vendor's cylinder. The SO_2-tank is then heated up in a silicon oil bath. Some kind of heating arrangement for the SO_2 source would have been necessary even without the vapor pressure

problem, because the latent heat of vaporization will have to be supplied to the cylinder.

Because the SO_2 vapor pressure must be maintained by heating it up at its source, the temperature of the entire reflux column will also have to be maintained at 55.5°C for the 10 atm operation. To accommodate the medium concentration sulfuric acid (1 ∿ 10 M) at this temperature, even Type 316 stainless steel will be unsatisfactory. The only possible material is Teflon or its equivalent (or lead). To provide the mechanical strength and the chemical resistance, we will have to have the inside surface of stainless steel refluxer column with a thick coat of Teflon. We believe we can fabricate such a column without trouble, especially because (cf: Figure 11) the condenser section at the top end of the refluxer does not have to be coated with Teflon, inasmuch as its inner wall will not be exposed to sulfuric acid. The internal cooling lines in the Pyrex system of Figure 11 will be replaced by a jacket of heating fluid surrounding the column.

There are two outlet lines from the refluxer, i.e., the NO-line and the waste sulfuric acid line. The NO is already at the exchange column pressure and it can be returned directly to the exchange column without much additional holdup. The waste H_2SO_4 can be released to the drain through a relief valve, which can be at room temperature, if SO_2 is completely consumed in the region of the column maintained at the elevated temperature. This can be accomplished by maintaining a length of the column between the reaction zone and the bottom of the column along which its temperature is gradually decreased.

Aside from the pressure of operation of the refluxer, NO_2 which is introduced at the top of the exchange column has to be heated to a temperature of 79.5°C to achieve a vapor pressure of 10 atm. A stainless steel cylinder identical to that used for heating SO_2 supply has been installed for this purpose.

Having been familiarized with operations of the refluxer, including its thermistor version, we are in a process of test-starting the all stainless steel exchange column system that we already built[1] and

re-assembled. For this phase of study at one atmosphere, we plan to use the Pyrex refluxer. Concurrently, we are working on a design of high pressure refluxer column.

(B-1-c) Operating Procedures of Pyrex Refluxer Column: Start-Up:

1. Flood the nitrogen oxide scrubbing tower with water. Drain and maintain a constant flow of ∿ 2 liter/min.

2. Pressurize the HNO_3 reservoir to 2 psig. This pressure is needed because the check valve leading to the scrubbing tower keeps the pressure inside the column at 1 psig above atmospheric pressure.

3. Start the flow of cooling water.

4. Flood the product refluxer with water by closing S_1 and opening V_5. This is done to wet the packing. Drain excess water and maintain a water flow of 1-2 cc/min. The small flow of dilute sulfuric acid at the top of the column is kept to reduce the amount of NO_2 going into the exchange column in the actual operation, and to cool the product refluxer. It is usually kept at 15 to 25% of the flow of nitric acid.

5. Start the oxygen flow to the scrubbing tower to oxidize the nitric oxide. Maintain a flow of about 75% (in moles) of that of SO_2 to assure an excess of O_2.

6. Start the SO_2 flow. Since the pressure inside the column at the level of SO_2-feed point will increase, the level of the liquid at the bottom will be lowered. To keep the level from going too far down and create the possibility of SO_2 discharging into the atmosphere, the right side of the Hypalon U-tube is raised. The Hypalon tubing can withstand concentrated H_2SO_4.

7. Start the HNO_3 flow to the desired level by opening S_3. After several minutes a band of NO_2 (brown gas) will appear.

8. With V_3 closed, V_2 is adjusted so that SO_2 is pumped into the refluxer at a rate required to maintain the boundary of the reaction zone at the level of the sensing element (thermistor or photocell). This flow is reduced by 15% by partially closing V_2 and then increased by 30% by adjusting the needle valve (V_4) with V_3 opened. During the run the height of the reaction zone is maintained constant by a Schmitt trigger which operates a relay that drives a 120 VAC solenoid valve which transmits pressure of either 0 or 50 psig to an all stainless steel pneumatic bellows-sealed valve, which results in opening or closing of the pneumatic valve, respectively. When the reaction zone falls, the thermistor senses the increase in temperature,

and the change in resistance causes the Schmitt trigger to trip at a preset voltage level, thus operating the relay. The pneumatic valve now cycles on the average of once every minute to provide the automatic control of SO_2 flow.

Shutdown:

1. Close S_1, S_2, S_3, V_1, V_2, and V_5.
2. Open T_1 to flush out the contents of the column into the scrubbing tower with N_2.
3. Open T_2 to flush out waste H_2SO_4 into the drainage system.
4. Vent the HNO_3 reservoir.
5. Shut off cooling water.
6. Close T_1 and T_2, open S_1 and S_2, vent the product refluxer and wash out the column by opening V_5.

Typical Flow Rates

	HNO_3(mmoles/min)	SO_2(mmoles/min)	O_2(mmoles/min)
1.	32	36	24
2.	18	20	13 1/2

(B-2) New Product Refluxer for Nitrox Process

by Motonari Adachi

The problem of chemical waste associated with a large scale Nitrox process in which ^{15}N is fractionated by isotope exchange between NO and HNO_3 was pointed out by Michaels and Schwind of Mound Laboratory. They estimated that the total H_2SO_4 generated by a Nitrox plant producing 300 metric tons of ^{15}N at 99% enrichment per year is 27×10^6 metric tons. Also, the correspondingly enormous amount of SO_2 will have to be transported to the site of the plant.

To avoid the needs for the large amount of chemical input and the problems of disposing of the large amount of chemical waste, Michaels and Nimitz of Mound Laboratory investigated an electrolytic reduction of nitric acid utilizing a specially designed, low-holdup electrolytic cell. The problem seems to be that of high overvoltage, which was verified in the presence of metal ion catalysts, at high (80°C) temperatures, and also with high cathode flow rates.

As a possible reducing agent which might replace SO_2 in the Nitrox or NO/N_2O_3 process we have investigated ferrous sulfate solution in sulfuric acid. Reduction of nitric acid by $FeSO_4$ in H_2SO_4 is well known as the "brown ring" method for the detection of nitrate. The "brown ring" is iron (II) nitrosyl complex, $FeNO^{2+}$. Recently, Pearsall and Bonner[17] conducted a careful study of reduction of $FeNO^{2+}$ by excess amounts of Fe^{2+} and concluded that, at the pH's below 4 and at room temperature, $FeNO^{2+}$ is stable and does not undergo any further reduction, although NO is reduced to N_2O at pH's between 4 and 7 and to N_2 above pH of 7.

Manchot and Haunschild[18] measured the equilibrium constant for the two-phase reaction,

$$Fe^{2+}(aq) + NO(g) \rightleftarrows FeNO^{2+}(aq) \quad , \qquad (23)$$

at temperatures between 2°C and 44°C, whose results are reproduced in Table 6 and Figure 13.

Table 6: Equilibrium Constant for Reaction (23)

t(°C)	K(atm^{-1})
2.6	3.02
11.9	1.77
18.6	1.08
25.5	0.66
31.4	0.415
44.0	0.133

Depending on the line of extrapolation used in Figure 13, the equilibrium constant at 100°K ranges from 0.002 atm^{-1} to 0.026 atm^{-1}. Using a compromised value of 0.012 atm we have made a sample design of a product refluxer, in which HNO_3 and $FeSO_4 + H_2SO_4$ concurrently flow down a column maintained at about 100°C mainly by boiling steam up the column from a still pot at the lower end of the column. Nitric oxide released by the decomposition of $FeNO^{2+}$ flows upward countercurrently to the liquid flow. Our calculation shows that the nitrogen content in liquid is reduced to the order of 1 ppm after only 2 stages, if we can assume that nitric oxide generated by the reduction of HNO_3 which is not complexed in the form of $FeNO^{2+}$ will immediately flow upward. After the liquid containing excess $FeSO_4$, H_2SO_4, and Fe^{3+} exits from the still, Fe^{++} may be regenerated by an electrolytic reduction. What follows is a sample calculation for the refluxer column.

The reduction of nitric acid by ferrous salt proceeds as follows:

$$HNO_3 + 3Fe^{2+} + 3H^+ \rightarrow NO + 3Fe^{3+} + 2H_2O \qquad (24)$$

$$\Delta G^\circ_{298} = -11.76 \text{ kcal}$$

$$K_{298} = 4 \times 10^8$$

Consider a packed column as shown in Figure 14. Because the reduction goes further than NO in a pH higher than 4, and because the sulfuric acid is diluted in the column, the concentration of H_2SO_4 fed with $FeSO_4$ has to be sufficiently high. Let it be 0.9 molar. A solution of $FeSO_4$ in

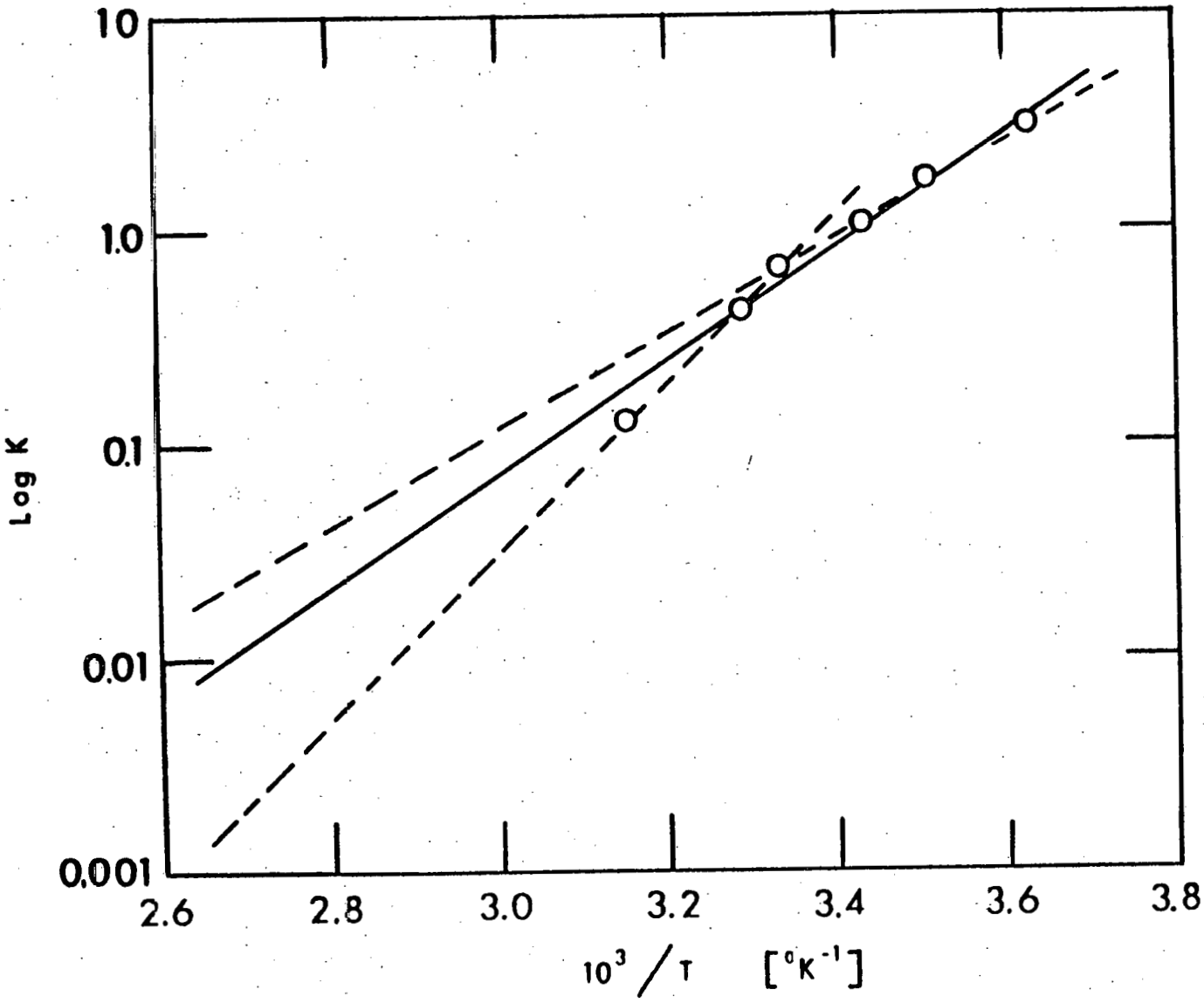

Figure 13. Formation Constant K for $Fe^{2+}(aq) + NO(g) \rightleftarrows FeNO^{2+}(aq)$

0.9 M - H_2SO_4 is fed at a higher elevation than the feed point for HNO_3 so that NO_2, N_2O_3, N_2O_4, etc. which may be generated in the side reactions may be efficiently scrubbed by sulfuric acid. Purpose of the still at the bottom end of the column is two-fold. The steam generated by the still flows up the column and acts as a carrier for nitric oxide generated by the decomposition of $FeNO^{2+}$ while, at the same time, keeping a low partial pressure of NO.

Operating Conditions Assumed:

Temperature of the still pot = 100°C

Feeds: HNO_3; 6 M, 2 ml/min

H_2SO_4; 0.9 M
$FeSO_4$; 1 M
} 70 ml/min

Steam generated in the still: 3 ℓ/min @ 100°C and 1 atm.
= 98 mmol/min = 1.76 gram/min

Stoichiometry

HNO_3 feed rate = 12 mmol/min

Fe^{2+} feed rate = 70 mmol/min

H^+ feed rate = 126 mmol/min

Rate of consumption of Fe^{2+} = 36 mmol/min

Composition of solution after the reduction:

0.459 M - Fe^{2+}; 1.22 M - H^+; 0.486 M - Fe^{3+}

NO generated = 12 mmol/min
= 367 ml (@ 100°C, 1 atm)/min

Total Liquid Flow-Rate: 70 + 2 + 1.7 = 74 ml/min

Total Gas Flow-Rate: 3000 + 367 = 3367 ml/min

Cross-sectional Area of Column: I.D. = 3 cm
Area = 7.07 cm^2

If the packing material is 3/16" I.D. glass helix, then the void ratio is 0.76, and the cross-sectional area of the void volume is 5.37 cm^2. If 10% of the void is occupied by liquid, the linear flow rate of liquid and gas are 2.3 cm/sec and 11.5 cm/sec, respectively. If 50% of the void is liquid, the linear flow rate of liquid and gas are 0.46 cm/sec and 20.8 cm/sec, respectively.

Material Balance and Equilibrium Relations:

If the total pressure of steam and NO is 1 atm, the partial pressures

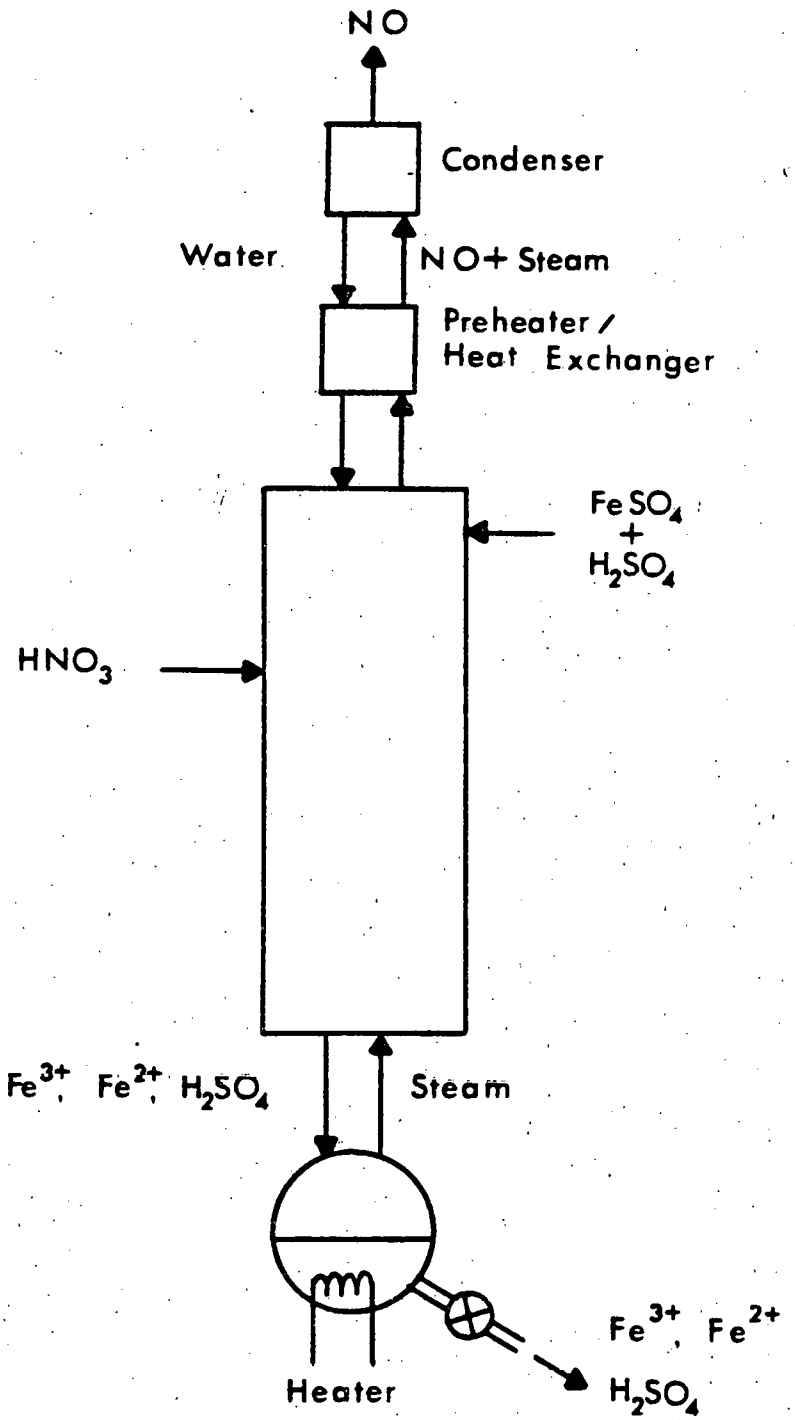

Figure 14. Schematic Diagram of HNO_3 Refluxer Utilizing $FeSO_4$-H_2SO_4

of steam and NO at the top of the column are 0.89 atm and 0.11 atm, respectively. (We assume the temperature is still 100°C since the liquid phase is a solution of H_2SO_4 and the salts.) $FeNO^{2+}$ at the top of the column is in equilibrium with this partial pressure of NO: $[FeNO^{2+}] = 6.7 \times 10^{-4}$ M at the top of the column. If we assume only that part of NO generated which forms the complex with Fe^{2+} moves toward the bottom of the column and that the remainder of NO is lost to the top of the column, the net feed rate of nitrogen to an envelope formed between the bottom of the column and the HNO_3 feed point will be 0.0495 mmol/min (cf: Figure 15a). If we require that there is zero nitrogen flow at the bottom of the envelope, 0.0495 mmol/min of NO has to come out at the top of the envelope: $P_{NO} = 5.07 \times 10^{-4}$ atm at the top of the envelope. Figure 15b shows the equilibrium concentrations of $FeNO^{2+}$ and equilibrium partial pressures of NO for the first few stages.

Both equilibrium and operating lines go through the origin. The slope of the equilibrium line is 181.5 atm/M, while that of the operating line is 0.754 atm/M.

Flooding:

We have used Lobo's empirical relation[19] to calculate the maximum allowable gas flow rate and found it to be four times the gas rates used in the calculations above.

We have fabricated a jacketed Pyrex column, 30 mm I.D. x 50 cm long, packed with 3/16" I.D. glass helices. It is designed to allow variable levels of feed points along the length of the column. The feed streams are preheated. The top of the column is connected to a condenser via a preheater for the condensate water returning to the column. We are about to start operations of this column at 1 atm to test its performance as a function of various flow rates, concentrations, temperatures, and steam boil-up rates. The liquid effluent will be analyzed for total nitrogen by the Kjeldahl/Nessler method developed for the sub-ppm level of nitrogen, which will be reported in the following section.

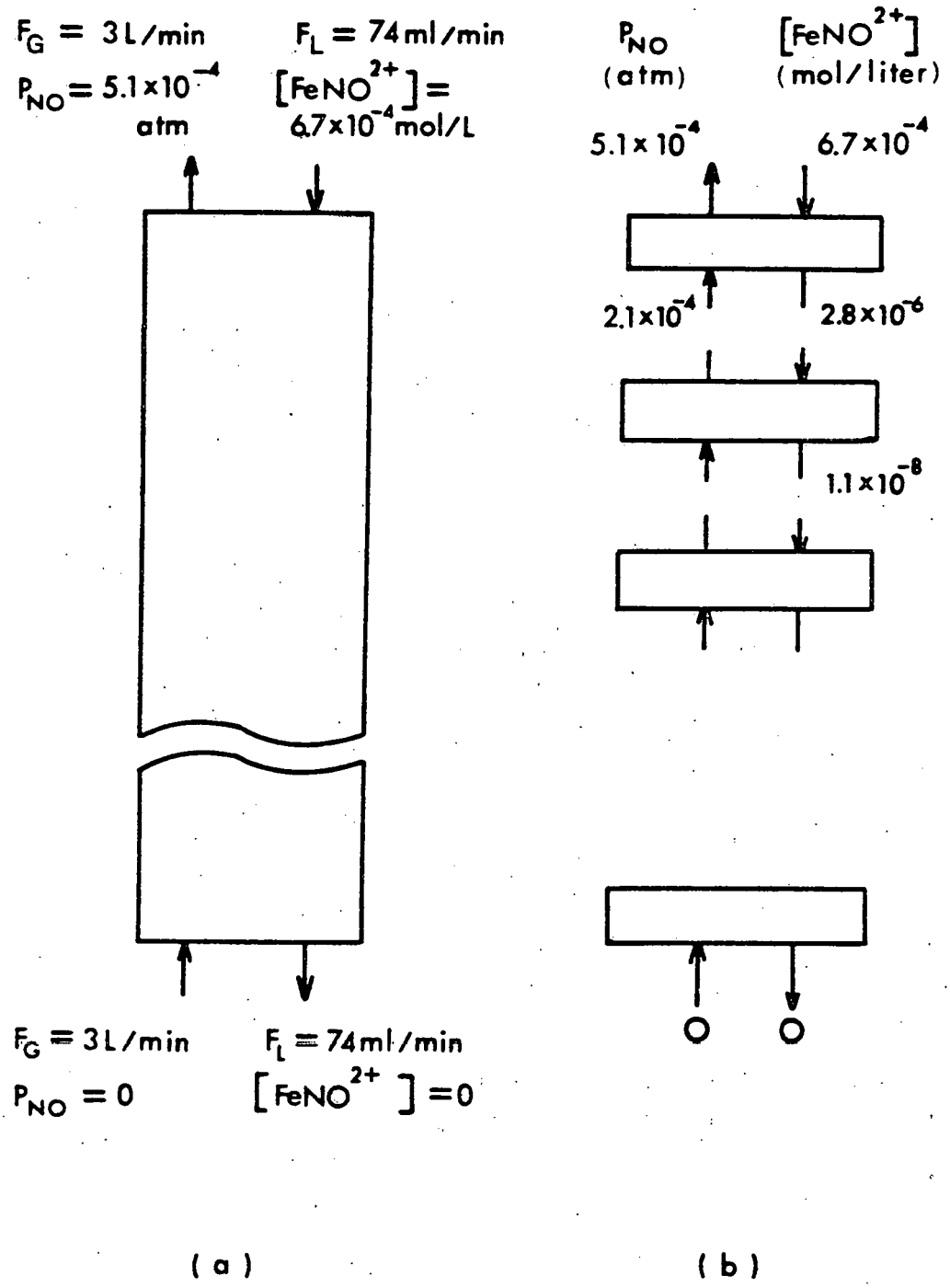

Figure 15. Equilibrium Relations

(B-3) New Analytical Procedure for Total Nitrogen

by Riazulla Rouhani Manshadi and Motonari Adachi

The Kjeldahl distillation for converting nitrogen compounds to ammonia followed by the Nesslerization of the ammonia for a colorimetric determination is a well accepted method for the quantitative analysis of total nitrogen. However, our tests showed that the method is unreliable when one tries to quantitatively analyze inorganic nitrogen at concentrations of the order of ppm or less. The problem is in the fact that ammonia dissolves well in water at room temperature: Small amounts of ammonia are easily lost between the Kjeldahl flask and a receiver flask when it is absorbed by water droplets formed on the inside walls of connecting tubes. We have developed a new procedure which solves this intermediate absorption problem. With the new method, we are able to analyze 0.1 ppm nitrogen with an accuracy better than ±10%.

Devarda's alloy is used for the reduction of nitrate. The alloy is 45% Al, 50% Cu, and 5% zn. The alloy is used in an alkali solution. For example,

$$3NO_3^- + 8Al + 5OH^- + 2H_2O \rightarrow 3NH_3 + 8AlO_2^- .$$

The apparatus (cf: Figure 16) consists of a reaction vessel, a jacketed connecting tube, and an absorption tube. The upper half of the reaction vessel and the connecting tube are formed into one integral unit. The upper and the lower halves of the reaction vessel are connected by means of an O-ring joint (60 mm I.D.), which provides means for cleaning of the vessel and introduction of liquid samples. The upper part of reaction vessel has two vertical ports and one horizontal port, each port being equipped with an Ace screw cap joint. One of the vertical ports is used to feed-through a thermometer, and the other is used to insert a tube for bubbling of helium through the solution. The bubbling is used to help expel the last trace of ammonia from the solution. The horizontal port is used to support a Teflon rod to which a glass cup container for Devarda's alloy is attached. The glass cup is detachable from the Teflon rod for cleaning. The alkalinity of the sample solution is adjusted in the reaction vessel. Devarda's alloy is added to the solution by

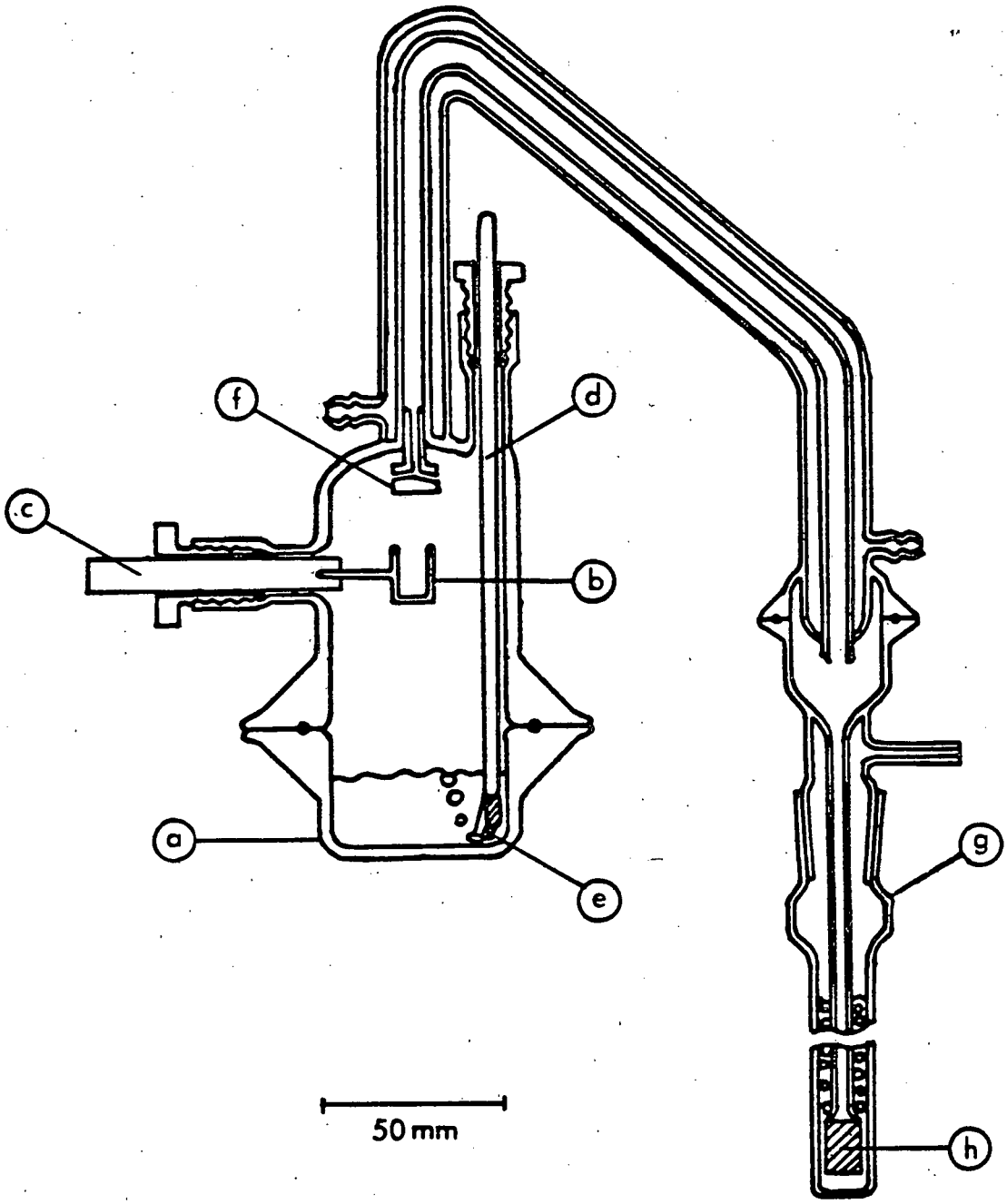

Figure 16. Micro-Kjeldahl Apparatus

[Legends for Figure 16 will be found on page 81.]

Figure Legends for Figure 16

(a) Reaction vessel

(b) Glass container for Devarda's alloy

(c) Teflon rod, rotatable around its axis

(d) Thermometer

(e) Helium bubble tube

(f) Teflon anti-mist insert

(g) Receiver tube

(h) Fritted cylinder

rotating the Teflon rod. To prevent water condensation inside of the dome of the reaction vessel, the entire vessel is enclosed in an electrical heating mantle.

The transfer tube is jacketed for its entire length so that hot water ($\sim$ 90°C) flowing through the jacket keeps water vapor from condensing. To prevent entraining of fine mist of sample solution into the receiver tube, a Teflon piece is inserted in the entrance end of the transfer tube. If the solution finds its way into the receiver tube, the subsequent Nesslerization of the absorber acid causes turbidity due to the metal ions from Devarda's alloy. The receiver tube consists of a fritted cylinder tube inserted in a 20 cm long cylindrical container of acid absorber.

What follows is a step-by-step procedure for the Devarda's alloy/Kjeldahl method and for the colorimetric determination by Nesslerization.

Devarda Reduction Procedure

(1) Weigh about 0.50±0.01 gr of Devarda's alloy, and transfer it to the glass cup designated by the letter (b) in Figure 16 by means of a clean, dry, glass funnel. During this process the glass cup is already attached to the Teflon rod, and the upper part of the reaction vessel has to be positioned upside down. After placing the alloy in the cup, hold the upper part of the flask by means of the Teflon rod (c), and rotate the upper half of the reaction vessel 180° around the axis of the Teflon rod in such a way that the sample cup is held right-side up all the time. Clamp the whole reaction vessel to a stand afterwards.

(2) Place 20 cc of sample solution containing NO_3^- (and/or NO_2^-) nitrogen in the reaction flask (a).

(3) Add 20 cc of 6.25N NaOH in the flask (a).

(4) Connect the reaction flask (a) to its upper half by means of O-ring clamp.

(5) Place 15 cc of 0.3N H_2SO_4 in the receiver tube and clamp it to the connecting tube.

(6) Connect a helium source to the bubble tube (e).

(7) Connect a thermometer to one of the vertical ports (d).

(8) Run a stream of hot water (90°C) through the jacket. Enclose the entire reaction vessel in an electrical heating mantle. Heat the upper half of the vessel to above 100°C.

(9) Pour Devarda's alloy into the reaction vessel by rotating the Teflon rod.

(10) Open a valve in the helium supply line very slowly. Control the rate of bubbling so that the bubbles through the receiver tube does

not push the acid level too high up.

(11) Heat the lower half of the reaction vessel by using a heating mantle. Temperature of the reacting liquid is maintained at 85°C.

(12) At the end of the reaction, which may last one hour, take the distillate by following these steps:

(a) Stop heating and disconnect hot water flow.

(b) Equalize the pressure by disconnecting the thermometer port (d).

(c) Stop the gas bubbling.

(d) Transfer the absorber acid into a 50 cc volumetric flask, and wash the receiver tube, pouring the wash solution into the volumetric flask. Add distilled water to bring the volume up to 50 cc in the volumetric flask.

Spectrophotometric Procedure

A spectrophotometer, Model SPECTRONIC-21 by Bausch & Lomb Company has been used with a sample holder with 1 cm light path and at a wavelength 410 nm and the slit width $\Delta\lambda$ = 10 nm.

Take 10 cc of the sample from Step (12) of the Kjeldahl procedure above. Add 1 cc of 1.00 N- NaOH, and mix the solution well by shaking the beaker. Add 1 cc of Nessler's reagent (described later) at the rate of 1 drop per second. Concentration of the NaOH after the final drop should fall within the range from 0.15 N to 0.5 N in order to obtain a good result. After NaOH is added, wait for 10 minutes to let the color fully develop.

The Nessler reagent used in this method is the Folin-Wu type purchased from Fisher Scientific Co. It consists of 1.5% W/V H_gI_2, 1.15% W/V KI, and 1.75 N NaOH.

Set the zero absorbance on the spectrophotometer by using the same size sample of distilled water that has undergone the Devarda reduction and Nesslerization procedures.

A calibration curve can be constructed by using a series of standard nitrate solution which are subjected to the Devarda reduction and the Nesslerization procedures. Our calibration curve is presented in Figure 17. A blank correction is always necessary. Since the Devarda's alloy contains a significant amount of nitrogen (cf: Figure 17), the amount of the alloy used has a significant consequence on the calibration curve.

This procedure can be used for concentrations ranging from 0.01 to 5 ppm nitrogen in the form of nitrate. However, 5 ppm is not the upper limit possible. It simply reflects the highest concentration we experimented for.

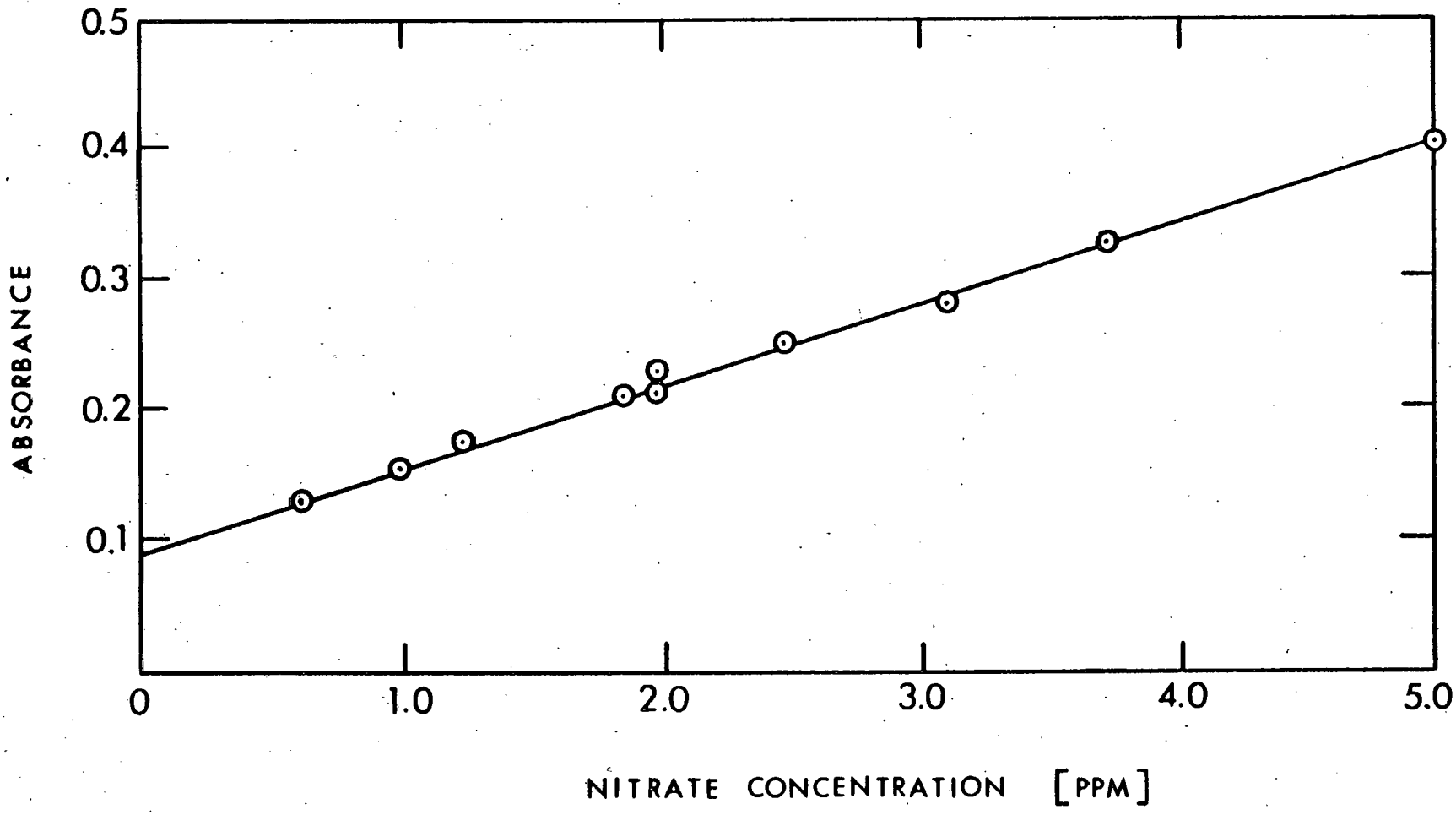

Figure 17. Calibration Curve for Kjeldahl-Nessler Microanalysis Procedure

(C) DIFFERENTIAL FORCE CONSTANT CHANGES AND ISOTOPE EFFECT

by Takanobu Ishida

(C-1) Approximation for the Differential Effect

Exact evaluation of direction and magnitude of an effect of a contemplated change in a force constant matrix element to isotope effect, i.e., $\ln(s/s')f$, is a time-consuming task, because it involves solving two secular problems (one for each isotope). In an effort to find a short-cut method for this problem, the study of effects of differential changes in various $\underset{\sim}{F}$-matrix elements to the isotopic reduced partition function ratio that was started last year has been continued. Last year,[1] we have developed a set of explicit formula for the first derivatives of $\ln(s/s')f$ with respect to force constants f_{ij}, based on the WIMPER approximation[20] of $\ln(s/s')f$. The approximation may be written as follows:

$$\frac{\partial}{\partial f_{pq}} [\ln \frac{s}{s'} f] = D_{pq}^{0} + D_{pq}^{1} + D_{pq}^{2} \qquad (25)$$

corresponding to the zero-th, first, and second-order terms in the WIMPER-approximation of $\ln(s/s')f$.

An extensive FORTRAN program, DIE (Differential Isotope Effect), has been written to test the errors of terminating the expansion after n = 1 term and then those after n = 2 terms for the differential effects of diagonal force constants as well as off-diagonal force constants. The program consists of the following subroutines:

(1) DIAG: This subroutine accepts information on an $\underset{\sim}{F}$-matrix and two $\underset{\sim}{G}$-matrices (one $\underset{\sim}{G}$-matrix for each isotopic molecule) from the main program, solves two secular equations; $|\underset{\sim}{FG}' - \lambda \underset{\sim}{I}| = 0$ and $|\underset{\sim}{FG} - \lambda \underset{\sim}{I}| = 0$, and returns two sets of exact eigenvalues.

(2) EXACT: This subroutine calculates the first derivative of $\ln(s/s')f$ with respect to a given force constant, f_{pp} or f_{pq}, at a specified temperature. This is done by varying the given f_{pp} or f_{pq} by 1% of its original value, evaluating exact eigenvalues for both isotopes for the new $\underset{\sim}{F}$-matrix, calculating exact $\ln(s/s')f$ for the new $\underset{\sim}{F}$-matrix,

and comparing it to the value of ln(s/s')f obtained for the original $\underset{\sim}{F}$-matrix.

(3) ZERO: This is to compute the differential effect of a given f_{pq} to the zero-th order term in the WIMPER approximation first as

$$D^{o}_{pq} = \frac{\partial}{\partial f_{pq}} \left[\ln \frac{s}{s'} f_o\right] \quad , \tag{26}$$

where

$$\ln \frac{s}{s'} f_o = \sum_{i=1}^{3N-6} \left[\ln b(u'_{io}) - \ln b(u_{io})\right] \quad , \tag{27}$$

in which

$$u_{io} = \frac{\hbar}{kT} \sqrt{f_{ii} g_{ii}} \quad , \tag{28}$$

and then as

$$D^{o}_{pq} \approx \frac{S(u_{po})}{2f_{pp}} \delta_{pq} \tag{29}$$

where

$$S(u) = \frac{1}{u} - \frac{ue^u}{(e^u-1)^2} \quad , \tag{30}$$

and u_{po} is given by Eq. (28), and δ_{pq} is the Kronecker delta. Eq. (29) is an approximation to Eq. (26), and subroutine ZERO makes the comparison of exact and approximate values.

(4) FIRST: This subroutine computes the differential effect of a given f_{pq} to the first order term in the WIMPER approximation, i.e.,

$$D^{1}_{pq} = - W_1 A_1 \left(\frac{\hbar}{kT}\right)^2 \delta g_{pq} \, (1-\delta_{pq}) \quad , \tag{31}$$

where W_1 is the modulating coefficient of WINIMAX approximation, $A_1 = 1/24$, $\delta g_{pq} = g'_{pq} - g_{pq}$ or the isotopic difference in the (p,q) element of $\underset{\sim}{G}$-matrices, and δ_{pq} is the Kronecker delta.

(5) SECOND: This subroutine computes the differential effect of a given f_{pq} to the second order term in the WIMPER approximation, i.e.,

$$D^{2}_{pq} = W_2 A_2 \left(\frac{\hbar}{kT}\right)^4 P^2_{pq} \quad , \tag{32}$$

where

$$p^2_{pq} = \delta \left\{ \frac{\partial Tr(\underset{\sim}{H}^2)}{\partial f_{pq}} - \frac{\partial Tr(\underset{\sim}{H}_o^2)}{\partial f_{pq}} \delta_{pq} \right\}, \tag{33}$$

in which $\underset{\sim}{H}^2 = \underset{\sim\sim}{FGFG}$ and $\underset{\sim}{H}_o^2 = \underset{\sim}{F}_o^2 \underset{\sim}{G}_o^2$, $\underset{\sim}{F}_o$ and $\underset{\sim}{G}_o$ being the diagonal matrices consisting of only the diagonal elements of $\underset{\sim}{F}$ and $\underset{\sim}{G}$, respectively. The second term on the right-hand side of Eq. (32) can be written, when $p = q$, as

$$\frac{\partial Tr(\underset{\sim}{H}_o^2)}{\partial f_{pp}} = 2 f_{pp} q_{pp}^2 \quad . \tag{34}$$

Since usefulness of the whole approximation for the differential effect depends on how well one can approximate the term, $\partial Tr(\underset{\sim}{H}^2)/\partial f_{pq}$, of Eq. (33) by a simple formula, we have tested several conceivable approximations for it. It has previously been shown[21] that

$$\frac{\partial Tr(\underset{\sim}{H}^2)}{\partial f_{pq}} = 2(\underset{\sim\sim}{GFG})_{pq} \quad . \tag{35}$$

Of the approximations for $(\underset{\sim\sim}{GFG})_{pq}$ we have tried, the following seemed most promising and reasonable so that this approximation is written into Subroutine SECOND:

$$(\underset{\sim\sim}{GFG})_{pq} \simeq g_{pq}(f_{pp}g_{pp} + f_{qq}g_{qq}) + f_{pq}(g_{pp}g_{qq} + g_{pq}^2) \tag{36}$$

This corresponds to the (p,q) element of the triple product of the (2x2) arrays,

$$\begin{bmatrix} g_{pp} & g_{pq} \\ g_{pq} & g_{qq} \end{bmatrix} x \begin{bmatrix} f_{pp} & f_{pq} \\ f_{pq} & f_{qq} \end{bmatrix} x \begin{bmatrix} g_{pp} & g_{pq} \\ g_{pq} & g_{qq} \end{bmatrix}.$$

If one uses a non-vanishing f_{pq} for an interaction between coordinates p and q, it is usually because these two coordinates are also kinetically coupled and, consequently, $g_{pq} \neq 0$. The neglected coupling terms g_{rs} are associated with f_{rs} and other interaction force constants, and such terms in $Tr(\underset{\sim}{H}^2)$ will vanish when differentiated with f_{pq}. Furthermore, Eq. (36)

keeps the required symmetry, $(\underset{\sim}{GFG})_{pq} = (\underset{\sim}{GFG})_{qp}$. Subroutine SECOND automatically compares the result of the approximation (36) among other approximations with the exact value of $(\underset{\sim}{GFG})_{pq}$.

The program is almost debugged. When finished, we plan to use this program for the differential effect calculations in molecules such as H_2O, CO_2, HCHO, CH_4, C_2H_4, C_2H_6, and C_6H_6. Hopefully, Eq. (25) gives a reliable approximation after the first or second order term.

(C-2) Differential Calculation for Vapor Pressure Isotope Effect

A program, P9042D, has been written to facilitate differential calculations related to the vapor pressure isotope effect (VPIE). After a set of experimental VPIE data are obtained, we always face the task of fitting an $\underset{\sim}{F}$-matrix of the condensed phase to reproduce the VPIE data, as well as some observed liquid frequencies. This is a tedious trial-and-error operation. Very often, one ends up using a few hundred liquid $\underset{\sim}{F}$'s before a reasonable fit is obtained. The study of the approximation for the differential effect reported in the preceding section, if successfully completed, will provide a means of short-cutting this process. In the meanwhile, however, we will have to continue to use the exact method. The program we have used in the past, i.e., a version of Schachtschneider-Snyder program allows us to use only one $\underset{\sim}{F}$-matrix at a time and the output contains sometimes repetitive and many non-essential information. The formats of output makes it usually too bulky to use in the remote terminal mode of computer usage.

Program P9042D has been written to accommodate inputs of as many $\underset{\sim}{F}$-matrix changes as needed in a single run, and the output format is tailored to provide only essential information needed for the differential VPIE calculation in a very compact form: It prints out the gas $\underset{\sim}{F}$-matrix and the basis liquid $\underset{\sim}{F}$-matrix (the matrix from which the subsequent changes are made) just once and only if so desired. The $\underset{\sim}{G}$-matrices are usually (unless instructed otherwise) not printed, because they are always printed out as an output of the $\underset{\sim}{G}$-matrix program. The gas frequencies and the liquid frequencies of both isotopes, the frequency isotope shifts, the frequency shifts upon condensation, $\ln(s/s')f_{gas}$, $\ln(s/s')f_{cond.}$, $\ln(f_c/f_g)$, $T\ln(f_c/f_g)$, and T are tabulated in a compact table for every modified $\underset{\sim}{F}$-matrix. It has been used very successfully in the liquid $\underset{\sim}{F}$-matrix fitting for the fluoroform VPIE-data. The listing of the program is attached to this report.

(D) REFERENCES

1) T. Ishida, "Stable Isotope Studies," Annual Progress Report to the U.S.D.O.E., COO-3127-31, December (1979).

2) T. Ishida, "Stable Isotope Studies," Annual Progress Report to the U.S.D.O.E., COO-3127-29, December (1978).

3) T. Ishida, "Stable Isotope Studies," Annual Progress Report to the U.S.D.O.E., COO-3127-26, December (1977).

4) F. D. Rossini et. al, NBS (US) Circ. No. C461, 121 (1947).

5) L. Borodinsky, H. J. Wieck, D. Mayfield, and T. Ishida, J. Chem. Phys. 68, 3279 (1978).

6) G. Glockler and W. F. Edgell, J. Chem. Phys. 9, 224 (1941).

7) D. H. Rank, E. R. Shull, and E. L. Pace, J. Chem. Phys. 18, 885 (1950).

8) R. Hajjar and G. MacWood, J. Chem. Phys. 49, 4567 (1968); R. Hajjar and G. MacWood, J. Chem. Eng. Data 15, 3 (1970).

9) "Handbook of Fundamentals," American Society of Heating, Refrigerating and Air-Conditioning Engineers, Inc., New York, N.Y., 1974.

10) D. A. Long, R. B. Gravenor, and D. T. L. Jones, Trans. Faraday Soc. 60, 1509 (1964).

11) V. Galasso, G. DeAlti, and G. Costa, Spectrochim. Acta 21, 669 (1965).

12) R. D'Cunha, J. Mol. Spectrosc. 43, 282 (1972).

13) R. D. Green, "Hydrogen Bonding by C-H Groups," John Wiley & Sons, New York (1974).

14) A. Allerhand and P. R. Schleyer, J. Am. Chem. Soc. 85, 1715 (1963).

15) T. Ishida and Wm. Spindel, J. Chem. Eng. Data 15, 107 (1970).

16) E. U. Monse, Wm. Spindel, L. N. Kauder, and T. I. Taylor, J. Chem. Phys. 68, 3501 (1978).

17) K. A. Pearsall, "Studies of Iron (II) Reduction of Nitric Oxide," Masters Thesis, State University of New York at Stony Brook, January, 1978.

18) W. Manchot and H. Haunschild, Z. anorg. allgem. Chem. 140, 22 (1924).

19) W. E. Lobo, et al., Trans. A.I. Ch. E. 41, 693 (1945).

20) J. Bigeleisen, M. W. Lee, T. Ishida, and P. E. Bigeleisen, J. Chem. Phys. 68, 3501 (1978).

21) T. Ishida, U.S. AEC Report COO-3127-4, January (1974).

APPENDIX-(A)

Listing of Program P9042D

```
C THIS IS A VARIATION OF 9042 PROGRAM FOR OBTAINING THE DIFFERENTIAL EFFECTS IN
C FREQUENCIES, LN(S/S')F FOR GAS OR LIQ PHASE, AND LN(FC/FG), DUE TO A CHANGE IN
C F-MATRIX OF GAS OR LIQUID. UP TO 24 F-MATRIX ELEMENTS MAY BE CHANGED
C SIMULTANEOUSLY IN EACH PHASE. INPUT SETS MAY BE STACKED TO PROCESS AS MANY
C DIFFERENTIAL EFFECTS AS NEEDED. ONLY ONE REFERENCE & UP TO TWO NON-REFERENCE
C ISOTOPES ARE ALLOWED FOR EACH PHASE.
C     THE ENTIRE MAIN PROGRAM BETWEEN STATEMENT NO. 90 AND THE END OF PROGRAM
C     IS REPEATED FOR EVERY ISOTOPIC SPECIES.
C *** ORDER OF INPUT:
C      1) ISOTOPE1, GAS ,NUMB=1        (=REFERENCE): READ GG(1, , ) & FF(1, , ,)
C      2)    "    , LIQ ,NUMB=2        (     "     ): READ GG(2, , ) & FF(2, , ,)
C      3) ISOTOTE2, GAS ,NUMB=3                     : READ GG(3, , )
C      4)    "    , LIQ ,NUMB=4                     : READ GG(4, , )
C      5) ISOTOPE3, GAS ,NUMB=5, IF ANY             : READ GG(5, , )
C      6)    "    , LIQ ,NUMB=6,   "                : READ GG(6, , )
C      7) ISOTOPE1, GAS ,NUMB=7,CHANGE IN F IF ANY : READ F-CHANGE INFORMATION
C      8)    "    , LIQ ,NUMB=8,     "      "      : READ F-CHANGE INFORMATION
C      9) ISOTOPE2, GAS ,NUMB=9,
C     10)    "    , LIQ ,NUMB=10,
C     11) ISOTOPE3, GAS ,NUMB=11,
C     12)    "    , LIQ ,NUMB=12,
C     13) ISOTOPE1, GAS ,NUMB=13,CHANGE IN F IF ANY: READ F-CHANGE INFORMATION
C     14)    "    , LIQ ,NUMB=14,    "      "      : READ F-CHANGE INFORMATION
C     15)
      IMPLICIT REAL*8 (A-H,O-Z)
      DIMENSION GG(6,18,18),FF(2,18,18),G(18,18),F(18,18),U(18,18),
     1DV(18),T(10),RECORD(80),NRO(170),NCO(170),NFO(170),Z(170),
     2FI(170),FJ(170),NROWG(4),NCOLG(4),DATING(4),NRL(170),NCL(170),
     3NFL(170),ZL(170),FIL(170),NRG(170),NCG(170),NFG(170),ZG(170),
     4FIG(170),IT(24),A(18,18),DG(18),DD(18),H(18,18),C(18,18),FNEW(24)


      CALL ERRSET (207,256,-1,0)
      CALL ERRSET (208,511,-1,0)

C READ GLOBAL INFORMATION FOR PRESENT MOLECULE.  "MOLECULES" ARE DIFFERENT IF
C DIFFERENT ISOTOPIC SPECIES, DIFFERENT PHASE, AND DIFFERENT F-MATRIX.  STACK
C AS MANY MOLECULES AS NEEDED, EXCEPT THAT THE TOTAL NUMBER MUST BE AN INTEGER
C MULTIPLE OF 4 OR 6
C     IND=-09 : THE PROGRAM CALLS EXIT OTHERWISE. PUT ONE BLANK CARD AT THE END
C               OF INPUT DECK.
C     NUMB    : SERIAL MOLECULE NUMBER.  SEE EXAMPLES.
C     NQ      : NUMBER OF INTERNAL COORDINATES USED FOR F- & G-MATRICES
C     NRED    : NO. OF REDUNDANT COORDINATES INCLUDED IN NQ.
```

```
C     IFS     : =2 IF STANDARD F-MATRIX, AND IF G-MATRIX INPUT IS PROVIDED
C             : =1 IF    "         "   , BUT NO     "      "        "
C             : =0 IF F-MATRIX IS TO BE MODIFIED.
C     NF      : NUMBER OF ELEMENTS IN FI-MATRIX.  THIS AND NOZ ARE SIGNIFICANT &
C               NEEDED ONLY WHEN NUMB=1 OR 2.
C     NOZ     : NUMBER OF ELEMENTS IN Z-MATRIX.
C     NIT     : NUMBER OF FI-MATRIX ELEMENTS TO BE CHANGED SIMULTANEOUSLY.  THIS
C               AND MODE BELOW ARE SIGNIFICANT & NEEDED ONLY WHEN
C               NUMB IS NOT 1 OR 2 AND IF KIND=1.
C     MODE    : =0 IF A CHANGE OF +1% IS IMPOSED ON EVERY F-MATRIX ELEMENT
C                  MODIFIED
C               =1 IF A CHANGE OF +0.1 MDYN/A IS IMPOSED ON EVERY ELEMENT
C                  MODIFIED
C               =2 IF EACH CHANGE IS BY +0.01 MDYN/A.
C               =3 IF EACH CHANGE IS BY +0.001 MDYN/A.
C               =4 IF NON-STANDARD CHANGES ARE MADE. THEN, FNEW INPUT IS NEEDED.
C     KIND    : =1 IF REFERENCE-GAS OR REFERENCE-LIQ MOLECULE.
C               =2 IF NON-REFERENCE MOLECULE USING THE STANDARD F-MATRIX.
C               =3 IF NON-REFERENCE MOLECULE USING A MODIFIED F-MATRIX.
C     ********* FOR FURTHER DISTINCTION AMONG KINDS, SEE "SUMMARY" BELOW.
   90 READ(5,5001) IND,NUMB,NQ,NRED,IFS,NF,NOZ,NIT,KIND,NOTEM,MODE,NCT
 5001 FORMAT(12I3)
C
C     ***************************************************************
C
C SUMMARY OF TYPICAL GLOBAL INPUT (FOR 2 NON-REFERENCE MOLECULES) FOLLOWS:
```

DESCRIPTION OF MOLECULE	NUMB	IFS	KIND	READ	CALCULATE	SAVE	PRINTOUT
STAND-F,REFERENCE,GAS	1	2	1	G,F,T	FREQ	FREQ	F
" " ,LIQ	2	2	1	G,F	FREQ	FREQ	F
" ISOTOPE-A,GAS	3	2	2	G	FREQ,RPFR	FREQ,RPFR	NONE
" " ,LIQ	4	2	2	G	FREQ,RPFR	FREQ,RPFR	FREQ(G',G)
					LN(FC/FG)		FREQ(L',L)
							DFREQ(ISOTOPE ,PHASE)
							RPFR(G,L,D)
" ISOTOPE-B,GAS	5	2	2	G	FREQ,RPFR	FREQ,RPFR	NONE
" " ,LIQ	6	2	2	G	FREQ,RPFR	FREQ RPFR	SAME AS FOR
					LN(FC/FG)		ISOTOPE-A
MOD'D-F,REFERENCE,GAS	7	1/0	1	IT	FREQ	FREQ	CHANGE IN F
" " LIQ	8	1/0	1	IT	FREQ	FREQ	" "
" ISOTOPE-A,GAS	9	1/0	3	NONE	ALL+DIFF.	ALL+DIFF.	NONE
" " ,LIQ	10	1/0	3	"	"	"	ALL+DIFF
" ISOTOPE-B,GAS	11	1/0	3	"	"	"	NONE
" " ,LIQ	12	1/0	3	"	"	"	ALL+DIFF

```
C ****
C NOTES:*ALL MEANS ALL ITEMS APPEARING FOR CORRESPONDING SPECIES IN STAND-F
```

```
C       *DIFF MEANS DIFFERENCE, MODIFIED-F MINUS STANDARD-F
C       *ONE OR BOTH IFS'S FOR GAS & LIQ IN MODIFIED-F CAN BE 1.  REPEAT PATTERN
C        OF IFS USED FOR REF FOR ALL OTHER ISOTOPIC MOLECULES, E.G.,IF IFS=1 & 0
C        FOR REF GAS & LIQ, USE IF=1 & 0 FOR ISOTOPE-A & -B ALSO.
C     **********************************************************************
      IF(IND.EQ.-9) GO TO 100
   95 CALL EXIT
  100 READ(5,5002)(RECORD(I),I=1,18)
 5002 FORMAT(9A8/9A8)
      WRITE(6,6001)(RECORD(I),I=1,18)
 6001 FORMAT(1H1,/5X,9A8,/)
  103 IF(IFS.EQ.2) GOTO 110
  104 NP=NCT
      DO 105 I=1,NQ
      DO 105 J=1,NQ
  105 G(I,J)=GG(NP,I,J)
      GO TO 130
  110 CONTINUE
      DO 112 I=1,NQ
      DO 112 J=1,NQ
      GG(NUMB,I,J)=0.0D0
  112 G(I,J)=0.0D0
      READ(5,5000)(RECORD(I),I=1,9)
 5000 FORMAT(9A8)
  113 READ(5,5003)(NROWG(L),NCOLG(L),DATING(L),L=1,3)
 5003 FORMAT(3(2I3,E18.9))
  115 DO 120 L=1,3
      IF(NROWG(L))122,610,117
  117 IF(NCOLG(L)-NROWG(L))610,118,118
  118 IF(NQ-NCOLG(L))610,119,119
  119 I=NROWG(L)
      J=NCOLG(L)
      G(I,J)=DATING(L)
      G(J,I)=G(I,J)
      GG(NUMB,I,J)=G(I,J)
  120 GG(NUMB,J,I)=G(I,J)
      GO TO 113
  122 IF(1+NROWG(L))610,130,610
  130 IF(NUMB-3)135,160,160
  135 READ(5,5004)(NRO(I),NCO(I),NFO(I),Z(I),I=1,NOZ)
 5004 FORMAT(4(3I3,F9.6))
      READ(5,5005)(FI(K),K=1,NF)
 5005 FORMAT(6F12.6)
      DO 138 K=1,NOZ
      IF(NQ-NCO(K))615,136,136
  136 IF(NCO(K)-NRO(K))615,137,137
  137 IF(NF-NFO(K))615,138,138
  138 CONTINUE
      IF(NUMB.EQ.1) GOTO 150
  140 DO 141 I=1,NOZ
      NRL(I)=NRO(I)
```

```
      NCL(I)=NCO(I)
      NFL(I)=NFO(I)
  141 ZL(I)=Z(I)
      DO 142 I=1,NF
  142 FIL(I)=FI(I)
      LG=2
      GO TO 300
  150 LG=1
      DO 151 I=1,NOZ
      NRG(I)=NRO(I)
      NCG(I)=NCO(I)
      NFG(I)=NFO(I)
  151 ZG(I)=Z(I)
      DO 152 I=1,NF
  152 FIG(I)=FI(I)
      IF(NOTEM.EQ.0) GO TO 300
      READ(5,5006)(T(I),I=1,NOTEM)
 5006 FORMAT(9F8.2)
      WRITE(6,5006)(T(I),I=1,NOTEM)
      GO TO 300
  160 IF(KIND.EQ.1) GOTO 166
  161 IF(NUMB.EQ.(NUMB/2)*2) GOTO 165
  162 LG=1
      GOTO 320
  165 LG=2
      GOTO 320
  166 IF(NIT.EQ.0) GO TO 161
      READ(5,5001)(IT(I),I=1,NIT)
      IF(MODE.NE.4) GOTO 171
      READ(5,5005)(FNEW(I),I=1,NIT)
      IF(NUMB.EQ.(NUMB/2)*2) GO TO 168
      DO 167 I=1,NIT
      J=IT(I)
  167 FIG(J)=FNEW(I)
      GO TO 171
  168 DO 169 I=1,NIT
      J=IT(I)
  169 FIL(J)=FNEW(I)
  171 IF(NUMB.EQ.(NUMB/2)*2) GOTO 175
  172 LG=1
      DO 173 I=1,NOZ
      NRO(I)=NRG(I)
      NCO(I)=NCG(I)
      NFO(I)=NFG(I)
  173 Z(I)=ZG(I)
      DO 174 I=1,NF
  174 FI(I)=FIG(I)
      GO TO 180
  175 LG=2
      DO 176 I=1,NOZ
      NRO(I)=NRL(I)
```

```
      NCO(I)=NCL(I)
      NFO(I)=NFL(I)
  176 Z(I)=ZL(I)
      DO 177 I=1,NF
  177 FI(I)=FIL(I)
  180 IF(IFS.NE.0) GO TO 300
      IF(MODE.GE.1) GO TO 190
  181 DO 185 I=1,NIT
      J=IT(I)
  185 FI(J)=FI(J)*1.01D0
      GO TO 300
  190 DO 195 I=1,NIT
      J=IT(I)
      M=-MODE
  195 FI(J)=FI(J)+10.D0**M
  300 CONTINUE
      DO 305 I=1,NQ
      DO 305 J=1,NQ
  305 FF(LG,I,J)=0.0D0
      DO 310 K=1,NOZ
      I=NCO(K)
      J=NRO(K)
      M=NFO(K)
      FF(LG,I,J)=FF(LG,I,J)+Z(K)*FI(M)
  310 FF(LG,J,I)=FF(LG,I,J)
      IF(NUMB.EQ.2) GO TO 6
      IF(NUMB.NE.1) GOTO 320
      WRITE(6,6004)
 6004 FORMAT(1H0,'STANDARD F-MATRIX FOR GAS:')
      WRITE(6,6005)
 6005 FORMAT(1H0,'              1           2           3           4
     1       5           6           7           8           9
     210')
      DO 312 I=1,NQ
  312 WRITE(6,6006) (FF(1,I,J),J=1,NQ)
 6006 FORMAT(9X,10F12.6)
      GO TO 320
    6 WRITE(6,6007)
 6007 FORMAT(1H0,'STANDARD F-MATRIX FOR LIQ:')
      WRITE (6,6005)
      DO 315 I=1,NQ
  315 WRITE(6,6006) (FF(2,I,J),J=1,NQ)
  320 DO 325 I=1,NQ
      DO 325 J=1,NQ
  325 F(I,J)=FF(LG,I,J)
  340 NR1=0
      IEGEN=0
  342 CALL HDIAG(G,NQ,IEGEN,A,NR1)
  343 DO 350 J=1,NQ
      IF(0.0005D0-G(J,J))347,345,345
  345 DG(J)=0.0D0
```

```
      GO TO 349
  347 DG(J)=G(J,J)
  349 DO 350 I=1,NQ
  350 W(I,J)=A(I,J)*DSQRT(DG(J))
  390 DO 400 J=1,NQ
      DO 395 L=1,NQ
      DD(L)=0.0D0
      DO 395 K=1,NQ
  395 DD(L)=DD(L)+F(L,K)*W(K,J)
      DO 400 I=1,NQ
      H(I,J)=0.0D0
      DO 400 M=1,NQ
  400 H(I,J)=H(I,J)+W(M,I)*DD(M)
  402 NR=0
      IEGEN=0
  404 CALL HDIAG(H,NQ,IEGEN,C,NR)
  406 DO 408 I=1,NQ
  408 DV(I)=DSQRT(DABS(H(I,I)/5.88852D-7))
      CALL THERM (NQ,NRED,DV,KIND,NUMB,IFS,LG,T,NOTEM,NCT,IT,MODE,NIT,
     1FNEW)
      GO TO 90
  610 WRITE(6,6002) NROWG(L),NCOLG(L),DATING(L)
 6002 FORMAT(1H0,' G-MATRIX ERROR. THE CARD READS ',2I3,F12.6)
      GO TO 95
  615 WRITE(6,6003) NRO(K),NCO(K),NFO(K),Z(K)
 6003 FORMAT(1H0,' Z-MATRIX ERROR. THE CARD READS ',2I3,F12.6)
      GO TO 95
      END
      SUBROUTINE HDIAG(H,N,IEGEN,U,NR)
      IMPLICIT REAL*8 (A-H,O-Z)
CHDIAGMIHDI3, FORTAN II DIAGONALIZATION OF A REAL SYMMETRIC MATRIX BY
C     THE JACOBI METHOD.
C     CALLING SEQUENCE FOR DIAGONALIZATION
C     CALL HDIAG( H, N, IEGEN, U, NR)
C     WHERE H IS THE ARRAY TO BE DIAGONALIZED.
C     N IS THE ORDER OF THE MATRIX, H.
C     IEGEN MUST BE SET UNEQUAL TO ZERO IF ONLY EIGENVALUES ARE TO BE
C     COMPUTED.
C     IEGEN MUST BE SET EQUAL TO ZERO IF EIGENVALUES AND EIGENVECTORS
C     ARE TO BE COMPUTED.
C     U IS THE UNITARY MATRIX USED FOR FORMATION OF THE EIGENVECTORS.
C     NR IS THE NUMBER OF ROTATIONS.
C     A DIMENSION STATEMENT MUST BE INSERTED IN THE SUBROUTINE.
C     DIMENSION H(N,N), U(N,N), X(N), IQ(N)
C     COMPUTER MUST OPERATE IN FLOATING TRAP MODE
C     THE SUBROUTINE OPERATES ONLY ON THE ELEMENTS OF H THAT ARE TO THE
C     RIGHT OF THE MAIN DIAGONAL. THUS, ONLY A TRIANGULAR
C     SECTION NEED BE STORED IN THE ARRAY H.
      DIMENSION H(18,18),U(18,18),X(18),IQ(18)
      IF (IEGEN) 15,10,15
   10 DO 14 I=1,N
```

```
      DO 14 J=1,N
      IF(I-J)12,11,12
   11 U(I,J)=1.0D0
      GO TO 14
   12 U(I,J)=0.0D0
   14 CONTINUE
   15 NR = 0
      IF (N-1) 1000,1000,17
C     SCAN FOR LARGEST OFF DIAGONAL ELEMENT IN EACH ROW
C     X(I) CONTAINS LARGEST ELEMENT IN  ITH ROW
C     IQ(I) HOLDS SECOND SUBSCRIPT DEFINING POSITION OF ELEMENT
   17 NMI1=N-1
      DO 30 I=1,NMI1
      X(I) = 0.0D0
      IPL1=I+1
      DO 30 J=IPL1,N
      IF(X(I)-DABS( H(I,J))) 20,20,30
   20 X(I)=DABS(H(I,J))
      IQ(I)=J
   30 CONTINUE
C     SET INDICATOR FOR SHUT-OFF.RAP=2**-27,NR=NO.OF ROTATIONS
      RAP=7.450580596D-9
      HDTEST=1.0D38
C     FIND MAXIMUM OF X(I) S FOR PIVOT ELEMENT AND
C     TEST FOR END OF PROBLEM
   40 DO 70  I=1,NMI1
      IF (I-1) 60,60,45
   45 IF(XMAX-X(I)) 60,70,70
   60 XMAX=X(I)
      IPIV=I
      JPIV=IQ(I)
   70 CONTINUE
C     IS MAX. X(I) EQUAL TO ZERO, IF LESS THAN HDTEST,REVISE HDTEST
      IF (XMAX) 1000,1000,80
   80 IF( HDTEST) 90,90,85
   85 IF (XMAX - HDTEST) 90,90,148
   90 HDIMIN = DABS ( H (1,1) )
      DO 110  I=2,N
      IF (HDIMIN - DABS ( H (I,I))) 110,110,100
  100 HDIMIN=DABS (H(I,I))
  110 CONTINUE
      HDTEST=HDIMIN*RAP
C     RETURN IF MAX.H(I,J)LESS THAN(2**-27)DABS(H(K,K)-MIN)
      IF (HDTEST-XMAX) 148,1000,1000
  148 NR= NR+1
C     COMPUTE TANGENT, SINE AND COSINE,H(I,I),H(J,J)
  150 TANG=DSIGN(2.0D0,(H(IPIV,IPIV)-H(JPIV,JPIV)))*H(IPIV,JPIV)/(DABS(H
     1(IPIV,IPIV)-H(JPIV,JPIV))+DSQRT((H(IPIV,IPIV)-H(JPIV,JPIV))**2+
     24.0D0*H(IPIV,JPIV)**2))
      COSINE=1.0D0/DSQRT(1.0D0+TANG**2)
      SINE=TANG*COSINE
```

```
      HII=H(IPIV,IPIV)
      H(IPIV,IPIV)=COSINE**2*(HII+TANG*(2.0D0*H(IPIV,JPIV)+TANG*H(JPIV,
     1JPIV)))
      H(JPIV,JPIV)=COSINE**2*(H(JPIV,JPIV)-TANG*(2.0D0*H(IPIV,JPIV)-TANG
     1*HII))
      H(IPIV,JPIV)=0.0D0
C     PSEUDO RANK THE EIGENVALUES
C     ADJUST SINE AND COS FOR COMPUTATION OF H(IK) AND U(IK)
      IF ( H(IPIV,IPIV) - H(JPIV,JPIV)) 152,153,153
  152 HTEMP = H(IPIV,IPIV)
      H(IPIV,IPIV) = H(JPIV,JPIV)
      H(JPIV,JPIV) =HTEMP
C     RECOMPUTE SINE AND COS
      HTEMP = DSIGN (1.0D0, -SINE) * COSINE
      COSINE =DABS (SINE)
      SINE =HTEMP
  153 CONTINUE
C     INSPECT THE IQS BETWEEN I+1 AND N-1 TO DETERMINE
C     WHETHER A NEW MAXIUM VALUE SHOULD BE COMPUTE   SINCE
C     THE PRESENT MAXIMUM IS IN THE I OR J ROW.
      DO 350 I=1,NMI1
      IF(I-IPIV)210,350,200
  200 IF (I-JPIV) 210,350,210
  210 IF(IQ(I)-IPIV) 230,240,230
  230 IF(IQ(I)-JPIV) 350,240,350
  240 K=IQ(I)
  250 HTEMP=H(I,K)
      H(I,K)=0.0D0
      IPL1=I+1
      X(I) =0.0D0
C     SEARCH IN DEPLETED ROW FOR NEW MAXIMUM
      DO 320 J=IPL1,N
      IF ( X(I) -DABS( H(I,J)) ) 300,300,320
  300 X(I) = DABS(H(I,J))
      IQ(I)=J
  320 CONTINUE
      H(I,K)=HTEMP
  350 CONTINUE
      X(IPIV) =0.0D0
      X(JPIV) =0.0D0
C     CHANGE THE ORDER ELEMENTS OF H
      DO 530 I=1,N
      IF (I-IPIV) 370,530,420
  370 HTEMP = H(I,IPIV)
      H(I,IPIV)= COSINE*HTEMP + SINE*H(I,JPIV)
      IF ( X(I) - DABS( H(I,IPIV)) )380,390,390
  380 X(I) = DABS(H(I,IPIV))
      IQ(I) = IPIV
  390 H(I,JPIV) = - SINE*HTEMP + COSINE*H(I,JPIV)
      IF ( X(I) - DABS ( H(I,JPIV)) ) 400,530,530
  400 X(I) = DABS(H(I,JPIV))
```

```
      IQ(I) = JPIV
      GO TO 530
  420 IF(I-JPIV) 430,530,480
  430 HTEMP = H(IPIV,I)
      H(IPIV,I) = COSINE*HTEMP + SINE*H(I,JPIV)
      IF ( X(IPIV) - DABS(H(IPIV,I)) ) 440,450,450
  440 X(IPIV) = DABS(H(IPIV,I))
      IQ(IPIV) = I
  450 H(I,JPIV) = - SINE*HTEMP + COSINE*H(I,JPIV)
      IF (X(I) - DABS( H(I,JPIV)) ) 400,530,530
  480 HTEMP = H(IPIV,I)
      H(IPIV,I) = COSINE*HTEMP + SINE*H(JPIV,I)
      IF ( X(IPIV) - DABS( H(IPIV,I)) ) 490,500,500
  490 X(IPIV) = DABS(H(IPIV,I))
      IQ(IPIV) = I
  500 H(JPIV,I) = - SINE*HTEMP + COSINE*H(JPIV,I)
      IF ( X(JPIV) - DABS( H(JPIV,I)) )510,530,530
  510 X(JPIV) = DABS(H(JPIV,I))
      IQ(JPIV) = I
  530 CONTINUE
C     TEST FOR COMPUTATION OF EIGENVECTORS
      IF(IEGEN) 40,540,40
  540 DO 550 I=1,N
      HTEMP=U(I,IPIV)
      U(I,IPIV)=COSINE*HTEMP+SINE*U(I,JPIV)
  550 U(I,JPIV)= -SINE*HTEMP+COSINE*U(I,JPIV)
      GO TO 40
 1000 RETURN
      END
      SUBROUTINE TRANS(AX,BX,CINT,CX,N)
      IMPLICIT REAL*8 (A-H,O-Z)
      DIMENSION AX(18,18),BX(18,18),CINT(18,18),CX(18,18)
    1 DO 5 I=1,N
      DO 5 J=1,N
      CINT(I,J)=0.0D0
    4 DO 5 K=1,N
    5 CINT(I,J)=CINT(I,J)+AX(I,K)*BX(J,K)
    6 DO 12 I=1,N
      DO 12 J=1,N
      CX(I,J)=0.0D0
      DO 10 K=1,N
   10 CX(I,J)=CX(I,J)+BX(I,K)*CINT(K,J)
      IF(0.00005-DABS(CX(I,J)))12,12,11
   11 CX(I,J)=0.0D0
   12 CONTINUE
   13 RETURN
      END
      SUBROUTINE REAR(A,N)
C THIS SUBROUTINE REARRANGES A ONE-DIMENSIONAL ARRAY A INTO DESCENDING ORDER.
C N IS THE NUMBER OF ELEMENTS IN A.
      IMPLICIT REAL*8 (A-H,O-Z)
```

```
      DIMENSION A(18),IT(18),B(18)
      DO 10 I=1,N
   10 IT(I)=0
      NC=1
   15 DO 20 I=1,N
      IF(IT(I).EQ.0) GOTO 21
   20 CONTINUE
   21 C=A(I)
      II=I
      DO 25 I=1,N
      IF(C.GE.A(I)) GOTO 25
      IF(IT(I).EQ.1) GOTO 25
      C=A(I)
      II=I
   25 CONTINUE
      B(NC)=C
      IT(II)=1
      NC=NC+1
      IF(NC.LE.N) GOTO 15
      DO 30 I=1,N
   30 A(I)=B(I)
      RETURN
      END
      SUBROUTINE THERM (NQ,NRED,DV,KIND,NUMB,IFS,LG,T,NOTEM,NCT,IT,MODE,
     1NIT,FNEW)
C THIS IS A 9042D-VERSION OF SUBROUTINE "THERMD". RPFR, ITS PHASE-DIFFERENCE,
C AND THEIR CHANGES DUE TO CHANGES IN F-MATRICES ARE COMPUTED.  ALL PRINTOUTS
C OF PROGRAM 9042D EXCEPT FOR THE ALPHAMERICS AND STANDARD F-MATRICES ARE
C DONE IN THIS SUBROUTINE.
      IMPLICIT REAL*8 (A-H,O-Z)
      DIMENSION DV(18),T(10),DVR(2,18),DVI(2,18),DVS(48,18),Y(2,24),
     1YS(6,24),D1(18),D2(18),D3(10),D4(18),D5(18),D6(18),D7(18),D8(18),
     2D9(18),D10(10),D11(10),D12(10),D13(10),D14(10),IT(24),FNEW(24)
      NQ=NQ-NRED
      NM1=NUMB-1
      CALL REAR(DV,NQ)
      IF(KIND.NE.3) GOTO 100
    5 NP=NCT
      NP1=NP-1
      DO 10 L=1,NOTEM
      X=0.0D0
      DO 7 I=1,NQ
      UR=1.4385*DVR(LG,I)/T(L)
      UI=1.4385*DV(I)/T(L)
      X=X+DLOG(UI/UR)+(UR-UI)/2.0D0+DLOG((1.0D0-DEXP(-UR))/(1.0D0-DEXP(
     1-UI)))
    7 CONTINUE
   10 Y(LG,L)=X
   11 DO 15 I=1,NQ
   15 DVI(LG,I)=DV(I)
      IF(LG.EQ.2) GOTO 20
```

```
      MQG=MQ
      GO TO 500
   20 DO 25 I=1,MQG
      D1(I)=DVR(1,I)-DVR(2,I)
      D2(I)=DVI(1,I)-DVI(2,I)
      D4(I)=DVR(1,I)-DVS(1,I)
      D5(I)=DVI(1,I)-DVS(NP1,I)
      D6(I)=DVR(2,I)-DVS(2,I)
      D7(I)=DVI(2,I)-DVS(NP,I)
      D8(I)=D4(I)-D6(I)
   25 D9(I)=D5(I)-D7(I)
      NL=MQG+1
      DO 30 I=NL,MQ
      D6(I)=DVR(2,I)-DVS(2,I)
   30 D7(I)=DVI(2,I)-DVS(NP,I)
      DO 35 L=1,NOTEM
      D3(L)=Y(2,L)-Y(1,L)
      D10(L)=(Y(1,L)-YS(NP1,L))*1.D2
      D11(L)=(Y(2,L)-YS(NP,L))*1.D2
      D12(L)=D11(L)-D10(L)
      D13(L)=T(L)*D3(L)
      D3(L)=D3(L)*1.D2
      D14(L)=T(L)*D12(L)
   35 D12(L)=D12(L)*1.D2
   40 WRITE(6,6001)
 6001 FORMAT(1H0,'                                FREQUENCY (CM-1)
     1                          REDUCED PARTITION FUNCTION RATIO')
      WRITE(6,6002)
 6002 FORMAT(1X, '-------------------------------------------------------
     1-------------------------------------------------------------
     2----')
      WRITE(6,6003)
 6003 FORMAT(1X, '           GAS                    LIQUID
     1 PHASE-SHIFT')

      WRITE(6,6004)
 6004 FORMAT(1X, '------------------------ ---------------------- -----
     1------------------')

      WRITE(6,6005)
 6005 FORMAT(1X, ' REFERENCE    ISOTOPE    REFERENCE    ISOTOPE    REFE
     1RENCE    ISOTOPE     TEMP       GAS        LIQ     100*DIFF   T*DI
     2FF')
      WRITE(6,6006)
 6006 FORMAT(1X, '------------ ---------- ---------- ---------- -----
     1------ ---------- --------- ---------- ---------- --------- -----
     2----')
      WRITE(6,6007)
 6007 FORMAT(1H0)
      DO 45 I=1,MQG
   45 WRITE(6,6008) DVR(1,I),DVI(1,I),DVR(2,I),DVI(2,I),D1(I),D2(I)
```

```
6008 FORMAT(1X,6F12.3)
     DO 46 I=NL,MQ
  46 WRITE(6,6009) DVR(2,I),DVI(2,I)
6009 FORMAT(25X,2F12.3)
     WRITE(6,6007)
     DO 50 L=1,NOTEM
  50 WRITE(6,6010) T(L),Y(1,L),Y(2,L),D3(L),D13(L)
6010 FORMAT(73X,F10.2,2F11.5,2F10.4)
  60 WRITE(6,6011)
6011 FORMAT(1H0,///1X,' EFFECT OF MODIFIED F-MATRIX FOLLOWS:
    1VALUES UNDER "CHANGE IN REDUCED PARTITION FUNCTION RATIO" ARE 100*
    2ACTUAL ')
     WRITE(6,6012)
6012 FORMAT(1H0,'                              CHANGE IN FREQUENCY (CM-1)
    1                        CHANGE IN REDUCED PARTITION FUNCTION RATIO')
     WRITE(6,6002)
     WRITE(6,6003)
     WRITE(6,6004)
     WRITE(6,6005)
     WRITE(6,6006)
     WRITE(6,6007)
     DO 65 I=1,MQG
  65 WRITE(6,6008) D4(I),D5(I),D6(I),D7(I),D8(I),D9(I)
     DO 70 I=NL,MQ
  70 WRITE(6,6009) D6(I),D7(I)
     WRITE(6,6007)
     DO 75 L=1,NOTEM
  75 WRITE(6,6010) T(L),D10(L),D11(L),D12(L),D14(L)
     GO TO 500
 100 DO 105 I=1,MQ
 105 DVS(NUMB,I)=DV(I)
     IF(KIND.NE.1) GO TO 200
 110 DO 115 I=1,MQ
 115 DVR(LG,I)=DV(I)
     IF(NUMB.LE.2) GOTO 500
 120 IF(LG.EQ.2.AND.IFS.EQ.0) GOTO 125
     IF(LG.EQ.1.AND.IFS.EQ.0) GOTO 121
     GO TO 500
 121 WRITE(6,6013) MODE
6013 FORMAT(1H0,' GAS F-MATRIX BEING MODIFIED:  MODE = ',I3)
     GO TO 130
 125 WRITE(6,6014) MODE
6014 FORMAT(1H0,' LIQUID F-MATRIX BEING MODIFIED:  MODE = ',I3)
 130 WRITE(6,6015) (IT(I),I=1,NIT)
6015 FORMAT(1X,' IT(I) = ',20I3)
     IF(MODE.NE.4) GOTO 500
     WRITE(6,6016) (FNEW(I),I=1,NIT)
6016 FORMAT(1X,' FNEW(I)= ',5F12.6)
     GO TO 500
 200 DO 210 L=1,NOTEM
     X=0.0D0
```

```
      DO 207 I=1,MQ
      UR=1.4385*DVR(LG,I)/T(L)
      UI=1.4385*DV(I)/T(L)
      X=X+DLOG(UI/UR)+(UR-UI)/2.0D0+DLOG((1.0D0-DEXP(-UR))/(1.0D0-DEXP(
     1-UI)))
  207 CONTINUE
  210 YS(NUMB,L)=X
  211 DO 215 I=1,MQ
  215 DVI(LG,I)=DV(I)
      IF(LG.EQ.2) GOTO 220
      MQG=MQ
      NL=MQG+1
      GO TO 500
  220 DO 225 I=1,MQG
      D1(I)=DVR(1,I)-DVR(2,I)
  225 D2(I)=DVI(1,I)-DVI(2,I)
      DO 235 L=1,NOTEM
      D3(L)=YS(NUMB,L)-YS(NM1,L)
      D13(L)=T(L)*D3(L)
  235 D3(L)=D3(L)*1.D2
  240 WRITE(6,6001)
      WRITE(6,6002)
      WRITE(6,6003)
      WRITE(6,6004)
      WRITE(6,6005)
      WRITE(6,6006)
      WRITE(6,6007)
      DO 245 I=1,MQG
  245 WRITE(6,6008) DVR(1,I),DVI(1,I),DVR(2,I),DVI(2,I),D1(I),D2(I)
      DO 246 I=NL,MQ
  246 WRITE(6,6009) DVR(2,I),DVI(2,I)
      WRITE(6,6007)
      DO 250 L=1,NOTEM
  250 WRITE(6,6010) T(L),YS(NM1,L),YS(NUMB,L),D3(L),D13(L)
  500 RETURN
      END
```